

Role of Coarse Aggregate Porosity on Chloride Intrusion in HPC Bridge Decks

**Final Report
March 2020**

IOWA STATE UNIVERSITY
Institute for Transportation

Sponsored by
Iowa Highway Research Board
(IHRB Project TR-728)
Iowa Department of Transportation
(InTrans Project 17-614)

About the Institute for Transportation

The mission of the Institute for Transportation (InTrans) at Iowa State University is to develop and implement innovative methods, materials, and technologies for improving transportation efficiency, safety, reliability, and sustainability while improving the learning environment of students, faculty, and staff in transportation-related fields.

Iowa State University Nondiscrimination Statement

Iowa State University does not discriminate on the basis of race, color, age, ethnicity, religion, national origin, pregnancy, sexual orientation, gender identity, genetic information, sex, marital status, disability, or status as a US veteran. Inquiries regarding nondiscrimination policies may be directed to the Office of Equal Opportunity, 3410 Beardshear Hall, 515 Morrill Road, Ames, Iowa 50011, telephone: 515-294-7612, hotline: 515-294-1222, email: eooffice@iastate.edu.

Disclaimer Notice

The contents of this report reflect the views of the authors, who are responsible for the facts and the accuracy of the information presented herein. The opinions, findings and conclusions expressed in this publication are those of the authors and not necessarily those of the sponsors.

The sponsors assume no liability for the contents or use of the information contained in this document. This report does not constitute a standard, specification, or regulation.

The sponsors do not endorse products or manufacturers. Trademarks or manufacturers' names appear in this report only because they are considered essential to the objective of the document.

Iowa DOT Statements

Federal and state laws prohibit employment and/or public accommodation discrimination on the basis of age, color, creed, disability, gender identity, national origin, pregnancy, race, religion, sex, sexual orientation or veteran's status. If you believe you have been discriminated against, please contact the Iowa Civil Rights Commission at 800-457-4416 or the Iowa Department of Transportation affirmative action officer. If you need accommodations because of a disability to access the Iowa Department of Transportation's services, contact the agency's affirmative action officer at 800-262-0003.

The preparation of this report was financed in part through funds provided by the Iowa Department of Transportation through its "Second Revised Agreement for the Management of Research Conducted by Iowa State University for the Iowa Department of Transportation" and its amendments.

The opinions, findings, and conclusions expressed in this publication are those of the authors and not necessarily those of the Iowa Department of Transportation.

Technical Report Documentation Page

1. Report No. IHRB Project TR-728	2. Government Accession No.	3. Recipient's Catalog No.	
4. Title and Subtitle Role of Coarse Aggregate Porosity on Chloride Intrusion in HPC Bridge Decks		5. Report Date March 2020	
		6. Performing Organization Code	
7. Author(s) Kejin Wang (orcid.org/0000-0002-7466-3451), Bharath Melugiri Shankaramurthy (orcid.org/0000-0001-7521-8440), and Franciszek "Franek" Hasiuk (orcid.org/0000-0002-6531-1710)		8. Performing Organization Report No. InTrans Project 17-614	
9. Performing Organization Name and Address Institute for Transportation Iowa State University 2711 South Loop Drive, Suite 4700 Ames, IA 50010-8664		10. Work Unit No. (TRAIS)	
		11. Contract or Grant No.	
12. Sponsoring Organization Name and Address Iowa Highway Research Board Iowa Department of Transportation 800 Lincoln Way Ames, IA 50010		13. Type of Report and Period Covered Final Report	
		14. Sponsoring Agency Code IHRB Project TR-728	
15. Supplementary Notes Visit https://intrans.iastate.edu for color pdfs of this and other research reports.			
16. Abstract <p>This study evaluated the effects of coarse aggregate pore system properties on the permeability and chloride ingress of high-performance concrete (HPC) mixes used in bridge decks in Iowa.</p> <p>Five coarse aggregates typically available in Iowa were studied, including three limestone and two dolostone aggregates with different water absorption capacities and porosity values. These coarse aggregates were used to make five concrete mixes with a given HPC mix proportion. (That is, the five concrete mixes differed only in terms of the coarse aggregate used.) A corresponding mortar mix was sieved from one of the concrete mixtures to eliminate coarse aggregate. The aggregates were analyzed for their pore characteristics, and the mortar and HPC mixes were evaluated for chloride intrusion using electrical and non-electrical tests. Relationships were determined between the aggregate properties and the results of the concrete chloride intrusion tests.</p> <p>The results showed that the aggregate critical and threshold pore sizes were strongly related to concrete surface resistivity and initial sorptivity but did not strongly affect the chloride penetration results of salt ponding tests. The different chloride intrusion tests indicated that the concrete mixes made with limestone and dolostone aggregates exhibited different behaviors. For a given coarse aggregate type (limestone or dolostone), concrete initial sorptivity increased with increasing aggregate critical pore throat size.</p> <p>Although aggregate absorption should not be used as the sole means of concrete durability control, it should be considered a key parameter for concrete aggregate evaluation. For concrete, the short-term initial sorptivity test (which takes six hours) can be used instead of a 90-day salt ponding test for a quick evaluation of chloride intrusion. This test can be used together with the aggregate absorption test to evaluate aggregate quality.</p>			
17. Key Words aggregate—chloride permeability—high-performance concrete—pore structure—porosity		18. Distribution Statement No restrictions.	
19. Security Classification (of this report) Unclassified.	20. Security Classification (of this page) Unclassified.	21. No. of Pages 84	22. Price NA

ROLE OF COARSE AGGREGATE POROSITY ON CHLORIDE INTRUSION IN HPC BRIDGE DECKS

**Final Report
March 2020**

Principal Investigators

Kejin Wang, Professor
Civil, Construction, and Environmental Engineering, Iowa State University

Franciszek “Franek” Hasiuk, Associate Scientist
Kansas Geological Survey, University of Kansas

Research Assistant

Bharath Melugiri Shankaramurthy

Authors

Kejin Wang, Bharath Melugiri Shankaramurthy, and Franciszek “Franek” Hasiuk

Sponsored by

Iowa Department of Transportation and Iowa Highway Research Board
(IHRB Project TR-728)

Preparation of this report was financed in part
through funds provided by the Iowa Department of Transportation
through its Research Management Agreement with the
Institute for Transportation
(InTrans Project 17-614)

A report from
Institute for Transportation
Iowa State University
2711 South Loop Drive, Suite 4700
Ames, IA 50010-8664
Phone: 515-294-8103 / Fax: 515-294-0467
<https://intrans.iastate.edu>

TABLE OF CONTENTS

ACKNOWLEDGMENTS	ix
EXECUTIVE SUMMARY	xi
1 INTRODUCTION	1
1.1 Problem Statement	1
1.2 Objectives and Approach	2
1.3 Scope of the Study	2
2 LITERATURE REVIEW	4
2.1 Specifications/Properties of Coarse Aggregate for Use in HPC for Bridge Deck Concrete	5
2.2 Test Methods for Rock/Aggregate Characterization	6
2.3 Test Methods for Chloride Penetration of Concrete	12
3 EXPERIMENTAL MATERIALS AND METHODS	15
3.1 Materials and Mix Proportions	15
3.2 Tests and Methods	18
4 RESULTS AND DISCUSSION	27
4.1 Aggregate Properties	27
4.2 Properties of Rock Cores	28
4.3 Fresh Concrete Properties	39
4.4 Hardened Concrete Properties	40
5 CONCLUSIONS AND RECOMMENDATIONS	60
REFERENCES	65

LIST OF FIGURES

Figure 2.1. Air void size measurement capabilities of various testing methods.....	11
Figure 3.1. Aggregate gradation	15
Figure 3.2. Sieving concrete using the #4 sieve (left) to obtain the mortar (right).....	18
Figure 3.3. Phunque flasks.....	18
Figure 3.4. Calibration check of air meter	19
Figure 3.5. Calibration tube shortened for aggregate correction factor test	19
Figure 3.6. Rock cores for resistivity measurement	21
Figure 3.7. Vacuum saturation of rock cores	22
Figure 3.8. Concrete plugs used for MIP analysis	22
Figure 3.9. Resipod used for SR measurement.....	23
Figure 3.10. Slab preparation and ponding	23
Figure 3.11. AASHTO T 260 procedure for chloride content determination.....	24
Figure 3.12. Nord test sample preparation and conditioning.....	25
Figure 3.13. Nord test procedure for determining chloride penetration depth	25
Figure 3.14. ASTM C1585 water sorptivity test procedure.....	26
Figure 4.1. Coarse aggregate correction factor versus absorption.....	28
Figure 4.2. Phunque absorption versus ASTM C127 absorption	28
Figure 4.3. Thin-section images of all rock samples (500 μm scale)	29
Figure 4.4. Helium porosity from rock plugs versus helium porosity from rock cores.....	30
Figure 4.5. Aggregate absorption versus rock core helium porosity	30
Figure 4.6. MIP test results for rocks.....	31
Figure 4.7. Determination of critical and threshold pore size from an MIP curve	33
Figure 4.8. Relationship between MIP porosity and helium porosity of rocks	33
Figure 4.9. Relationship between mercury intrusion volume and aggregate water absorption.....	34
Figure 4.10. Rock core water sorptivity versus absorption	34
Figure 4.11. Relationship between rock pore size and initial sorptivity.....	35
Figure 4.12. Resistivity of rock cores	35
Figure 4.13. Rock resistivity versus aggregate absorption	36
Figure 4.14. Dynamic uptake of CsCl solution by mortar	37
Figure 4.15. Path of CsCl salt solution movement	37
Figure 4.16. CT sample and scanning facility at the CNDE at ISU	38
Figure 4.17. CT scan images of DM1 and DM2 rock slices	39
Figure 4.18. Thin-section micrograph of a concrete specimen.....	40
Figure 4.19. Thin-section micrograph highlighting deterioration of a fine aggregate grain	41
Figure 4.20. Thin-section micrograph highlighting a fine aggregate grain	41
Figure 4.21. Thin-section micrograph of fine aggregate grains in porous dolostone.....	42
Figure 4.22. Thin-section micrographs of paste-coarse aggregate interface in all concrete mixes	42
Figure 4.23. Thin-section micrograph of low-porosity paste	43
Figure 4.24. Thin-section micrograph of fine aggregate-paste interface.....	43
Figure 4.25. Thin-section micrograph of Alden sample	44
Figure 4.26. Thin-section micrographs of concrete mixes showing mineral growth in air voids.....	44

Figure 4.27. Compressive strengths of the concrete mixes	45
Figure 4.28. SR development with specimen age.....	46
Figure 4.29. 28-day concrete SR versus critical and threshold pore throat diameter in rocks	47
Figure 4.30. Rock SR versus 28-day concrete SR	47
Figure 4.31. Variation of concrete SR values with aggregate absorption values	48
Figure 4.32. Concrete SR versus rock SR considered separately for the limestone (a) and dolostone (b) series	50
Figure 4.33. Concrete DNSSM values versus aggregate ASTM C127 absorption values	51
Figure 4.34. Concrete DNSSM values versus rock pore throat diameter values.....	52
Figure 4.35. Relationship between SR values and DNSSM.....	52
Figure 4.36. 28-day water sorptivity of concrete mixes versus ASTM C127 aggregate absorption values.....	53
Figure 4.37. 28-day initial sorptivity in concrete versus initial sorptivity in LS rocks	54
Figure 4.38. 28-day initial sorptivity of concrete versus pore throat diameter of rocks.....	54
Figure 4.39. Chloride content in concrete versus ASTM C127 absorption values.....	55
Figure 4.40. Concrete chloride content versus the critical and threshold pore throat diameters of the corresponding rocks in the concrete.....	56
Figure 4.41. 28-day concrete sorptivity versus 28-day concrete SR	57
Figure 4.42. Concrete chloride content versus concrete SR at 28 days and 56 days.....	58
Figure 4.43. Concrete chloride content versus concrete initial sorptivity	59

LIST OF TABLES

Table ES1. Main features of the pore structure of the aggregates studied	xii
Table 2.1. DOT requirements for coarse aggregates in HPC or bridge deck concrete.....	6
Table 3.1. Coarse aggregate sources, lithologies and range of absorptions	15
Table 3.2. Chemical composition of the cementitious materials	16
Table 3.3. Mix proportions for all mixes	17
Table 3.4. Test methods and number of samples.....	17
Table 4.1. Tests performed in the present study	27
Table 4.2. Coarse aggregate properties.....	27
Table 4.3. Pore characteristics of rock plugs	32
Table 4.4. Fresh concrete properties	39
Table 5.1. Main features of the pore structure of the aggregates studied	60

ACKNOWLEDGMENTS

The authors would like to thank the Iowa Department of Transportation (DOT) and Iowa Highway Research Board (IHRB) for sponsoring this research project. The authors also acknowledge and thank Kaitlyn Roling and Mitchell Vanderveen at the Iowa DOT for their assistance in the chemical analysis of chloride content in concrete, Burton Chaska and Michael Coles at the Iowa DOT for their help in carrying out chloride tests, and the technical advisory committee (TAC) members, Kevin Jones, Jeff Devries, Todd Hanson, Bob Dawson, Michelle Barger, and Ahmad Abu-Hawash, for providing valuable and timely input during the course of the project.

EXECUTIVE SUMMARY

To control concrete permeability and chloride ingress, the Iowa Department of Transportation (DOT) has been using low-permeability high-performance concrete (HPC) for the decks and substructures of bridges on higher traffic roadways over past several years. Most of the development work on low-permeability HPC has focused on the paste portion of concrete mixes. Very limited work has been done to investigate the role of aggregate, especially coarse aggregate, on the intrusion of chloride into HPC in bridge decks. In Iowa, many carbonate aggregates with relatively high absorption values (greater than 3%) have been used in HPC. Because chemical fluids generally penetrate concrete via advection through pores, requiring low-permeability HPC without considering the porosity of the coarse aggregate in the concrete poses risks.

In recent years, the Iowa DOT has found that the chloride permeability values of some HPC mixes are not as low as expected (RFP IHRB-17-05). These permeability values are often measured using electrical test methods, such as AASHTO T 277, Standard Method of Test for Rapid Determination of the Chloride Permeability of Concrete, and AASHTO T 358, Standard Method of Test for Surface Resistivity Indication of Concrete's Ability to Resist Chloride Ion Penetration. HPC with high permeability values as measured by rapid electrical methods is often associated with highly absorptive coarse aggregate. It is not clear whether this trend would still exist if a non-electrical test method (such as AASHTO T 259, Standard Method of Test for Resistance of Concrete to Chloride Ion Penetration) were used to measure concrete permeability.

To address the above issues, the aim of this research project was to identify an effective test method to reduce uncertainty concerning the use of certain Iowa aggregate sources for manufacturing HPC for bridge decks. The specific objectives of the study were as follows:

1. To identify rock properties (such as porosity, median or critical pore throat diameter, etc.) that describe the main features of the coarse aggregate pore structure
2. To evaluate test methods for quantifying these properties
3. To examine the relationship between coarse aggregate pore properties and HPC permeability (i.e., chloride ingress) measured using both electrical and non-electrical test methods
4. To provide recommendations for evaluating Iowa coarse aggregates and permeability of HPC

The following tasks were conducted during this project to fulfill the abovementioned objectives:

1. A literature review was conducted on aggregates used in HPC and their effects on concrete properties.
2. Rocks and their corresponding coarse aggregates from five Iowa sources as well as other concrete materials were collected for concrete preparation. These five coarse aggregates are typically available in Iowa and include three limestone and two dolostone aggregates with different water absorption capacities and porosity values.
3. The pore structure of the selected rocks and aggregates was characterized using water absorption, helium porosity, mercury intrusion porosity (MIP), and petrographic thin-section test methods. Surface resistivity and water sorptivity tests were also performed on the rocks.

4. Concrete specimens (cylinders and ponding slabs) were prepared from five concrete mixes made with a single HPC mix proportion but different coarse aggregates. A corresponding mortar mix to serve as a control was sieved from one of the concrete mixtures to eliminate coarse aggregate.
5. Two electrical tests (surface resistivity and Nord) and two non-electrical permeability/chloride penetration tests (water sorptivity and ponding) were performed on the concrete specimens. Some tests were also performed on the rocks and the mortar sieved from one of the concrete mixes.
6. The potential relationships between the parameters describing the aggregate pore structure and the chloride penetration resistance of concrete were examined.
7. Conclusions and recommendations were made for testing Iowa coarse aggregates and HPC concrete permeability.

The following major findings were obtained from this study:

1. The main features of the pore structure of the aggregates studied are summarized in Table ES1.

Table ES1. Main features of the pore structure of the aggregates studied

Rock ID	Absorption (%)	Ave. rock He porosity (%)	Ave. MIP porosity (%)	Mean throat pore size (µm)	Critical pore throat size (µm)	Threshold pore throat size (µm)
LS1	0.7	1.0	3.2	0.02	0.02	0.04
LS2	2.9	6.7	8.4	0.29	0.15	0.4
LS3	3.5	12.5	15.9	1.94	3.63	11
DM1	4.1	15.0	18.4	1.25	1.49	2.1
DM2	6.8	21.0	25.8	5.34	20.4	25

2. The following observations were made regarding the test methods for quantifying the pore system of coarse aggregates:
 - Absorption test – This test is simple and quick to run. The absorption values affect many concrete properties, but they are not directly related to concrete chloride penetration.
 - Sorptivity test – The initial sorptivity values of rock plugs are related to concrete chloride penetration (ponding test results), but it is important to know the coring orientation of the rock plugs because rock plugs with different coring orientations provide quite different test results.
 - MIP test – The results of this test provide detailed information on the pore structure (such as total porosity, intruded volumes for given pore size ranges, and the average, critical and threshold pore throat sizes) of tested samples, but the test requires equipment, operational skills, and dealing with the used mercury.

- Thin-section test – This test provides information on mineralogy, the relative abundance of grain and pore types and grain and pore sizes, and pore connectivity.
 - Helium test – This test measures the total porosity of the connected pores in a sample and shows a good relationship with the total porosity measured from MIP tests.
3. Different trends were observed from the electrical and non-electrical test methods:
- In the electrical tests, concrete surface resistivity decreased with increasing aggregate absorption, which is consistent with the Iowa DOT's findings that the chloride permeability values of some HPC mixes are not as low as expected (RFP IHRB-17-05). However, the diffusion non-steady state migration (DNSSM) measured from Nord tests increased with increasing aggregate absorption.
 - In the non-electrical tests, the same trends were obtained from the sorptivity and ponding tests. Concrete initial sorptivity and chloride content in the top surface layer (1/16 to 1/2 inch) increased with limestone aggregate absorption, but they decreased with dolostone aggregate absorption.
4. The effects of coarse aggregate absorption on concrete chloride content were as follows:
- The mortar samples sieved from the C-LS1 Ames mix had a higher chloride content than all five of the concrete mixes made with coarse aggregate with different absorption values. As a result, fluids and chemicals were able to intrude into the concrete through the mortar to the coarse aggregate.
 - Concrete made with a higher absorption limestone coarse aggregate had higher chloride content after the salt ponding tests. Concrete made with dolostone aggregate had reduced chloride content with increasing aggregate absorption. Based on these findings, aggregate absorption values cannot be simply used to estimate concrete chloride intrusion resistance.
5. The effects of coarse aggregate pore system on concrete permeability and chloride intrusion were as follows:
- Concrete surface resistivity decreased non-linearly while the Nord chloride migration coefficient increased non-linearly with the critical and threshold pore sizes of the rocks used as coarse aggregates in the concrete.
 - For limestone aggregates, concrete initial sorptivity and chloride content (measured from the salt ponding tests) increased non-linearly with the critical and threshold pore sizes of the rocks used as coarse aggregates in the concrete. However, the effects of the critical and threshold pore sizes of the rocks on concrete chloride content are very small.
 - Different from the limestone aggregates, the dolostone aggregates showed a decreased trend in initial sorptivity and chloride content with increasing critical and threshold pore sizes of their rocks.
6. Other important relationships that were identified included the following:

- There is a close relationship between coarse aggregate absorption and specific gravity.
- There is a close relationship between coarse aggregate absorption and helium porosity.
- There is a strong linear relationship between coarse aggregate helium and MIP porosity.
- The surface resistivity of concrete made with limestone coarse aggregate increased linearly while the surface resistivity of concrete made with dolostone coarse aggregate decreased with the surface resistivity of the corresponding rocks.
- For the limestone aggregates, concrete chloride content (measured from the ponding tests) decreased with increasing concrete surface resistivity values. For the dolostone aggregates, concrete chloride content decreased with increasing concrete surface resistivity values.
- For either coarse aggregate lithology (limestone or dolostone), concrete chloride content increased with concrete initial sorptivity.

The following recommendations are proposed for further study:

1. Recommendations for aggregate pore structure characterization:

- Coarse aggregate absorption is a key parameter related to many other aggregate and concrete properties. However, the effects of aggregate absorption on concrete sorptivity and chloride intrusion also depend upon coarse aggregate type because of the difference in surface physics between the two lithologies with respect to the wetting fluid (water). Therefore, coarse aggregate absorption should not be used as a sole criterion for concrete durability control.
- Helium porosity provides an easy, non-destructive, and dry test for the total porosity of a rock or concrete's connected pore network. If the sample has a simple geometry (e.g., a cylinder or prism), the test is also quick (less than 30 minutes).
- The critical and threshold pore sizes of aggregate obtained from MIP testing can be used to provide quantitative information on the pore connectivity of aggregate, mortar, and concrete as needed. Because mercury is a non-wetting fluid with respect to mineral surfaces, it will provide more accurate results.
- Thin-section tests provide detailed information on coarse aggregate quality (e.g., coarse aggregate grain size, pore characteristics). These tests also provide visual, spatial relationships between concrete components (e.g., coarse aggregate's bond with mortar). More thin-section tests should be conducted on a variety of Iowa aggregates in the near future.

2. Recommendations for concrete permeability and chloride intrusion tests:

- When a surface resistivity test is used, it is important to know the concrete's coarse aggregate type (i.e., limestone or dolostone), because the relationship between concrete surface resistivity is negatively correlated to concrete initial sorptivity and chloride content in limestones but positively correlated in dolostones.
- The initial sorptivity test (which takes six hours) can be performed instead of a 90-day salt ponding test for a quick evaluation of chloride intrusion in concrete because for any

given coarse aggregate type, the chloride content measured from the salt ponding tests always increased with the initial sorptivity of the concrete.

3. Recommendations for future study:

- Only aggregates from three limestone sources and two dolostone sources were examined in the present study. More Iowa aggregate sources, especially those of mixed lithology (“intermediates” in the terminology of the Iowa DOT), should be studied to verify the trends observed in the present study.
- The mortar had the highest chloride content after 90 days of the ponding test, and fluids and chemicals can penetrate into aggregate through the mortar. In the future, concrete mixes with a lower water-to-binder ratio (w/b) should also be studied. As the mortar becomes less permeable with a lower w/b, it can encase and seal the permeable aggregate particles, thus preventing chloride penetration into the aggregate and improving the chloride resistance of the HPC.
- Many test results in the present study showed opposite trends between the limestone aggregate concrete and dolostone aggregate concrete. For example, initial sorptivity and chloride measurements increased with the absorption of limestone aggregates but decreased with the absorption of dolostone aggregates. This behavior is probably due to a potential cement reaction with the surface of the dolostone and the internal curing ability provided by the stored water in the more porous aggregates. High-porosity dolostone aggregates should be studied further due to the potential cement reaction with the surface of the dolostone and the internal curing ability.
- A comparison study should be conducted involving the construction of two field HPC overlays, one made with a low-absorption and low-sorptivity aggregate and the other made with a high-absorption and especially high-sorptivity aggregate. The aggregates can be selected from the limestone series or the dolostone series. The overlays can be monitored for surface resistivity and chloride penetration over time. The results can be used to verify the findings from the present study.

1 INTRODUCTION

1.1 Problem Statement

Permeability is a key parameter controlling concrete durability. In reinforced concrete structures such as bridge decks, the ingress of chloride ions from applied deicing chemicals often results in corrosion of reinforcing steel, leading to concrete expansion, cracking, and failure. Significant efforts have been made to reduce the permeability of concrete. One approach has been to utilize low-permeability high-performance concrete (HPC).

The Iowa Department of Transportation (DOT) has been using low-permeability HPC for the decks and substructures of bridges on higher traffic roadways over the past several years. Most of the development work on low-permeability HPC has focused on the paste portion of concrete mixes. Concrete research and practice in Iowa have proven that combinations of blended cement (Type IS or IP), or slag with Type I/II cement, and fly ash significantly reduce the permeability of concrete and the potential for critical chloride intrusion at the steel level.

Because the permeability of HPC paste is substantially reduced, the permeability of the HPC's aggregate then becomes a critical component of the overall permeability of the HPC. Hence, it is important to investigate the role of aggregate, especially coarse aggregate, on chloride intrusion in HPC bridge decks.

In Iowa, some high-quality carbonate aggregates have a relatively high water absorption (greater than 3%). Because chemical fluids generally penetrate concrete via advection through pores, creating an HPC mix without considering the porosity of the coarse aggregate in the concrete poses risks. If low-permeability aggregates are locally available, the use of these aggregates for HPC is the most cost-effective approach to ensuring durable bridge decks; otherwise, selection of aggregates for HPC with low permeability is challenging. Ideally, a lower permeability paste may be designed and produced to isolate the permeable aggregate particles in the concrete and thereby reduce the bulk concrete permeability. Unfortunately, few systematic studies have been conducted to evaluate the effects of aggregate pore system properties (e.g., porosity, permeability) on concrete, especially HPC. As HPC is increasingly used in the decks and substructures of US bridges, detailed research on this subject is necessary.

In recent years, the Iowa DOT has found that the chloride permeability values of HPC in some Iowa projects were not as low as expected (RFP IHRB-17-05). These permeability values were often measured using electrical test methods, such as AASHTO T 277, Standard Method of Test for Rapid Determination of the Chloride Permeability of Concrete, and AASHTO T 538, Standard Method of Test for Surface Resistivity Indication of Concrete's Ability to Resist Chloride Ion Penetration. According to the Iowa DOT's specifications, HPC should have a maximum 28-day permeability of 2,000 coulombs for the substructure (or greater than 20 K ohm-cm surface resistivity [SR]) and 1,500 coulombs for the deck (or greater than 30 K ohm-cm SR) as a target.

It has also been observed that HPC with high permeability measured by rapid electrical methods was associated with highly absorptive coarse aggregate. However, it is not clear whether this trend would still exist when a non-electrical test method (such as AASHTO T 259, Standard Method of Test for Resistance of Concrete to Chloride Ion Penetration) is used to measure concrete permeability.

The study reported herein was intended to bridge the abovementioned knowledge gaps using an experimental program based on standard aggregate characterization and chloride permeability testing of rocks, mortar, and cement concrete.

1.2 Objectives and Approach

The overall goal of this research was to identify an effective test method to reduce uncertainty concerning the use of certain Iowa aggregate sources for manufacturing HPC for bridge decks. The approach was to investigate Iowa HPC coarse aggregates with a range of water absorbances and study the relationships between the aggregate properties, especially the pore system properties, and concrete permeability. The specific objectives of the study included the following:

1. Examine the relationship between coarse aggregate pore properties and concrete permeability/chloride ingress measured using different methods (e.g., natural chloride penetration and electrical methods)
2. Identify the properties (e.g., porosity or median pore throat diameter) that describe the main features of the aggregate pore structure
3. Evaluate the test methods for quantifying the key pore system properties of coarse aggregates
4. Provide recommendations for characterizing Iowa coarse aggregates and testing low-permeability HPC

1.3 Scope of the Study

The following tasks were conducted during this project to fulfill the abovementioned objectives:

1. A literature review was conducted on aggregates used in HPC and their effects on concrete properties.
2. Rock and coarse aggregates from five different sources as well as other concrete materials were collected for concrete preparation.
3. The collected materials were characterized, especially the aggregates and corresponding rock cores.

4. Concrete specimens were prepared from five concrete mixes, all of which were made with a given HPC mix proportion but different coarse aggregates.
5. Two electrical and two non-electrical permeability/chloride penetration tests were performed on rock, mortar, and concrete specimens.
6. The potential relationships between the parameters describing the aggregate pore structure and the chloride penetration resistance of concrete were examined.
7. All related information was analyzed and conclusions and recommendations were provided for testing Iowa coarse aggregates and HPC concrete permeability.

2 LITERATURE REVIEW

Various attempts have been made to identify better aggregate characterization methods and to modify specifications to extend the use of available aggregate sources to improve the service life of pavements (e.g., Bektas et al. 2015, Ridzuanet al. 2016).

Concrete permeability is determined by the characteristics of its air void system, cement paste, coarse and fine aggregates, and the interfacial transition zones (ITZ) between the aggregate and cement paste. Generally, the porosity of most natural aggregates used for durable concrete is much lower than the capillary porosity of a cement paste in normal strength concrete (NSC), which is approximately 30% to 40% depending on the water-to-binder ratio (w/b) and degree of binder hydration (Mehta and Monteiro 2014). It has been previously suggested that aggregate porosity could influence the chloride diffusivity of concrete but that the effect is negligible compared to the effect of the porosity of the cement matrix (Nilsson et al. 1996). Consequently, the effects of aggregate pore structure on concrete permeability and chloride diffusivity have not been widely studied.

However, the aggregate properties that affect the quality, quantity, and tortuosity of the ITZs (such as aggregate type, size, shape, surface texture, etc.) are well known to affect concrete permeability. This is because the ITZs in NSC are more porous than the cement paste and are interconnected with pores in the cement paste. It is this interconnectivity that facilitates fluid permeation through NSC. As a result, one way to reduce concrete permeability is to alter the ITZs in NSC to reduce their porosity. This can be simply achieved by use of a low w/b and supplementary cementitious materials (SCMs), like what is used in HPC, where permeability of both the cement paste and ITZs is reduced. Research has also indicated that the use of high-porosity aggregate, like lightweight aggregate, can also reduce porosity in the ITZs in NSC because little to no bleeding water could accumulate underneath porous aggregate particles that would lead to the formation of porous ITZs. In addition, the water stored in porous aggregate particles, which functions as an internal curing agent, can contribute to hydration of the surrounding cement paste and further reduce porosity in ITZs. Therefore, in normal weight NSC, water penetration generally occurs through the paste and ITZs, whereas in well-designed and well-produced lightweight concrete, the water penetration mainly occurs through the paste due to the low porosity of the ITZs (Vaysburd 1992).

The penetration of chloride into concrete can be carried out by various mechanisms, commonly advection and diffusion (Wattanapornprom and Ishida 2017), convection (Nilsson et al. 1996), permeation (Basheer et al. 2001, Zhutovsky and Hooton 2019), and fluid absorption (Wei et al. 2017). However, because most fluid penetration into concrete occurs via advection, many DOTs specify a limit on the maximum absorption of aggregates. For instance, for bridge superstructures, the Minnesota DOT (MnDOT) has specified a maximum absorption of 1.75% for Class B aggregate, which includes crushed quarry or mine rock such as carbonates, rhyolite, and schist (MnDOT 2018, Bektas et al. 2015). A water absorption test (as a proxy for porosity) is often used to provide insight into the pore structure or permeability of aggregate. Low absorption is often considered as a sign of low permeability because numerous geological and porous media studies have shown the correlation between porosity and permeability. However, few studies in

the civil engineering literature have related the petrophysical (e.g., absorption, pore size distribution) and petrographic (e.g., pore type, rock type) properties of aggregates to subsequent concrete permeability and chloride intrusion.

2.1 Specifications/Properties of Coarse Aggregate for Use in HPC for Bridge Deck Concrete

The following sections summarize various DOT specifications regarding aggregate type selection and the absorption limit for aggregates.

2.1.1 Indiana DOT (INDOT)

The maximum allowable absorption for coarse aggregate class AP (the highest classification) is 5%. Coarse aggregates having absorption values between 5.0 and 6.0 that pass AP testing can be used in portland cement concrete (PCC).

2.1.2 Kansas DOT (KDOT)

Coarse aggregate consisting of crushed or uncrushed gravel, chat (siliceous carbonate rock), or crushed stone (limestone, calcite-cemented sandstone, rhyolite, quartzite, basalt, and granite are considered to be crushed stone) can be used for structural concrete construction. For coarse aggregate used for wear and absorption, the absorption limit is 2%. For coarse aggregate used in prestressed concrete beams, the absorption limit is 3% (KDOT 2007).

For bridge decks in Kansas, the predominant coarse aggregate is limestone. However, the Kansas City Metro Materials Board limits the maximum absorption to 0.5%, thus necessitating the use of imported aggregates, typically granite or quartzite (McLeod 2009). The city of Overland Park, Kansas, requires the coarse aggregate to be granite, with a maximum absorption of 0.5% and an average specific gravity of 2.62.

2.1.3 Michigan DOT (MDOT)

Coarse aggregate meeting the requirements of Class 6AA or 17A is used for bridge structures, and the maximum absorption limit is 2.5% (MDOT 2012).

2.1.4 MnDOT

Coarse aggregate for bridge superstructures should meet the requirements of Class B (crushed quarry or mine rock types including carbonates, rhyolite, and schist) and have an absorption limit of 1.75%. For concrete bridge decks and bridge barriers, the absorption limit is 1.10% (MnDOT 2018).

2.1.5 New Jersey DOT (NJDOT)

For coarse aggregate used in concrete, NJDOT specification 901.06.01 mandates the following: “use coarse aggregate that is broken stone or washed gravel [...], except do not use carbonate rock for concrete surface courses, bridge approach[es], or bridge decks.” The maximum allowable percentage absorption for fine aggregate is 2% and for coarse aggregate (#9 and larger) is 1.8%, and the maximum allowable chloride content is 0.06% (NJDOT 2007).

2.1.6 Pennsylvania DOT (PennDOT)

Different quality specifications exist for different types of coarse aggregate used in concrete (with the type of structure not specified). The aggregate types include Type A, Type B, and Type C, with Type A being the highest quality and Type C being the lowest. The maximum absorption limit is 3% for Type A coarse aggregate and 3.5% for Type B, with no absorption limit specified for Type C (PennDOT 2003).

The requirements used by various DOTs to select coarse aggregates for use in HPC or bridge deck concrete are summarized in Table 2.1.

Table 2.1. DOT requirements for coarse aggregates in HPC or bridge deck concrete

State DOT	Max. Allowable Absorption (%)	Aggregate	Structure
Indiana	5.00	-	-
Kansas	0.50	Limestone, granite, or quartzite	Bridge decks
Michigan	2.50	-	Bridge structures
Minnesota	1.75	Crushed quarry or mine rock types including carbonates, rhyolite, and schist	Bridge superstructures
	1.10		Bridge decks and bridge barriers
New Jersey	1.80	Broken stone or washed gravel	-
Pennsylvania	3.00	-	For highest quality Type A aggregates

2.2 Test Methods for Rock/Aggregate Characterization

2.2.1 Characterization of Pores in Rock/Aggregate

Pores in rocks can be classified in numerous manners. The International Union of Pure and Applied Chemists has established the following classification system for pores based on the behavior of gas sorption in porous materials: micropores (less than 2 nm in diameter), mesopores (2 to 50 nm), macropores (greater than 50 nm) (Rouquerol et al. 1994). This classification is not useful to geologists, where pores can range from the nanometer scale all the way up to cave size, since caves are, by definition, pores that a person can fit into (Choquette and Pray 1970).

A more pragmatic attempt by Zhang et al. (2016) to classify pore sizes includes the following ranges: nanopores (less than 0.1 μm), micropores (0.1 to 0.5 μm), mesopores (0.5 to 2.5 μm), macropores (2.5 to 10 μm), and megapores (greater than 10 μm). Choquette and Pray (1970) classify pores by their genetic origin. Lucia (1995) classifies pores by their effect on flow, resulting in only four major pore types: interparticle pores, micropores, separate vugs, and touching vugs.

Pore structure refers to the sizes of the pores and their geometry, distribution, connectivity, etc. Total porosity is the volume fraction of all pores in the rock, regardless of their connectivity, whereas effective porosity quantifies only the volume fraction of the pores that are interconnected to form a flow system (Rouquerol et al. 2012). The characterization of pore structures includes parameters such as porosity, pore and pore throat size distribution, tortuosity, and specific surface area. The test method chosen for analyzing pore structure can have a significant influence on the interpretation of the test results obtained (Yan et al. 2015). Techniques that are available for characterizing rock/aggregate pore structure are summarized below.

Helium Porosimetry/Pycnometry

Helium porosimetry combines measurement of grain volume with measurement of bulk volume to determine porosity. The technique is based on the gas expansion method, where helium gas is used as the saturating gas because of its small molecular size (Richards and Bouazza 2007). The testing process consists of four steps: determining the sample's weight, obtaining its grain volume via helium pycnometry, obtaining the bulk volume, and calculating porosity as well as bulk and grain density. The calculation of grain volume is based on Boyle's Law ($P_1V_1 = P_2V_2$), where a known volume of helium gas at a fixed pressure is isothermally expanded into an unknown void volume (Ridzuan 2016, Oliveira et al. 2016). Post expansion, the resultant pressure is measured and the grain volume (sometimes also referred to as the skeletal volume) is determined. Using the grain density obtained through helium pycnometry, the porosity of the sample is determined using the following equation (Ridzuan 2016):

$$\Phi (\%) = \frac{\rho_e - \rho_s}{\rho_s} \times 100$$

where, Φ is helium porosity in %, ρ_e is envelope density, and ρ_s is grain density.

Iowa Pore Index (IPI) Test

The IPI test utilizes water intrusion for determining the volume ratio of macropores to micropores present in a rock/aggregate (Myers and Dubberke 1980, Bektas et al. 2016). In this test, water is intruded progressively into 4.5 kg of oven-dried crushed aggregate at a pressure of 240 kPa. The intruded water volume is recorded at time intervals of 1 and 15 minutes. The recorded values correspond to macropore and micropore volumes, respectively, and are also respectively termed as the primary and secondary indices. This method has several advantages

over conventional petrophysical test methods that are used to determine porosity and pore size distribution in rocks. These advantages are summarized by Ridzuan (2016) as follows:

- The test requires only water and air for the analysis of samples. No chemicals or other hazardous materials such as mercury or alcohol are required. Hence, the test poses a low environmental hazard, making the test relatively inexpensive.
- The test is non-destructive. The samples tested using the IPI largely maintain their integrity in terms of their shape, weight, and volume after each test. As a result, the same samples can be retested (or further subsampled) for any further analysis, such as for petrographic thin sections.
- The test is relatively fast, with each test taking only 30 minutes.
- The test investigates a reasonably significant amount of rock (4.5 kg). This improves the comparability of the test results to the quarry scale relative to other test methods, which use smaller sized samples like core plugs (e.g., for the mercury intrusion porosimetry [MIP] test).
- The IPI test uses crushed rock instead of a whole rock core. As a result of using crushed rock, the intruding liquid used in the test penetrates the sample's pore system at a faster rate due to the higher surface area.
- This test method can be used in conjunction with techniques such as x-ray diffraction and x-ray fluorescence for effectively predicting aggregate performance in PCC.

Mercury Intrusion Porosimetry (MIP)

MIP involves intruding mercury into an evacuated sample at increasing pressures to measure the volume fraction of increasingly smaller pore throats (Ridzuan 2016). Mercury is a non-wetting fluid and thus will not penetrate the pores through capillary action. It requires external pressure to penetrate into the pores (Yao and Liu 2012). The larger pore spaces are saturated initially, and the smaller pores are progressively invaded by mercury as the external pressure increases. Due to the high pressure that can be achieved, nearly the entire connected pore system, including even the smallest pore throats, can be completely saturated (Giesche 2006). The volume of mercury intruded at each pressure step determines the non-wetting mercury saturation and hence the porosity in the sample at the pore throat size that corresponds to that pressure step (Ridzuan 2016). The method is governed by the Washburn equation for non-wetting liquid penetration (Giesche 2006, Rouquerol et al. 2011, Dong et al. 2018, Ridzuan 2016). Two assumptions that are made to convert the pressure, P , to the pore throat size, d_c , are that (1) the pores are cylindrical and (2) the pores are entirely and equally accessible to the outer surface of the specimen (Dong et al. 2018).

MIP can directly measure pore volumes per given pore sizes, pore throat size distribution (PTSD), total porosity, and the bulk and grain density of a material, from which other pore characteristics can be calculated, such as critical pore throat size (i.e., the pore diameter at which hydraulic conductance is maximum), total pore surface area, and median pore diameter (i.e., the diameter corresponding to 50% of the total area on the plot of cumulative pore area versus diameter). The method has many advantages, and it is the most commonly used method for pore structure characterization (Gane et al. 2004). The advantages of the method are as follows:

- The test is quick, usually taking about 1 to 2 hours per sample (Zhang et al. 2016).
- The test uses a high measuring pressure (up to 60,000 psi), which makes it suitable for cores with high, medium, or low permeability, and a complete capillary pressure curve can be obtained for further analysis.
- The test can analyze irregularly shaped samples.
- The test can evaluate pore throat sizes across a large size range (Li et al. 2018), from approximately 3 nm to 500 μm (Zhang et al. 2016).

The primary limitations of the technique are as follows:

- Mercury is toxic to humans and so strict laboratory procedures must be followed to work with and dispose of the mercury used in the test as well as samples contaminated during the test.
- MIP is considered a destructive test because samples are irreversibly contaminated with mercury during the analysis.
- Only the features of effective pores are reflected in the test results.
- The general model of cylindrical pores used for analysis might cause errors if the actual measured pore shape is not cylindrical. Errors can also be caused by the contact angle between the mercury and the pores' surfaces (Li et al. 2018).
- The determined pore throat size can be influenced by damage to the sample caused by crushing or pressurized mercury during MIP measurement, the amount of drying the sample undergoes before MIP measurement, or the sample size used for testing (Dong et al. 2018). It is worth noting that there are contradictory findings regarding the effect of sample size on PTSD, and a detailed discussion on the issue is still not present (Dong et al. 2018).
- Measurement errors may occur due to the "ink bottle" effect. In the interpretation of MIP measurements, one assumption is that pores in the tested material are connected either to the sample surfaces directly or through large pores. Pores not meeting this assumption are called ink bottle pores. Natural rocks may have pores of different sizes and shapes, and some large pores (referred to as the bottom of an ink bottle) are connected through small pore throats or narrow openings (referred to as the neck of an ink bottle) and thus do not meet the abovementioned assumption. Intrusion of mercury into the large pores may not occur during the MIP test unless a higher pressure is applied to force the mercury into the narrow openings. As a result, MIP measurement in some cases overestimates the smaller pore sizes (Dong et al. 2018).

In order to overcome the shortcomings of conventional (i.e., pressure-controlled) MIP due to the ink bottle effect, a constant rate-controlled MIP (CMP) method has been developed. The principle of CMP is to maintain quasi-static mercury intrusion at a very low intrusion speed, i.e., the injection rate is kept the same and the mercury capillary pressure is monitored (Yao and Liu 2012). The main pore throat size is determined by the pressure of the breaking point, and the value of the porosity is determined by the intruded mercury volume. As a result, the size and number of throats can be clearly reflected in the mercury intrusion pressure curve (Yan et al. 2015).

Gas Adsorption

For the range of pore sizes that cannot be measured by MIP, in particular pores with a diameter less than 0.01 μm , the gas adsorption method can be used (Yao and Liu 2012). The procedure uses nitrogen (N_2), carbon dioxide (CO_2), or noble gasses as an adsorbate. In this test, the gas pressure is increased gradually at a constant temperature, and then the amount of the gas that the sample adsorbs is measured. The partial pressure can also be gradually reduced to measure the corresponding desorption amount. The pore volume is determined by the amount of adsorbate at the boiling temperature. Under low temperatures and pressures (i.e., less than -196° and 0.127 MPa), N_2 isothermal adsorption can reflect pore size distribution in the range of approximately 2 to 50 nm, and CO_2 isothermal adsorption can reflect pore size distributions in the range of approximately 0.35 to 2 nm. The gas adsorption method is an effective means for characterizing pores with sizes smaller than 50 nm, but the application of the test is restricted by the narrow testing range (Yan et al. 2015).

X-ray CT / Micro-CT Scan

X-ray computed tomography (CT) / micro-CT scanning is one of the most useful and powerful tools among the non-destructive imaging techniques. When used on rocks, it can provide information about the relative abundance of components, component size, shape and distribution, pore connectivity, particle surface structure, and other characteristics. It is the only semi-quantitative method that is capable of imaging both open and closed pores inside rock samples non-destructively. It allows for an excellent three-dimensional visualization of porous structures (Gane et al. 2004) with a spatial resolution of several microns (Yao and Liu 2012).

However, due to its resolution, CT scanning can only identify porosity above the micron scale. Concrete has a large range of pore sizes, and the volume of pores with a diameter greater than a micron is only a portion of the total pore volume. Based on the above understanding, pore data obtained through CT scanning should be considered with care (Yan et al. 2015).

The limitations of CT scanning are as follows (Yan et al. 2015):

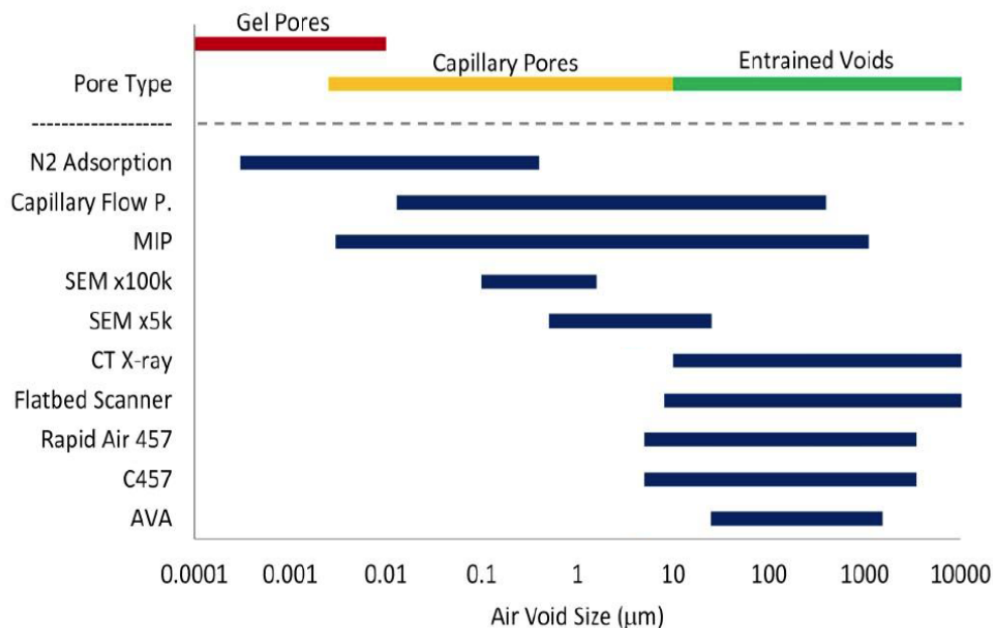
- The cost associated with CT analysis is very high (about 20 times as high as MIP).
- The detection range is limited by the method's poor resolution. At present, the best resolution that CT instruments can obtain is in the micron range, and the maximum horizon is about 1,000 to 2,000 times larger than the resolution, which implies that only pores within approximately two to three orders of magnitude can be detected.
- Artificial image processing is needed after CT imaging, and the artificial threshold affects the results to some extent because it is difficult to identify the boundaries between pores and other entities.
- High-resolution analysis requires smaller samples, and the process of machining can easily produce secondary cracks that might cause deviations in the test results.

Scanning Electron Microscopy (SEM)

SEM analysis can evaluate and visualize the pore network in rocks, as well as the degree of connectivity among the pores (Gane et al. 2004, Rushing et al. 2008). The method can qualitatively characterize pore images, but quantitative data on pore size distribution requires laborious measurement of individual particles. In addition, SEM requires processed rock samples, and to some extent the processing might destroy the internal structure and external morphology of the pores in the rock samples and cause a distortion in the observations. Moreover, the greater the magnification, the smaller the field of view; as a result, it is easy to overgeneralize the observations and miss important information. Because nanoscale pores are difficult to observe clearly through SEM, field emission SEM (FESEM) can be used to observe the samples after argon ion polishing (Li et al. 2018).

Notes on the Use of Different Test Methods

To visualize the applicable ranges and limits of different test methods for characterizing pores in concrete materials, the chart shown in Figure. 2.1 was developed by Kejin Wang and Gilson Lomboy.



Wang and Lomboy, National Concrete Pavement Technology Center 2016

Figure 2.1. Air void size measurement capabilities of various testing methods

The figure illustrates that no single test method can capture the entire size range of pores or pore throats in concrete materials. As a result, multiple methods have been used to characterize the pore structure of concrete materials in order to capture the entire spectrum of pores. It should be noted that different test methods differ and sometimes overlap in terms of the sizes of pores

identified, and proper analyses of the test results is essential when making comparisons across orders of magnitude in size.

2.2.2 Petrographic Analysis

In petrographic analysis, a thin-section sample is often prepared. Because different minerals in the sample have different optical properties, they alter the color and intensity of light. Therefore, most rock-forming minerals can easily be identified. Thin sections are typically constructed of ultra-thin slices (30 μm thick) of rock in which the pore volume is impregnated under vacuum conditions with a low-viscosity blue or red fluorescent epoxy resin. Most rock minerals transmit light at a thickness of 30 μm . Therefore, it is possible to evaluate the pore structure, grain framework and texture, and matrix material from transmitted polarized light microscopy (Scholle and Ulmer-Scholle 2003, Ulmer-Scholle et al. 2015). It should be noted that since pores larger than 5 μm can also be seen in MIP, there is an overlap between the MIP and thin-section methods (Ridzuan 2016). Thin-section analysis allows for void space size to be determined at a much greater range of identification than the IPI test. However, thin-section analyses provide a two-dimensional view of a three-dimensional system, and therefore it is not possible to view all of the complexities in the pore structure (Scholle and Ulmer-Scholle 2003). Future research combining mercury porosimetry with thin-section analysis would help to obtain the most accurate pore size distribution data (Gustafson et al. 2015).

2.3 Test Methods for Chloride Penetration of Concrete

2.3.1 Surface Resistivity

Electrical resistivity can be an indicator of fluid transport in concrete. The Wenner four-probe surface resistivity technique is a resistivity measurement technique that can be used both in the laboratory and for on-site assessment. It is a non-destructive, quick, and simple test that assesses the resistance of concrete to corrosion (Andrade 1993, Andrade and Alonso 1996). In this method, four equally spaced point electrodes are pressed onto the concrete surface. The two outer electrodes induce a current flow, whereas the two inner electrodes measure the potential drop. The resistivity of the concrete, ρ , is calculated from the resistance, which is the ratio of the potential difference to the current. Resistivity, ρ , is dependent on the quantity and conductivity of the pore solution and the size, interconnectivity, and tortuosity of the pores (Andrade et al. 2007). According to Andrade et al. (2013), the major factors affecting the resistivity of concrete are age, water saturation, and temperature. In terms of resistivity, many classification criteria for concrete quality have been proposed by different researchers. Some researchers have tried to link resistivity and corrosion risk (Andrade et al. 2004, Andrade and Alonso 1996), and they have found that a certain inverse relationship between both variables appears to exist.

2.3.2 Nord NT Build492

The Nord test (also called the rapid migration test) is an accelerated test that is an alternative to ASTM C1202. This test is based on the procedure initially developed by Luping and Nilsson

(1992). The American Association of State Highway and Transportation Officials (AASHTO) version of this test (TP 164-03, Predicting Chloride Penetration of Hydraulic Cement Concrete) is based on further development by Stanish et al. (1997). The result of the Nord test, known as the diffusion non-steady state migration (DNSSM) coefficient, is an indicator of chloride permeability. The main advantage of this test over ASTM C1202 is that the test results are not affected by the conductivity of the pore fluid. Therefore, the test is applicable to concrete with calcium nitrite corrosion inhibitor.

2.3.3 Water Sorptivity

Sorptivity is an index of moisture transport into an unsaturated porous material, and it is determined from a simple test that measures the unidirectional water uptake capability of unsaturated concrete through capillary action (Hall and Tse 1986). Since the moisture content (or degree of saturation) of the tested sample and its uniformity have a considerable effect on the rate of water absorption, it is very important to condition test samples (Wei et al. 2017). In addition, the temperature of the tested samples is also very important because fluid properties (e.g., viscosity) vary with temperature. In order to prevent decomposition of hydration products (e.g., ettringite) and reduce microcracking due to heating and drying, ASTM C1585 requires that samples be conditioned by drying for 3 days at 50°C followed by 15 days in a sealed container at 85% relative humidity (RH).

During a sorptivity test, the driving force for water ingress into a tested sample is capillary suction within the pore spaces of the sample. Therefore, sorptivity helps the tester understand the pore characteristics of porous materials such as concrete, rocks, and bricks (Hall and Tse 1986). In a recent study, Zhutovsky and Hooton (2019) found that compared with ASTM C1585, DIN 52617, which requires more rigorous drying at 60°C until a constant mass is obtained, provided a better correlation between concrete sorptivity and pore structure parameters.

The sorptivity test involves recording incremental mass change measurements at relatively frequent intervals during the first six hours after the sample comes in contact with water and subsequently taking one measurement every day for the next eight days. The amount of absorbed water is normalized by the cross-section area of the specimen exposed to the fluid:

$$i = \frac{M_t}{a \times \rho}$$

where i is the normalized absorbed fluid volume, M_t is the change in specimen mass at time t , a is the area of the specimen exposed to the fluid (i.e., that of the bottom face), and ρ is the density of the absorbed fluid (taken to be 1,000 kg/m³ at 23°C for water).

These absorbed fluid volumes are then plotted as a function of the square root of time. The initial sorptivity is determined as the slope of the curve during the first six hours, while secondary sorptivity is determined using the slope of the same measurements between one and eight days, according to ASTM C1585.

Sorptivity is positively correlated to porosity by the following equation:

$$\frac{Mass_{Sample+Water} \times Sorptivity}{\rho_{water} \times Volume_{Sample}} = Porosity_{Sample}$$

2.3.4 Salt Ponding

This is a long-term test for measuring the penetration of chloride into concrete. A 3% NaCl solution is ponded over the test specimens (i.e., test slabs) for a period of 90 days (as per AASHTO T 259). Since the bottoms of the test specimens are exposed to a 50% RH atmosphere during ponding, there is water vapor transmission from the wetted side of the concrete to the drier surrounding atmosphere at the external surface for the duration of the ponding. This causes more water to penetrate into the concrete, bringing chloride ions with it (Qiao et al. 2018, Stanish et al. 1997). At the end of the ponding, the penetration of chloride in terms of chloride content is determined at various depths to obtain the chloride profile over depth in the specimen. The 90-day ponding duration might still be too short to develop a sufficient chloride profile when higher quality concrete (e.g., HPC) is considered for evaluation.

3 EXPERIMENTAL MATERIALS AND METHODS

3.1 Materials and Mix Proportions

3.1.1 Aggregates

Coarse aggregates with varying absorption values obtained from five different sources were selected and collected with the help of the technical advisory committee (TAC) members at the Iowa DOT. The details of the sources, lithologies, and ranges of absorptions of the coarse aggregates are provided in Table 3.1, where LS denotes a limestone rock and DM denotes a dolostone rock, which is composed primarily of the mineral dolomite.

Table 3.1. Coarse aggregate sources, lithologies and range of absorptions

Aggregate/ Rock ID	Source	Lithology	Absorption Range (%)
LS1	Ames (Lime Creek Fm)	Limestone	< 1
LS2	Alden (Gilmore City Fm)	Limestone	3
LS3	Durham (Bed 101, North Hill Grp)	Limestone	3–4
DM1	Douds (Spergen Fm)	Dolostone	5–6
DM2	Bowser	Dolostone	5–9

The fine aggregate used for the mixes was river sand obtained from Hallett Materials in Ames, Iowa. The gradation of fine and coarse aggregate used, along with the specified upper and lower limits, is shown in Figure 3.1.

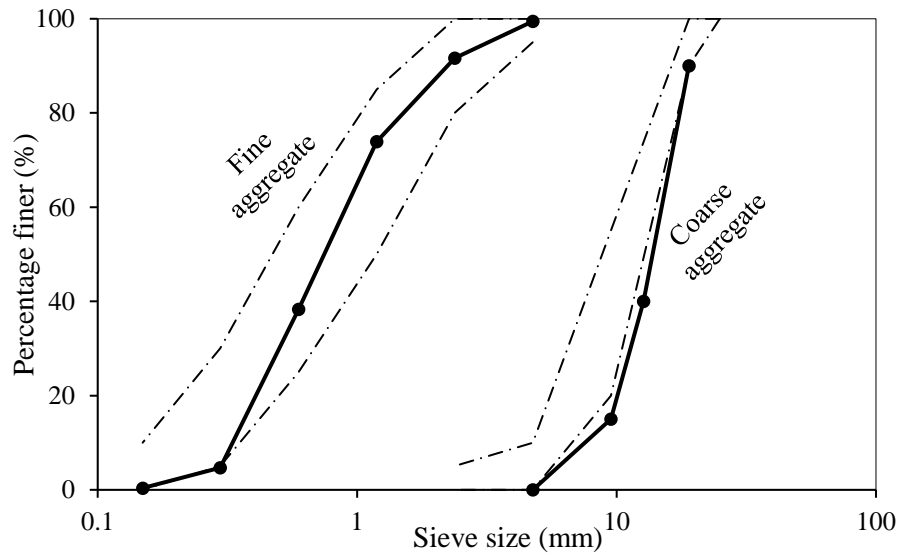


Figure 3.1. Aggregate gradation

3.1.2 Cementitious Materials

Type IS 20 cement (80% by weight of binder) and class C fly ash (20% by weight of binder) were used as cementitious materials. The chemical composition of the cement and fly ash as provided by X-ray fluorescence is given in Table 3.2.

Table 3.2. Chemical composition of the cementitious materials

Chemical Composition	IS20 Cement	C-Fly ash
C ₃ A	11.91	-
SiO ₂ (wt %)	23.51	36.22
Al ₂ O ₃ (wt %)	6.02	18.50
Fe ₂ O ₃ (wt %)	2.39	6.01
CaO (wt %)	56.17	26.44
MgO (wt %)	4.05	5.27
SO ₃ (wt %)	3.18	1.13
Na ₂ O (wt %)	0.15	1.69
K ₂ O (wt %)	0.65	0.52
Na ₂ O. Equiv. (wt %)	0.58	2.03
LOI (wt %)	3.00	0.77

3.1.3 Chemical Admixtures

An air entraining agent (AEA), Euclid AEA 92, and a mid-range water reducer (MRWR), Euclid WR91, were used to achieve the target air content of 6.5% (by concrete volume) and the required workability in terms of a slump value of 4 inches (as per the Iowa DOT specifications for concrete bridge decks).

3.1.4 Mix Proportions and Test Samples

A total of six mixes, five HPC mixes and one high-performance mortar mix, were cast for the study with constant volume proportions of materials. The mix proportions and details of the test specimens (prepared per mix) for all mixes are given in Table 3.3 and Table 3.4, respectively.

Table 3.3. Mix proportions for all mixes

Mix ID	Mix	Cement (lbs/cy)	Fly ash (lbs/cy)	Water (lbs/cy)	Coarse Aggregate (lbs/cy)	Fine Aggregate (lbs/cy)
C-LS1	Ames	501	125	251	1,507	1,479
C-LS2	Alden	501	125	251	1,434	1,479
C-LS3	Durham	501	125	251	1,405	1,479
C-DM1	Douds	501	125	251	1,417	1,479
C-DM2	Bowser	501	125	251	1,338	1,479
Mortar*	-	501	125	251	1,507	1,479

*Mortar was sieved using the #4 sieve from the concrete mix prepared using Ames coarse aggregate at the Portland Cement Concrete Laboratory (PCC lab) at Iowa State University (ISU).

Table 3.4. Test methods and number of samples

Test Name	Specimen Dimensions	No. of Specimens per Mix	Test Age (days)
Salt Ponding (AASHTO T 259)	14" x 10.5" x 3.5" Slab	2	28 days (total duration = 132 days)
Nord Test (NT Build 492)	4" x 8" Cylinder	3	28 days
Surface Resistivity (AASHTO T 358) / Compressive Strength	4" x 8" Cylinder	6	SR – 1 to 120 days Strength – 28 days
Water Sorptivity (ASTM C1585)	4" x 8" Cylinder	2	28 days

3.1.5 Preparation and Mixing

Different sized coarse aggregates were soaked in water separately overnight and then brought to their saturated surface dry (SSD) condition. The SSD-conditioned coarse aggregates were then combined to achieve the gradation specified by the Iowa DOT, as indicated in Figure 3.1 and then used in preparing mixes according to the mix proportions specified in Table 3.3. Fine aggregate was also soaked overnight in water in a similar way and then brought to SSD condition before being used for mixing. Thus, all aggregates were used in their SSD condition for mixing.

3.1.6 Concrete Mixing

All five concrete mixes were prepared in a rotating drum mixer with a capacity of 3 cubic feet. Mixing was done according to ASTM C192. For the mortar mix, concrete was mixed initially using Ames coarse aggregate from the PCC lab at ISU, and then the mortar was sieved from the prepared concrete mix using a #4 sieve, as shown in Figure 3.2.



Figure 3.2. Sieving concrete using the #4 sieve (left) to obtain the mortar (right)

3.2 Tests and Methods

3.2.1 Tests on Aggregate

Specific Gravity and Water Absorption

The specific gravity and water absorption values of the aggregates were determined using three different methods:

1. For the coarse aggregates, specific gravity and water absorption were determined according to ASTM C127, Standard Test Method for Relative Density (Specific Gravity) and Absorption of Coarse Aggregate, and AASHTO T 354, Standard Method of Test for Specific Gravity and Absorption of Aggregate by Volumetric Immersion Method. The Phunque flask used for AASHTO T 354 is shown in Figure 3.3.
2. For the fine aggregates, specific gravity and water absorption were determined according to ASTM C128, Standard Test Method for Relative Density (Specific Gravity) and Absorption of Fine Aggregate.



© Humboldt Manufacturing Company

Figure 3.3. Phunque flasks

Aggregate Correction Factor

Because the coarse aggregates had varying porosities, an aggregate correction factor test was performed on all of the aggregates to correct and control the concrete air content. The test was performed in accordance with AASHTO T 152 using a Type B Washington-type air meter. Calibration of the air meter was checked according to the standard before testing (Figure 3.4).



(a) Air meter reading zero with full water during calibration



(b) Water removed (429.5 g) during calibration



(c) Air meter reading 6.5% after removing 429.5 g water during calibration

Figure 3.4. Calibration check of air meter

The correction factor test on the coarse aggregate was performed by removing a measured quantity of water (429.5 g), the equivalent of 6.5% air (targeted air) in concrete, from the aggregate. The inside calibration tube was cut short (Figure 3.5) to prevent drawing sand into the water during water removal. The water used for the test was left to stand in a bucket for two days before the test to make sure that the water being used did not contain air bubbles that would affect the test measurements.



(a) Shortened calibration tube



(b) Shortened calibration tube attached to the air meter

Figure 3.5. Calibration tube shortened for aggregate correction factor test

3.2.2 Tests on Rock Cores

Petrophysical and Petrographic Analysis

Sample Preparation. Blockstones were collected from each source that were approximately cubic with 50 cm sides. From these blockstones, four-inch-diameter cores were drilled using a water-cooled, trailer-mounted concrete coring rig provided by the Iowa DOT. From each blockstone, a vertical and a horizontal core were collected. Permeability is usually at its maximum parallel to bedding (horizontal, K_h) and at its minimum perpendicular to bedding (vertical, K_v). From each four-inch-diameter core, one-inch-diameter cores were drilled using a water-cooled drill coring bit on a standard shop drill press and a water-cooled coring bit. The one-inch-diameter cores were then cut to one inch long using a water-cooled tile saw and stored in a desiccator. When each core plug had dried for several days, digital calipers (Mitutoyo, precision ± 0.01 mm) were used to measure the diameter and height six times. The average of each property was used to compute the bulk volume of each core plug geometrically. Each core plug was then weighed on an analytical balance (Mettler Toledo Me204e, precision ± 0.1 mg).

Thin-Section Petrography. The trimmed ends resulting from cutting the one-inch-diameter core plugs to one inch long were used to prepare petrographic thin sections. The thin sections were approximately 30 μm thick and prepared with blue-dyed epoxy to better highlight the pores. Thin-section samples were prepared by TPS Enterprises (Houston, Texas) and analyzed and imaged with an Olympus BX53 petrographic microscope.

SEM Petrography. The core plug samples were analyzed via scanning electron microscope (JEOL ITS-100) at 20 kV, at a 12 mm working distance, at a 60 nA probe current, and under high vacuum. Integrated JEOL electron dispersive spectroscopy (EDS, 30 mm² detector) was employed to qualitatively identify the elemental compositions of the materials.

Porosity and Pore Structure

Helium Pycnometry. A helium pycnometer (Micrometrics AccuPyc II 1460) was used to measure the grain volume of each core plug (i.e., the volume of the solid material). The method uses Boyle's Law:

$$P_1V_1 = P_2V_2$$

where P_1 is the pressure at t_1 , V_1 is the known volume of the device, P_2 is the pressure at t_2 , and V_2 is the known volume less the sample volume. This measurement samples all pore spaces that are (1) larger than a helium atom (approximately 0.1 nm) and (2) connected to the outer surface of the sample. Any fully isolated pores (i.e., "blind" pores) are not sampled and are counted as part of the volume of the solid phase. Petrographic methods like thin-section petrography, SEM, or CT scanning can identify these voids. From the grain volume, grain density (in g/cm³) and porosity (pore volume per bulk volume expressed as a percentage) were computed. Helium

pycnometry was performed at the Petrographic Industrial Research Laboratory operated by the Geology Program at ISU. The background pressure of the helium was 19.5 psi.

MIP. A mercury intrusion porosimeter (Quantachrome Poremaster 33) was used to measure the PTSD of the one-inch by one-inch core plugs obtained from the four-inch by eight-inch cores using the Washburn equation:

$$P_c = \frac{2\gamma\cos\theta}{r}$$

where P_c is the capillary pressure, γ is the interfacial tension, θ is the contact angle, and r is the pore throat radius. PSD is often mistaken for a measurement of pore size distribution, but the measurement is actually of the connections between the pore bodies. Measuring PSD would be analogous to measuring the sizes of doors that connect rooms, where the volume of the room is assigned to the width of the door. The analysis was performed at the Petrographic Industrial Research Laboratory operated by the Geology Program at ISU. Intrusion was performed over a range from 2 to 33 kpsi (approximately 210 MPa). The intrusion and extrusion mercury contact angles were 140°. The mercury's temperature was approximately 22°C.

Surface Resistivity

Surface resistivity measurements were made on the four-inch by eight-inch rock cores obtained from the blockstones (Figure 3.6). The cores were immersed in a lime bath for 48 hours before the measurements were taken. For each aggregate source except for the Ames and Bowser sources, the measurements were taken on both the horizontal (marked with "H") and vertical (marked with "V") rock cores. The blockstones from the Ames and Bowser sources had only one core.



Figure 3.6. Rock cores for resistivity measurement

Water Sorptivity

The water sorptivity test was conducted on four-inch by two-inch rock slices obtained from the four-inch by eight-inch cylindrical cores obtained from the field in accordance with ASTM C1585. The cores were first saturated in accordance with the vacuum saturation procedure specified in ASTM C1202 (Figure 3.7) to ensure uniform moisture conditions across all cores.

While doing so, the step for coating the side surfaces of the specimens was omitted, as recommended in ASTM C1585.

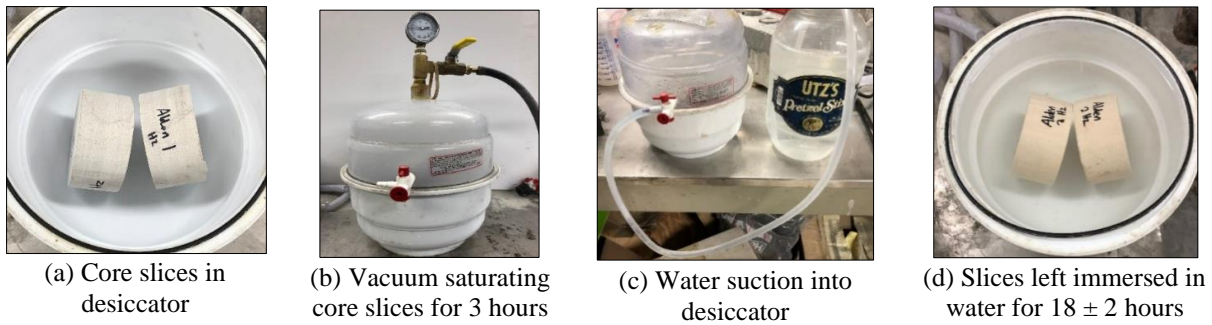


Figure 3.7. Vacuum saturation of rock cores

3.2.3 Tests on Fresh Concrete

Fresh concrete properties were measured according to ASTM C143 (for slump), AASHTO T 152 (for air content), and ASTM C138 (for unit weight).

3.2.4 Tests on Hardened Concrete

Compressive Strength

Compressive strength was tested on standard four-inch by eight-inch cylindrical concrete specimens at the age of 28 days according to ASTM C39. Three cylinders from each mix were used to determine the average strength of each mix.

MIP

Analysis of pore throat size distribution was performed on one-inch by one-inch core plugs (Figure 3.8) obtained from the four-inch by eight-inch concrete cylinders used for compressive strength testing. The MIP test was similar to that used to measure the porosity of the rock plug samples.



Figure 3.8. Concrete plugs used for MIP analysis

Surface Resistivity

Surface resistivity values were measured on standard four-inch by eight-inch cylinder specimens according to AASHTO T 358. Three cylinders were examined at the ages of 1, 3, 7, 14, 28, 56, 90, and 120 days to determine the average SR of a particular mix at each respective age. The SR measurements were made using a commercially available resipod (Wenner four-probe resistivity meter) with a probe spacing of 38 mm. See Figure 3.9.



© Proceq

Figure 3.9. Resipod used for SR measurement

Salt Ponding Test

For each mix, two slabs of dimensions 14 inches by 10.5 inches by 3.5 inches were prepared in accordance with the minimum dimension requirements of AASHTO T 259. The slabs were cast in plastic pan molds, as shown in Figure 3.10.



Figure 3.10. Slab preparation and ponding

The base of each pan was cut out and temporarily taped back in place before pouring the concrete/mortar, as shown in the figure. Once the slabs were cast, they were left undisturbed until the bleed water (if any) evaporated from the surface. Then the surface of the slabs was finished using a soft paint brush to provide an even texture. A mortar wall (to hold the NaCl solution in place) of approximately 1 inch in height was made around the perimeter of the slab surface when the concrete surface was still fresh to ensure a proper bond between the concrete surface and the mortar wall to prevent leaking of salt solution.

The cast specimens in the pans were cured in a moist room at $95 \pm 3\%$ RH and $23 \pm 2^\circ\text{C}$ for 14 days. The slabs were then shifted to a room with a RH of 50%. Here the cut portions of the plastic pans that were temporarily taped to the bases of pans were removed to expose the base of the cast samples to the 50% RH of the room. In this conditioning environment, the slabs were left to dry for 28 days (until a total sample age of 42 days). After 28 days of conditioning in this environment, the inner sides of the mortar walls were coated with paraffin wax prior to salt

solution ponding. This was to prevent the salt solution from leaking. Then a 3% NaCl solution was poured on the top surface of the slabs to an approximate depth of 13 mm (0.5 inch). The slab surfaces were then covered with polythene sheets to prevent evaporation of the salt solution. The depth of the salt solution was maintained at 13 mm by pouring fresh 3% NaCl solution as and when required for a period of 90 days (until total sample age of 132 days). After 90 days of ponding, the salt solution was removed from the slabs and the surfaces were allowed to dry. The surfaces were later wire-brushed until all salt crystal buildup was completely removed.

Chloride content was determined using powdered samples extracted from the coring slab samples at two different depths (1/16 to 1/2 inch and 1/2 to 1 inch). The test for chloride content was done according to AASHTO T 260 using the titration method (Figure 3.11). The test was performed at the Iowa DOT Construction and Materials Bureau's chemical laboratory.

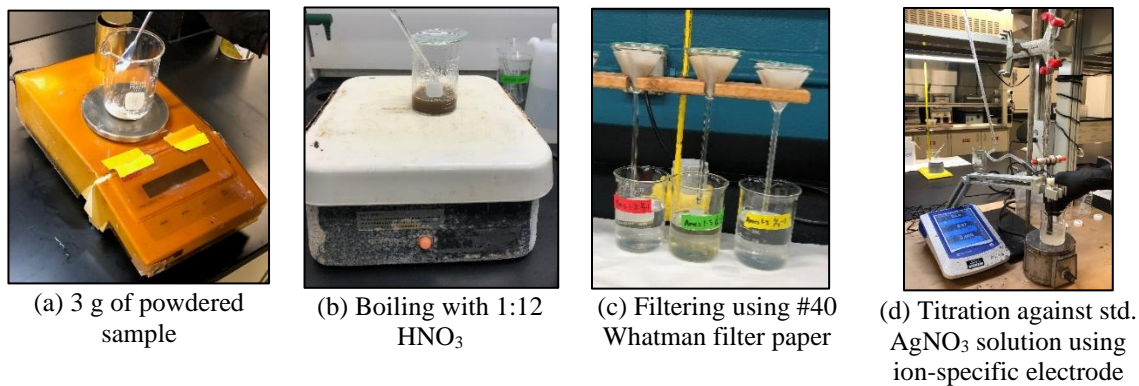


Figure 3.11. AASHTO T 260 procedure for chloride content determination

The titration endpoint was when a value of about 225 mv was obtained on the meter (display). The chloride content was determined using the following equation:

$$\% \text{ Chloride} = \frac{35.453 N V}{10 W}$$

where N is the normality of a standard silver nitrate solution, V is the volume of titrant obtained at the given endpoint (ml), W is the original weight of the sample (g), 35.453 is the atomic weight of Cl⁻, and 10 is a factor.

Rapid Migration Test (Nord Test)

One four-inch by two-inch test slice was cut off from each four-inch by eight-inch cylinder specimen belonging to same mix. The test slice was cut off from the four-inch by eight-inch cylinder after the top two inches of the cylinder were discarded (Figure 3.12).

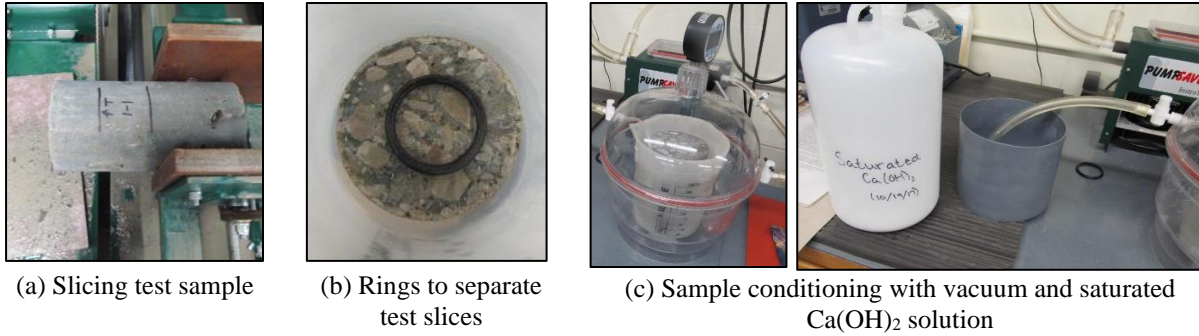


Figure 3.12. Nord test sample preparation and conditioning

The Nord test was performed according to Nord NT BUILD 492 at the sample age of 29 days. The test slices were wiped to remove excess water from their surfaces. Surface-dry samples were then placed in a vacuum container (desiccator). Rubber rings were used to separate the slices from each other and to prevent the slices from touching the bottom of the container. The slices inside the desiccator were vacuum saturated (similar to vacuum saturation in ASTM C1202) using $\text{Ca}(\text{OH})_2$ solution, with the pressure inside the desiccator reduced to below 700 mm mercury. The conditioned slices were then used for chloride penetration depth determination using a ProoveIT cell assembly and the ProovePC computer program to adjust the voltage (set to 30 V) and test time (usually 24 hours). The initial temperature and current were noted before beginning the test. Once the test was complete, the samples were removed from the cells and then rinsed, sawed, and sprayed with 0.1 M silver nitrate to determine the chloride depth (Figure 3.13). Nine depth readings with a spacing of 10 mm were taken on the tested split samples.

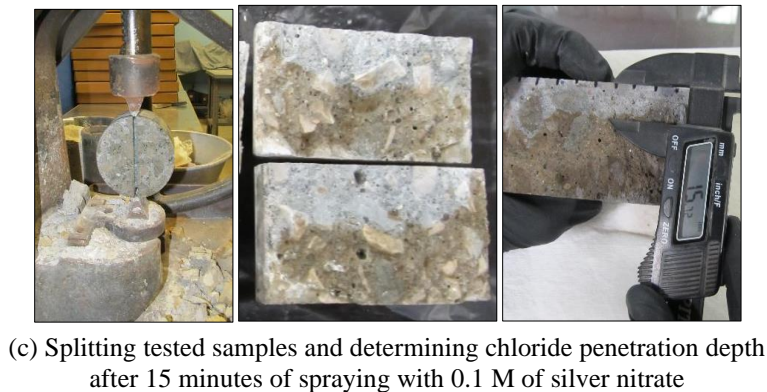
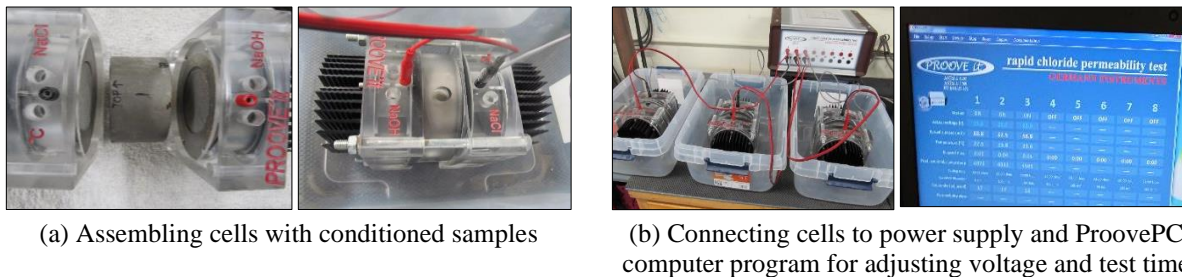


Figure 3.13. Nord test procedure for determining chloride penetration depth

Rate of Water Absorption

A rate of water absorption (water sorptivity) test was conducted at a sample age of 28 days on four-inch by two-inch slices cut from standard four-inch by eight-inch cylindrical specimens according to ASTM C1585. Two cylinders (a total of six slices, three from each cylinder) were used to perform the test. The sample conditioning was done in two stages. First, slices were cut from the cylinders and then conditioned at $50 \pm 2^\circ\text{C}$ and an RH of $80 \pm 3\%$ for 3 days. The required RH conditioning was maintained using a saturated solution of potassium bromide (KBr). For this, the cut slices were placed in air-tight containers with the saturated KBr solution poured into the bottom of the containers. The slices were placed over plastic grids (Figure 3.14) to make sure that there was no contact between the solution and the test samples.

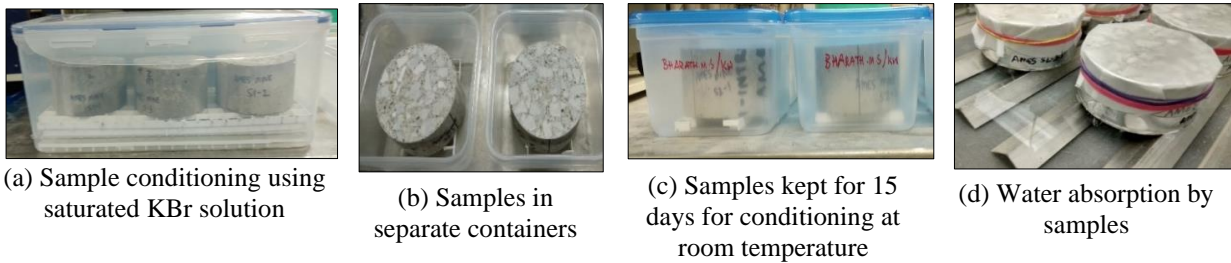


Figure 3.14. ASTM C1585 water sorptivity test procedure

The containers were then placed in oven at $50 \pm 2^\circ\text{C}$ for 3 days. After 3 days, the slices were removed from the containers and placed in different air-tight boxes over the supports to make sure that they did not touch the inner sides of the boxes. These air-tight boxes were placed at room temperature for a period of 15 days. After 15 days, the slices were sealed by first coating their sides using epoxy paint and then placing aluminum tape over it. The top surfaces of the samples (opposite to the side exposed to water) were covered using a plastic sheet loosely held in place with elastic bands. The water absorption test was then conducted with the samples supported over L-shaped aluminum bars such that the water was 3 mm above the bottom of the samples.

4 RESULTS AND DISCUSSION

Table 4.1 summarizes the tests performed for the various materials studied in the present project. The discussions of the test results are given in the following sections.

Table 4.1. Tests performed in the present study

Aggregate	Rock Cores	Concrete/Mortar
1. Specific gravity	1. Helium porosimetry	1. Air content
2. Water absorption	2. MIP	2. Unit weight
3. Correction factor for aggregate air void	3. Thin-section petrography	3. Compressive strength
	4. CT petrography	4. Surface resistivity
	5. Surface resistivity	5. Nord NT Build 492
	6. Water sorptivity	6. Water sorptivity
		7. Salt ponding

4.1 Aggregate Properties

4.1.1 Absorption, Specific Gravity, and Correction Factor

The water absorption, specific gravity, and correction factor test results for all coarse aggregates are given in Table 4.2.

Table 4.2. Coarse aggregate properties

Aggregate ID	Coarse Aggregate Source	Specific Gravity	ASTM C127 Absorption (%)	AASHTO T 354 Phunque Absorption (%)	Correction Factor (%)
LS1	Ames	2.67	0.7	0.47	0.29
LS2	Alden	2.54	2.9	1.39	0.39
LS3	Durham	2.49	3.5	2.18	0.50
DM1	Douds	2.51	4.1	2.88	0.70
DM2	Bowser	2.37	6.8	4.48	1.90

The variation of coarse aggregate correction factor with coarse aggregate absorption is shown in Figure 4.1, and the relationship between Phunque absorption and ASTM C127 absorption is shown in Figure 4.2.

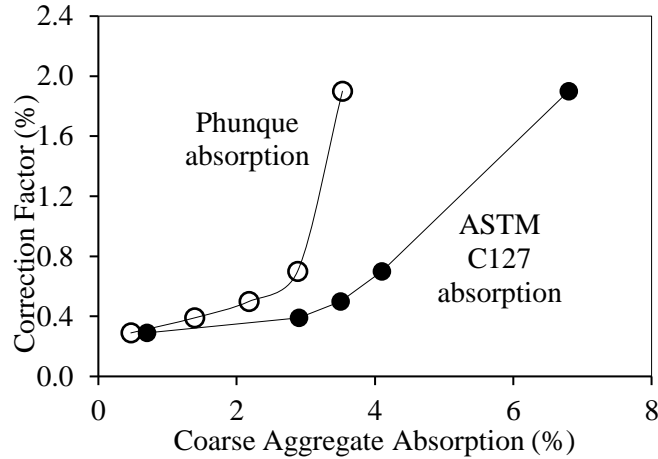


Figure 4.1. Coarse aggregate correction factor versus absorption

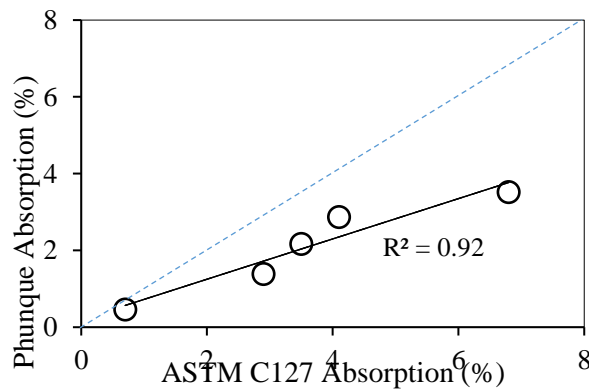


Figure 4.2. Phunque absorption versus ASTM C127 absorption

As Figure 4.1 shows, the coarse aggregate correction factor values increased exponentially with an increase in the coarse aggregate water absorption values. A very good correlation is observed between the correction factor and water absorption values determined by both the ASTM C127 and Phunque test methods. The coarse aggregate absorption values obtained from the Phunque test were relatively lower than those obtained from the ASTM C127 method. Nonetheless, a very good linear relationship exists between the absorption values obtained by both methods, as indicated in Figure 4.2.

4.2 Properties of Rock Cores

4.2.1 Thin-Section Imaging

Thin-section images of all rock samples indicating different porosities are shown in Figure 4.3.

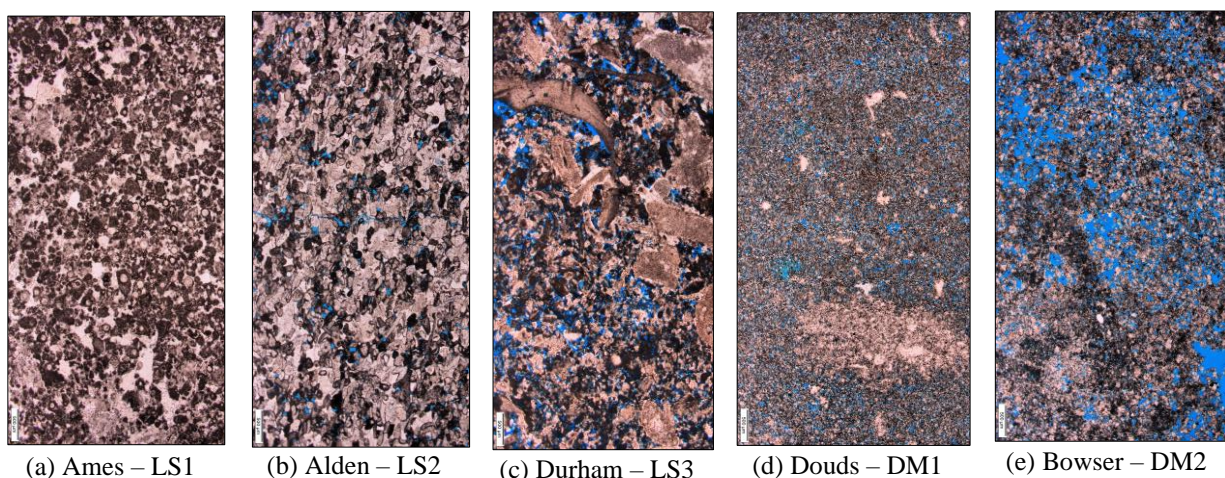


Figure 4.3. Thin-section images of all rock samples (500 μm scale)

In these images, the porosity of each rock is shown in blue due to the blue-dyed epoxy used during sample preparation to better highlight the pores. The reference bar (scale) shown at the bottom left of each picture represents 500 μm . In Image (a), very few permeable pores, indicated by a blue color, are seen in the aggregate from Ames. This rock is a fine-grained peloid skeletal lime grainstone that is well cemented. In Image (b), small inter-grain pores (mostly 10 to 50 μm) are visible in the aggregate from Alden, and a small percentage of these pores are visibly connected. This rock is similar in composition to the Ames aggregate, a fine-grained skeletal lime grainstone that is well cemented. In Image (c), many more large pores (mostly 100 μm and some up to 500 μm) between or along the edges of the grains of the aggregate from Durham are observed. The rock texture is much coarser than that of the rocks in samples LS1 and LS2. It is classified as a coarse-grained skeletal lime grainstone. In Image (d), a large amount of very fine pores (about 10 μm) are visible and are uniformly distributed in the aggregate from Douds, and very few pores are larger than 100 μm . This is a fine-grained dolostone. In Image (e), many large pores (mostly larger than 100 μm) are visible in the aggregate from Bowser. Many of them are clustered and interconnected. This is a coarse-grained dolostone. These observations are consistent with the absorption values observed for the aggregates.

4.2.2 Helium Porosimetry

Figure 4.4 shows the relationship between the helium porosity values obtained from the one-inch by one-inch rock plugs and the four-inch by eight-inch rock cores.

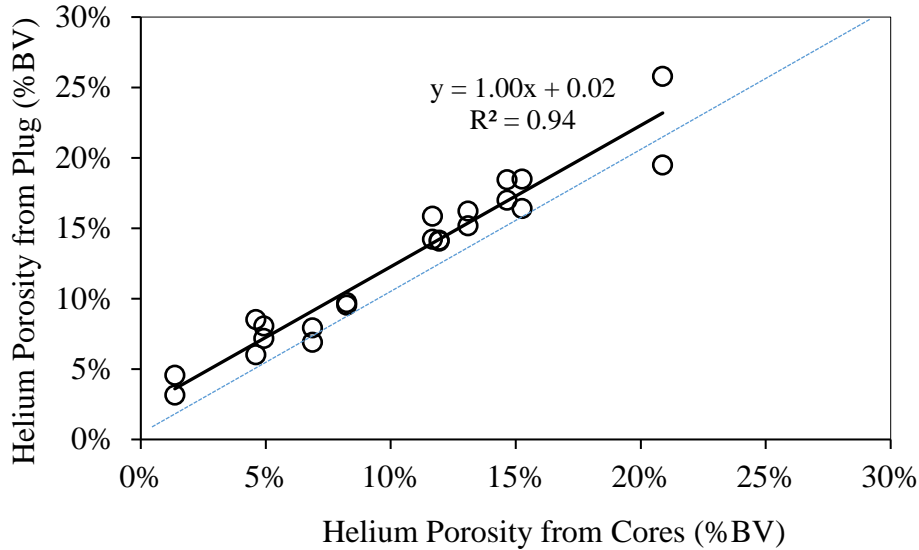


Figure 4.4. Helium porosity from rock plugs versus helium porosity from rock cores

A very good linear correlation is seen to exist between the porosity values obtained using the two methods. The helium porosity values of the small samples are all slightly higher than those of the large samples, except for the sample with the highest porosity.

Good linear correlations also exist between the absorption values of the coarse aggregates and the helium porosity values of the corresponding rock cores (Figure 4.5).

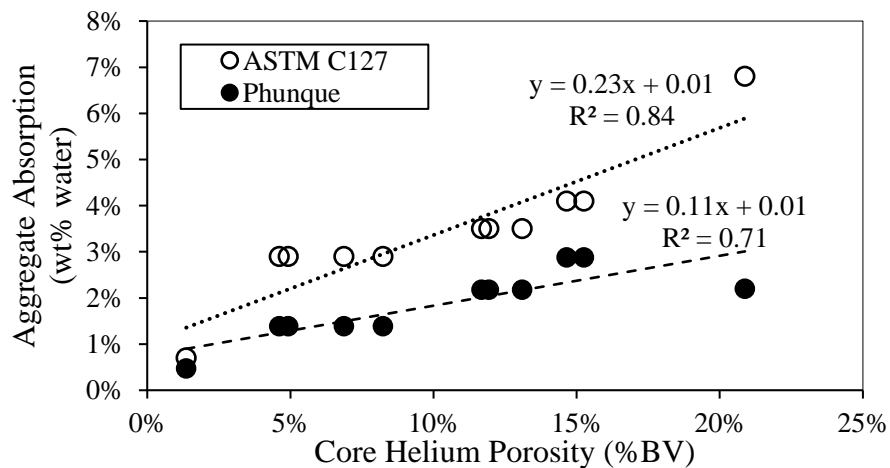


Figure 4.5. Aggregate absorption versus rock core helium porosity

The correlation between the helium porosity of the rock cores and the absorption of the coarse aggregate obtained using ASTM C127 is better than that between the helium porosity values of the rock cores and the absorption values obtained from the Phunque test. For both aggregate absorption test methods, the helium porosity of a rock core is positively correlated with aggregate absorption values.

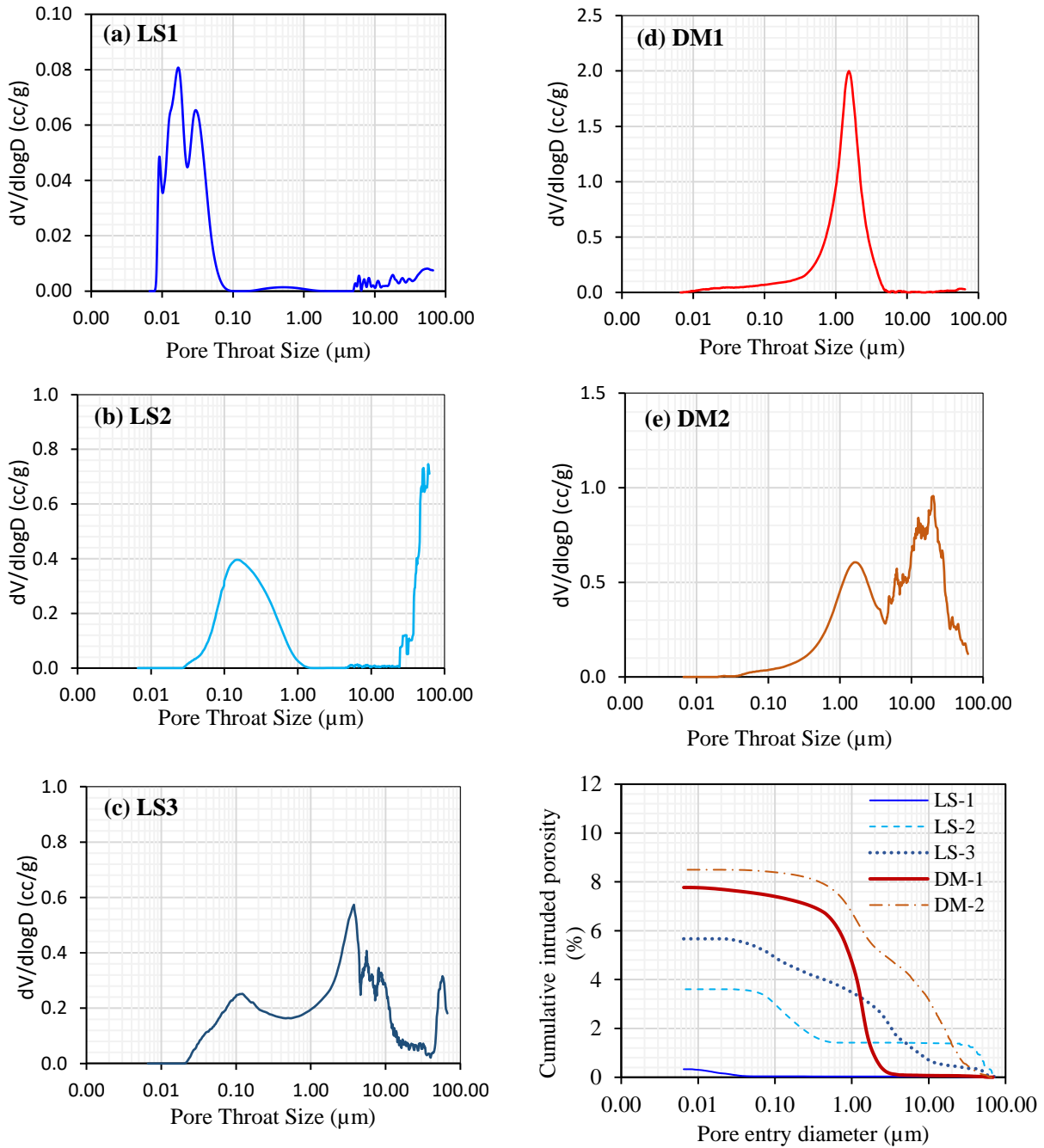


Figure 4.6. MIP test results for rocks

4.2.3 MIP

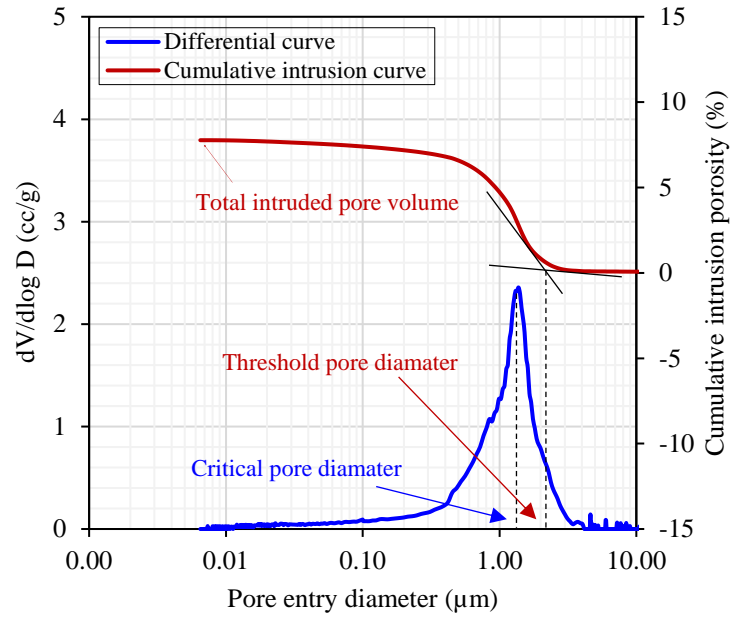
MIP measures the pore throat (entry) size and should not be confused with the pore diameter. The differential, DV ($dv/d\log D$), and the cumulative pore volume, CV (cc/g), curves for the LS rock plugs are given in Figures 4.6 (a) through (c), while those for the DM rock plugs are given in Figures 4.6 (d) through (e). Only pores with a size less than 100 μm were considered in the MIP data analysis.

As seen in Figure 4.6 (f), the trend of the total intruded volumes of the rocks is similar to that of the corresponding aggregate absorption, where LS1 had the lowest while DM2 had the highest intruded volumes. For rock LS1, according to Figure 4.6 (a), most pores had a size ranging from 0.008 to 0.100 μm . For rock LS2, according to Figures 4.6 (b) and (f), over 50% of the total pores had a size ranging from 0.03 to 0.15 μm , and about 25% of the total pores had a size ranging from greater than 45 μm . For rock LS3, according to Figures 4.6 (c) and (f), the pore sizes were well distributed in the range of 0.02 to 45 μm . For the DM rocks, their total porosity, reflected by the total intruded volume, was much higher than that of the LS rocks. However, for rock DM1, according to Figures 4.6 (d) and (f), most sizes were around 1.5 μm , and very few pores had a size greater than 5 μm . For rock DM2, according to Figures 4.6 (e) and (f), the sizes of about 95% of the total pores were well distributed in a range of 4 to 80 μm .

A summary of the MIP characteristics is given in Table 4.3, where the critical and threshold pore throat diameters are determined according to Figure 4.7. The critical pore throat diameter is obtained from the steepest part of the cumulative curve, and the threshold pore throat diameter is defined as the diameter obtained at the intersection of two tangents of the cumulative curve. The critical pore throat diameter is considered to be the pore size at which hydraulic conductance is maximum. The threshold pore throat size is understood to be the smallest pore throat size that is continuous throughout the entire sample.

Table 4.3. Pore characteristics of rock plugs

Rock	ASTM C127 Absorption (%)	Critical pore throat diameter (μm)	Threshold pore throat diameter (μm)	Cumulative intruded volume (cc/g)
LS1	0.7	0.02	0.04	0.05
LS2	2.9	0.15	0.40	0.49
LS3	3.5	3.63	11.0	0.75
DM1	4.1	1.49	2.10	0.97
DM2	6.8	20.4	25.0	1.14



Data from Soja et al. 2019 and Dhandapani and Santhanam 2017

Figure 4.7. Determination of critical and threshold pore size from an MIP curve

Figure 4.8 shows a strong linear relationship between the MIP and the helium porosity of the rocks studied. Figure 4.9 shows a polynomial relationship between the cumulative mercury intrusion volume and the water absorption value of the aggregate.

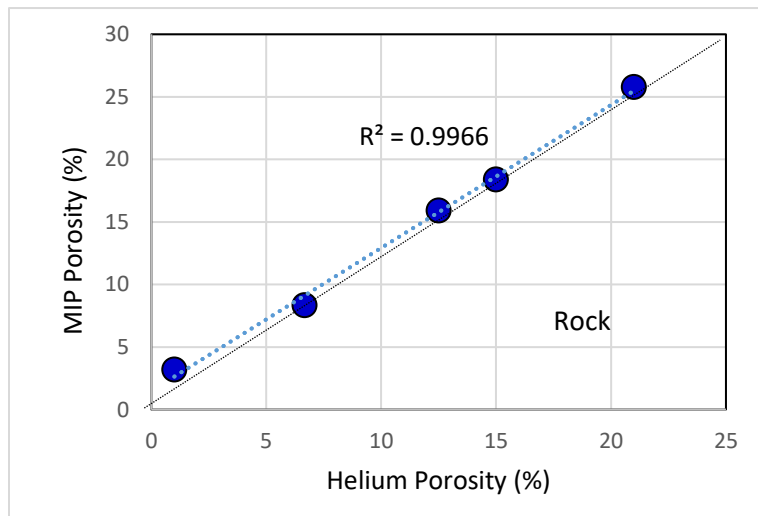


Figure 4.8. Relationship between MIP porosity and helium porosity of rocks

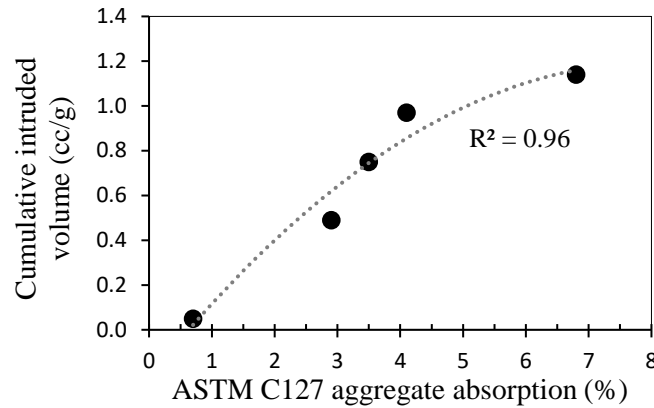


Figure 4.9. Relationship between mercury intrusion volume and aggregate water absorption

4.2.4 Water Sorptivity

The rock cores' water sorptivity results obtained in this study are shown in Figure 4.10. From the figure, among the limestone rocks LS1 showed the lowest initial sorptivity value, 8×10^{-4} (mm/s)^{1/2}, and LS3 showed the highest initial sorptivity, 152×10^{-4} (mm/s)^{1/2}. Among the dolostone rocks, DM1 and DM2 showed initial sorptivity values of 77×10^{-4} (mm/s)^{1/2} and 230×10^{-4} (mm/s)^{1/2}, respectively. Therefore, it could be concluded that DM2 had the largest pores and thus could absorb the most amount of water and that LS1 had the smallest pores among all rocks and thus could absorb the least amount of water.

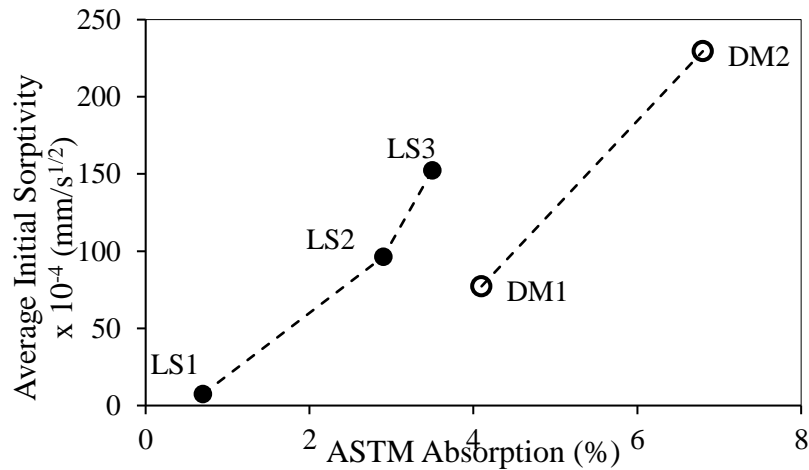


Figure 4.10. Rock core water sorptivity versus absorption

Figure 4.11 shows that the initial sorptivity values had a power correlation with both the threshold and critical pore throat diameters obtained from MIP tests. That is, initial sorptivity values of the rocks generally increased with their threshold and critical pore throat diameters, and the increase was more significant when the threshold or critical pore throat diameters were

small (less than 5 μm). Although having a higher absorption and higher porosity, rock DM1 showed a lower initial sorptivity than LS3.

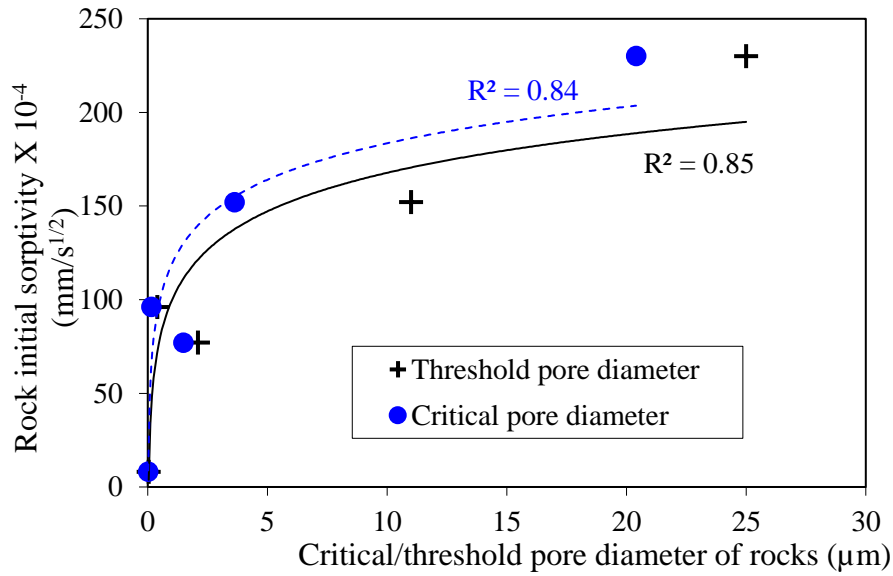
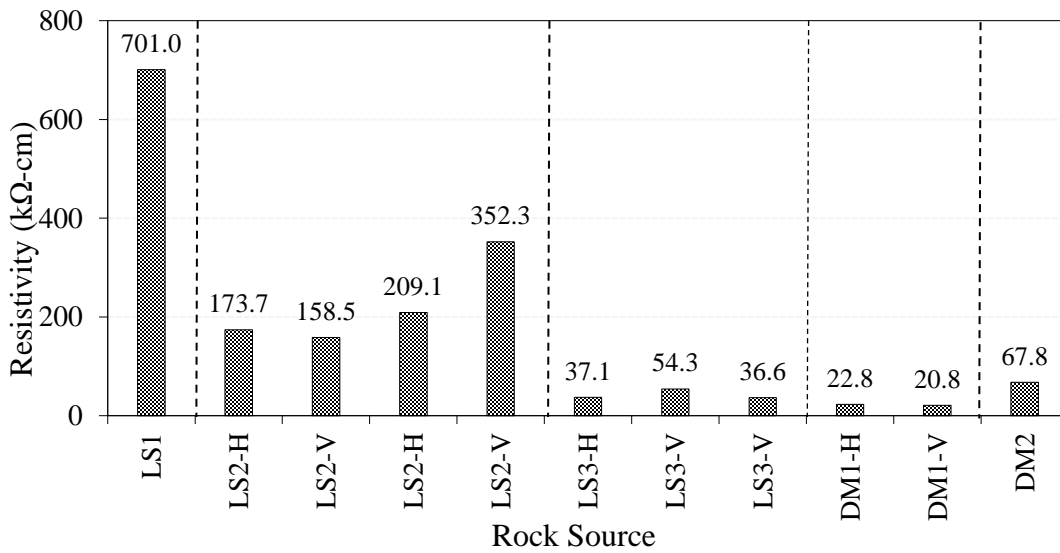


Figure 4.11. Relationship between rock pore size and initial sorptivity

4.2.5 Surface Resistivity

SR was measured on the four-inch by eight-inch rock cores after immersing the cores for 48 hours in a lime bath. The values obtained are shown in Figure 4.12, and the variation in rock resistivity with the rocks' water absorption values is shown in Figure 4.13.



H or V following the sample number indicates the horizontal or vertical rock core obtained from the blockstone for that sample, respectively.

Figure 4.12. Resistivity of rock cores

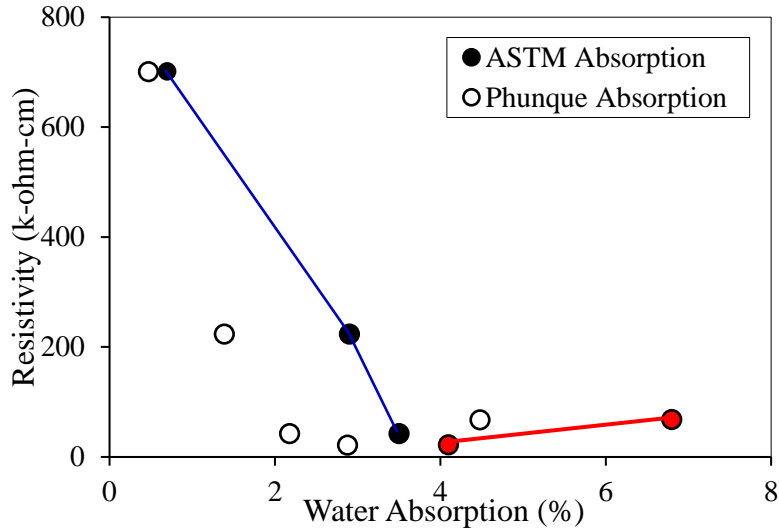


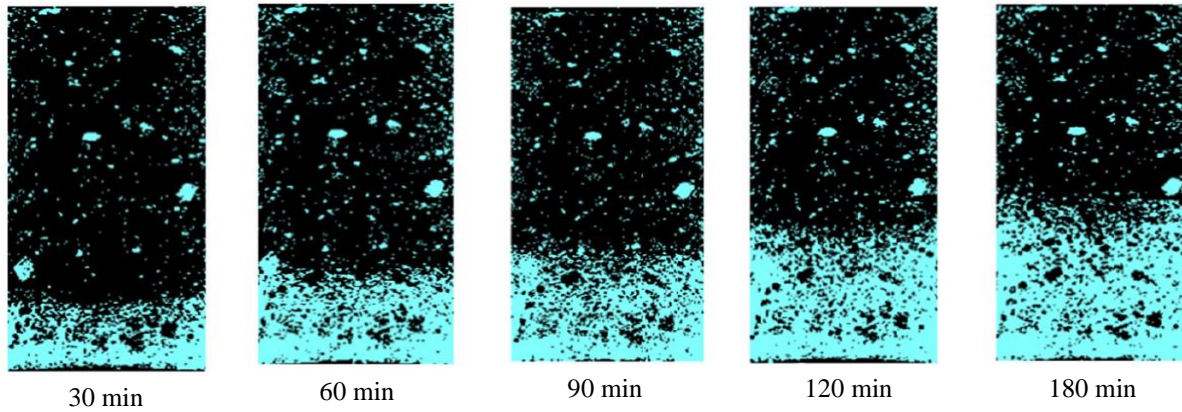
Figure 4.13. Rock resistivity versus aggregate absorption

LS1 had the highest resistivity and DM1 had the lowest resistivity. Though DM2 had a higher porosity than DM1, DM1 showed the lowest resistivity. This might be attributed to the significant variation in the resistivity values among the rock cores even within the same group. For example, the resistivity values of the LS2 rock cores vary in the range of 158.5 to 352.3 k Ω -cm. Overall, the resistivity of the rock cores decreased with an increase in the rocks' water absorption (i.e., porosity) values. The reduction was observed to be sudden and significant as the aggregate water absorption (ASTM C127) increased from 0.7% to 2.9% (LS1 to LS2) and from 2.9% to 3.5% (LS2 to LS3). The change in the resistivity values was relatively smaller when the absorption increased from 3.5% to 4.1% (LS2 to DM1) and from 4.1% to 6.8% (DM1 to DM2). Because SR provides an indication of matrix permeability, a reduction in SR values is an indication of the increased pore connectivity that resulted from a high rock core porosity.

4.2.6 CT Scan

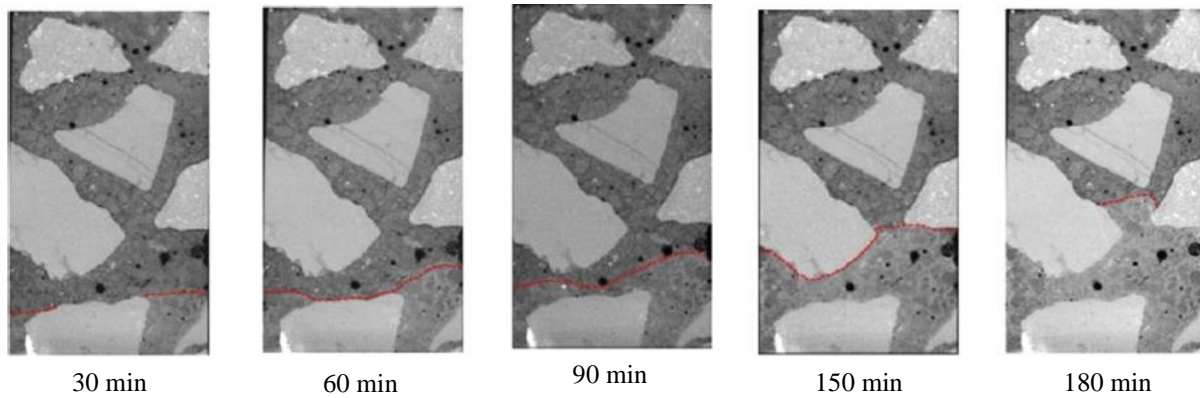
CT scanning, a non-destructive technique, utilizes high-energy x-rays to obtain images of the object under study. The highly energetic rays have a strong capability to penetrate objects and thereby provide insights into the object's interior. Different materials in the test samples have different X-ray absorption rates, and hence the different materials can be distinguished.

Recently, the technique has been used to understand the dynamic fluid uptake behavior of porous materials such as rocks (Derluyn et al. 2013), paste (Zeng et al. 2019), mortar, and cement concrete (Yang et al. 2019) through running continuous x-ray scans to monitor and visualize the movement and path of fluids. Studies have reported the use of water, salt solution such as cesium chloride (Yang et al. 2019), and ethanol (Zeng et al. 2019) as absorbate fluids. Figure 4.14 and Figure 4.15 provide images from one such study (Yang et al. 2019), showing the absorption of CsCl solution (5% by weight) in mortar (as manifested by the rise in the height of the liquid in the system) and the path of the water around the aggregates in the concrete (with the waterfront marked with a red line in Figure 4.15).



© Lin Yang, Danying Gao, Yunsheng Zhang, Jiyu Tang, and Ying Li 2019

Figure 4.14. Dynamic uptake of CsCl solution by mortar



© Lin Yang, Danying Gao, Yunsheng Zhang, Jiyu Tang, and Ying Li 2019

Figure 4.15. Path of CsCl salt solution movement

Recently, in addition to tomography, neutron radiography has also been explored to achieve a detailed quantitative analysis of fluid uptake and transport in porous media (Derluyn et al. 2013, Khanzadeh Moradllo et al. 2019). In the present study, an attempt was made to visualize the path of chloride ions as they were absorbed by the rock and concrete samples using a CT scanning facility at the Center for Non-Destructive Evaluation (CNDE) at ISU (Figure 4.16).

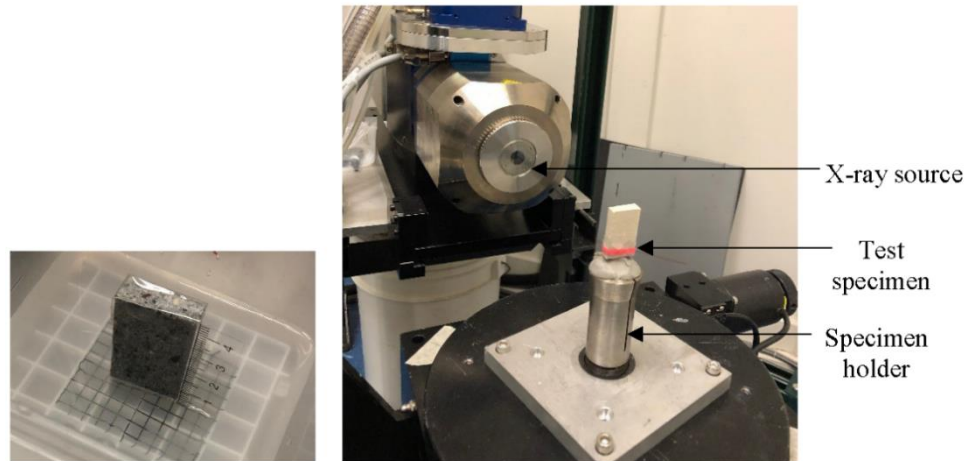


Figure 4.16. CT sample and scanning facility at the CNDE at ISU

A salt solution consisting of 5% CsCl with tap water was used as an absorbate. Attempts were made with varying scanning parameters, including applied voltage, source current, and exposure time. Initial tests were conducted on 4 cm × 2.5 cm × 0.4 cm sample slices sealed with duct tape on the outside surface. The top surface was covered with loosely held plastic, whereas the bottom surface in contact with the fluid was left unsealed to ensure the unidirectional flow of the absorbate.

The sample was CT-scanned before the beginning of the absorption test to visualize the initial condition of the sample. Later, the sample was placed in the salt solution such that the bottom of the sample was 5 mm inside the solution (Figure 4.16). The depth of the solution was maintained at 5 mm throughout the test by pouring in additional solution as and when required to maintain the depth of the solution. The sample was taken out of the solution for scanning at different time intervals, after which the sample was returned to the solution. This procedure was continued, and the scanning was done at different time intervals ranging from few minutes to days. Some of the representative images obtained during the trials with the key parameters set at 80kV, 800 μ A, and an exposure time of 6500 ms are shown in Figure 4.17. The waterfront is indicated by a dashed line. No visible differences were seen in the samples before (0 minutes) and after (20 minutes) being placed in 5 mm of water.

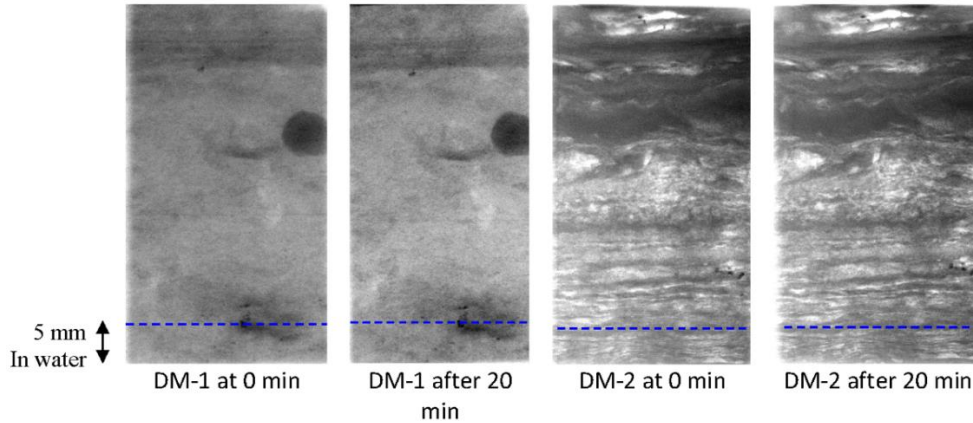


Figure 4.17. CT scan images of DM1 and DM2 rock slices

However, different from the results presented in Yang et al. (2019), the uptake of liquid could not be visualized, even after the sample was made to absorb the salt solution for few days. A probable reason for this is that the age of the concrete and mortar samples was more than 1.5 years old, while the samples used in the literature were tested at early ages (3 to 28 days). The samples were not tested earlier in the present study because of the unavailability of the testing equipment. The sorptivity of the 1.5-year-old samples might have been very low, and the amount of the water absorbed by these samples might not have been sufficient to be visualized by CT scanning. Nevertheless, liquid uptake was also not observed in the rock samples, which would not have been affected by age. Therefore, it is not clear why the testing conducted for this project did not yield similar results to those presented in literature. Another possibility is that the raw CT scan images were not post-processed sufficiently because access to and operation of the scanning equipment was restricted. Therefore, the CT scan study was terminated due to the project's timeframe and because it had only been proposed as an optional exploration for the project.

4.3 Fresh Concrete Properties

The fresh concrete properties of all mixes are given in Table 4.4. As mentioned above, the concrete mix proportions were the same for all mixes (by volume). The slumps of all concrete mixes made with different aggregates were controlled at 4 inches by the use of a mid-range water-reducing agent.

Table 4.4. Fresh concrete properties

Mix ID	Coarse Aggregate Source	Slump (in.)	Unit Weight (pcf)	Measured Concrete Air Content (%)	Corrected Concrete Air Content (%)
C-LS1	Ames	4	142	7.6	7.3
C-LS2	Alden	4	139	8.4	8.0
C-LS3	Durham	4	138	8.5	8.0
C-DM1	Douds	4	140	8.2	7.5
C-DM2	Bowser	4	138	9.0	7.1

4.4 Hardened Concrete Properties

4.4.1 Thin-Section Imaging

Figures 4.18 to 4.26 show the images of different thin-section specimens. Each sample was impregnated with blue-dyed epoxy before sectioning to accentuate the air voids.

In Figure 4.18, a thin-section photomicrograph shows three phases: fine aggregate (fa), paste (p), and entrained air voids (v). Two kinds of fine aggregate were used, quartz (fa-q) and chert (fa-ch). Some areas of the paste were microporous (mp), as evidenced by a blue-tinge. However, some voids were either partially (v2) or not (v3) intruded.

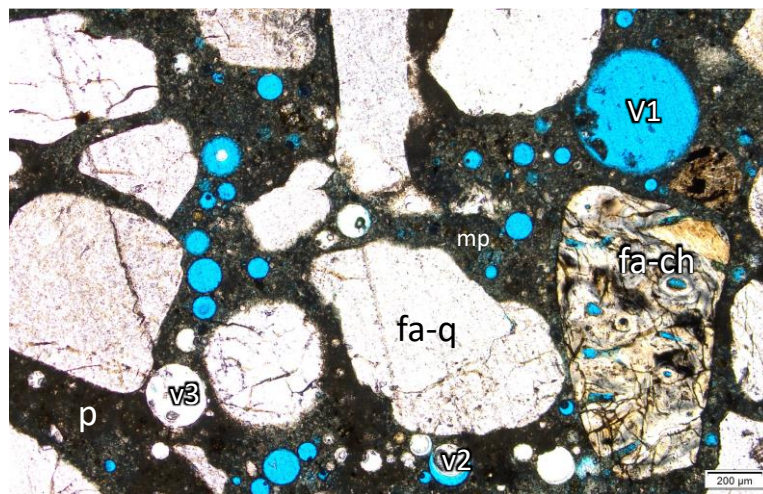


Figure 4.18. Thin-section micrograph of a concrete specimen

Figure 4.19 presents a thin-section photomicrograph showing extreme deterioration of a fine aggregate grain, likely a shale particle. Other fine aggregates present include quartz (fa-q) and an igneous rock fragment (fa-ig), which are more resistant to deterioration. The paste includes entrained air voids (v), many of which have not been intruded by the blue-dyed epoxy used to make the thin section.

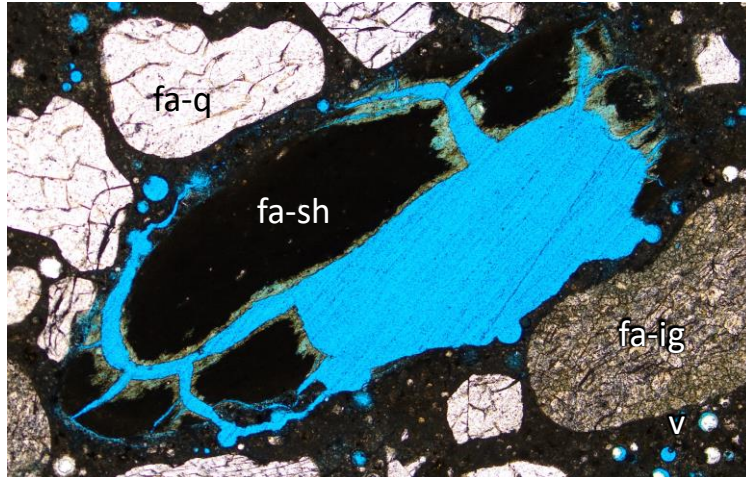


Figure 4.19. Thin-section micrograph highlighting deterioration of a fine aggregate grain

Figure 4.20 shows a thin-section photomicrograph showing a rounded fine aggregate grain of plagioclase feldspar (fa-p) that exhibits characteristic tartan twinning of the crystal in cross-polarized transmitted light. This plagioclase grain has inclusions of other minerals in it that may weather at a different rate than the plagioclase crystal itself.

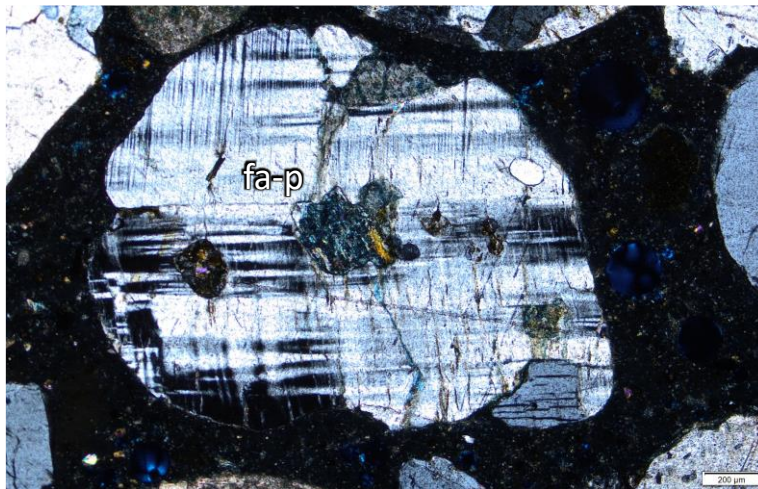


Figure 4.20. Thin-section micrograph highlighting a fine aggregate grain

Figure 4.21 shows a thin-section photomicrograph showing rounded fine aggregate grains of porous dolostone of two different types (d1, d1), as well as quartz (q). Entrained air voids are also present.

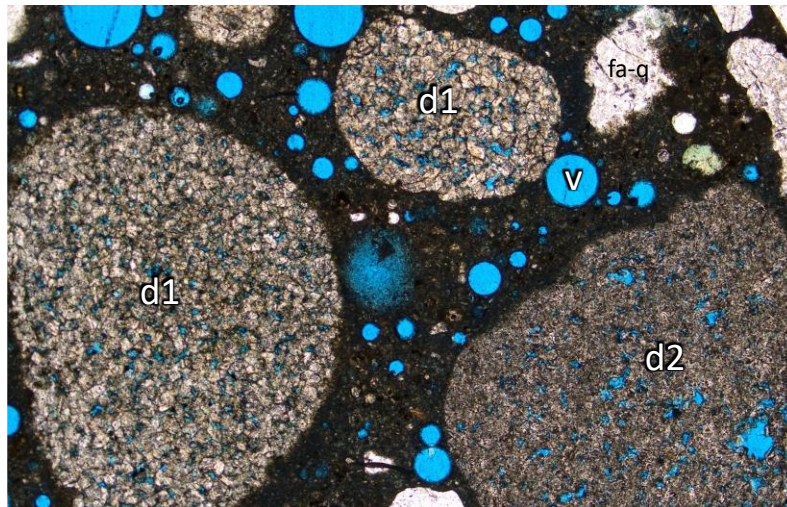


Figure 4.21. Thin-section micrograph of fine aggregate grains in porous dolostone

Figure 4.22 shows five thin-section photomicrographs (all at the same scale) of concrete samples made with different coarse aggregates. In addition to the features of the aggregates, the features of the cement pastes and the aggregate-paste interfacial transition zones can also be observed. In Image A, some air voids are clustered in the area close to the Ames aggregate surface. The high porosity of the interfacial transition zone between the paste and the coarse aggregate can be clearly distinguished in all of the images, identified by either a blue or dark color and indicated by an arrow in each image.

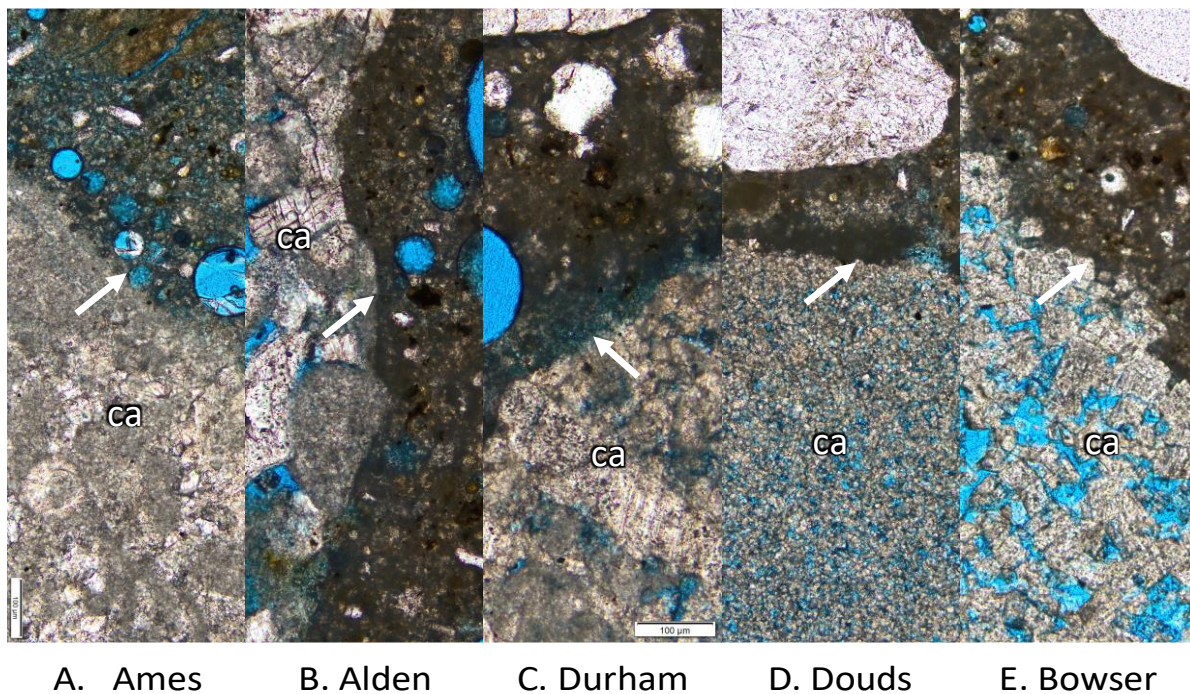


Figure 4.22. Thin-section micrographs of paste-coarse aggregate interface in all concrete mixes

Figure 4.23 shows a thin-section photomicrograph of a sample impregnated with blue-dyed epoxy. The porosity of the paste differs across the section. Lighter colored areas (pl) are less porous, while darker colored areas are more porous (pd). The fine aggregate is mostly quartz (fa-q). Most of the air voids (v1) were not intruded (v2) by the blue dye, possibly due to the low porosity of the paste, which restricted epoxy flow into those voids.

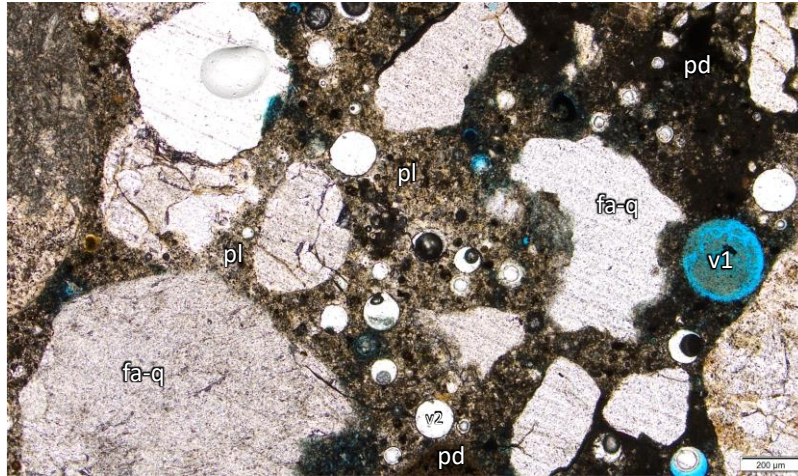


Figure 4.23. Thin-section micrograph of low-porosity paste

Figure 4.24 shows a thin-section photomicrograph of a sample impregnated with blue-dyed epoxy that possibly shows the interaction between a quartz grain (fine aggregate, fa-q) and paste at the margin of the grain indicated by the arrow.

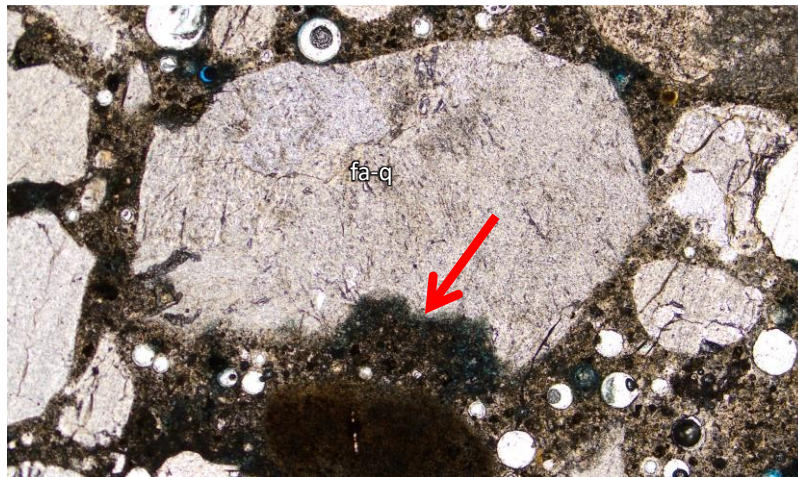


Figure 4.24. Thin-section micrograph of fine aggregate-paste interface

Figure 4.25 shows a thin-section photomicrograph of an Alden sample impregnated with blue-dyed epoxy that shows a range in porosity from highly porous (php) to less porous (plp) areas. The paste is so low in porosity that the air voids (v) were unable to be intruded by the blue-dyed epoxy used to make the thin section. The coarse aggregate grains are limestone (ca-ls).

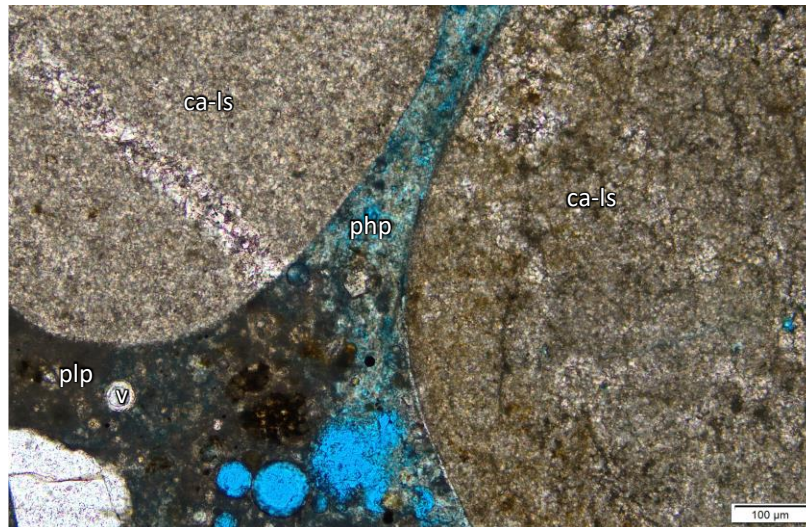


Figure 4.25. Thin-section micrograph of Alden sample

Figure 4.26 shows four thin-section photomicrographs of samples impregnated with blue-dyed epoxy that show the variation among the sample in terms of the amount of mineral growth into the air voids. The sample made with Alden aggregate (A) shows a mesh of acicular crystals. The sample made with Douds aggregate (B) shows a matrix of microcrystals. The sample made with Bowser (C) shows both acicular minerals and a microcrystalline matrix in the air voids. The sample made with Durham aggregate (D) shows a void-lining matrix of microcrystals.

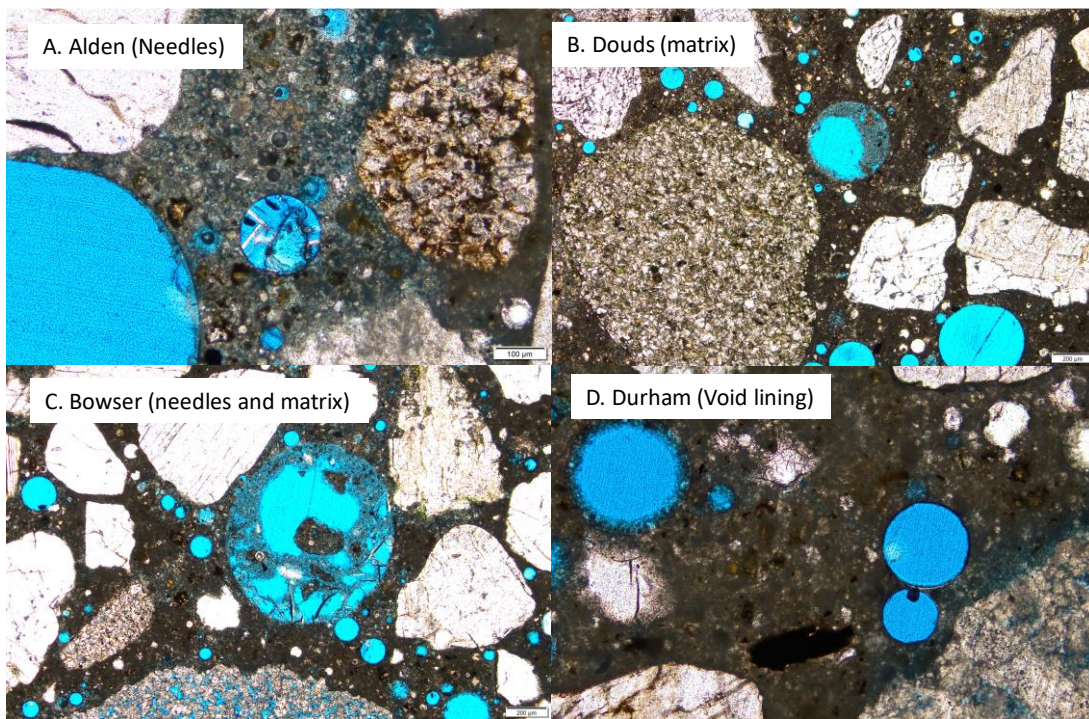


Figure 4.26. Thin-section micrographs of concrete mixes showing mineral growth in air voids

4.4.2 Compressive Strength

The 28-day compressive strength test results for the concretes are shown in Figure 4.27.

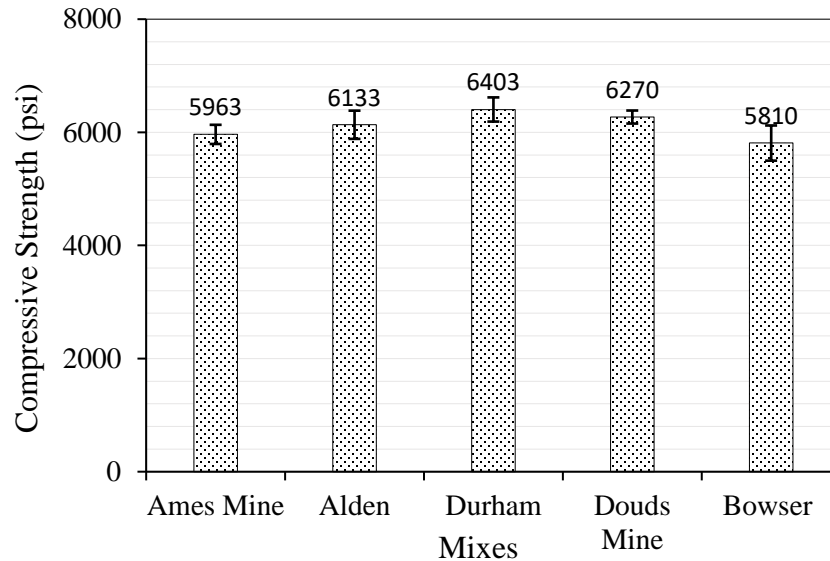


Figure 4.27. Compressive strengths of the concrete mixes

All concretes mixes had similar compressive strength values. This implies that the properties of the coarse aggregate (e.g., absorption and porosity) had a very limited influence on concrete compressive strength and that the compressive strength of the concrete mixes was primarily controlled by the strength of the mortar.

4.4.3 Surface Resistivity

Figure 4.28 shows the development of SR with sample age for all of the mixes studied. As expected, the SR values of the mixes increase as the sample age increases. Up to the age of 28 days, the SR values of the mixes with limestone aggregates (C-LS1 through C-LS3) were higher than those of the mixes with dolostone aggregates (C-DM1 and C-DM2). C-LS1 showed the highest and C-DM2 showed the lowest SR values up to 28 days. However, the mixes with dolostone aggregates exhibited higher SR values after 28 days. Overall, the SR values of all mixes increased after a sample age of 28 days up to 120 days of SR measurement.

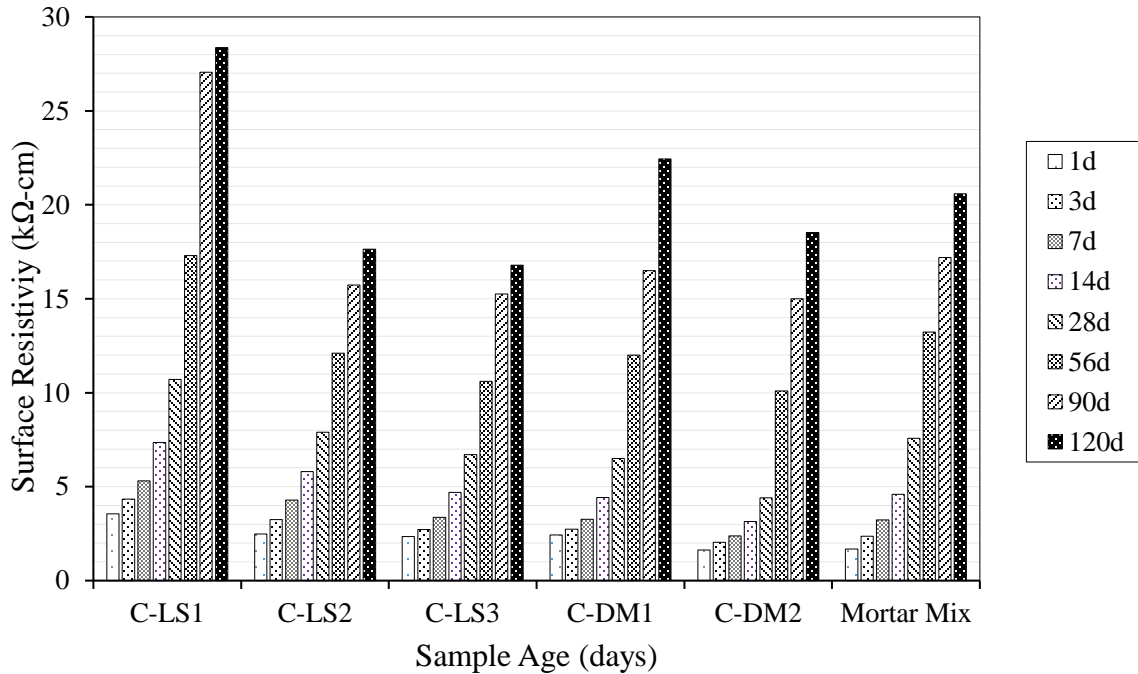


Figure 4.28. SR development with specimen age

The difference between the SR values of the mortar mix and the concrete mixes containing coarse aggregates of different porosities (Figure 4.28) indicates the influence of aggregate porosity on the properties of concrete. From the figure, comparing C-LS1 (the mix containing the aggregate with the lowest absorption, 0.7%) with the mortar mix, it is evident that C-LS1 showed relatively better performance in terms of higher SR values at all ages than the mortar mix. This superior behavior exhibited by C-LS1 compared to the mortar mix might be attributed to the higher resistance offered by the LS1 aggregates present in the mix.

However, as the coarse aggregate absorption increased, it was observed that the SR values of the mixes generally decreased, indicating an inverse relationship between aggregate absorption (i.e., porosity) and concrete SR at all sample ages (up to 120 days). A similar decrease in SR due to the presence of aggregates with higher absorption values was also observed by Bentz et al. (2017) for a variety of sedimentary, igneous, and metamorphic rock types from around the US.

Figure 4.29 shows the relationship between rock pore parameters and 28-day concrete SR, and Figure 4.30 shows the relationship between rock SR and 28-day concrete SR.

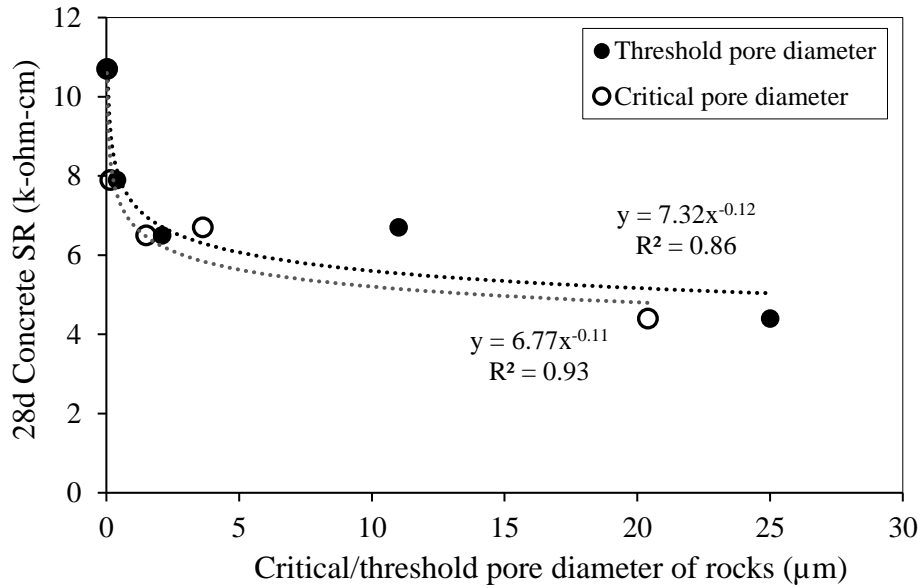


Figure 4.29. 28-day concrete SR versus critical and threshold pore throat diameter in rocks

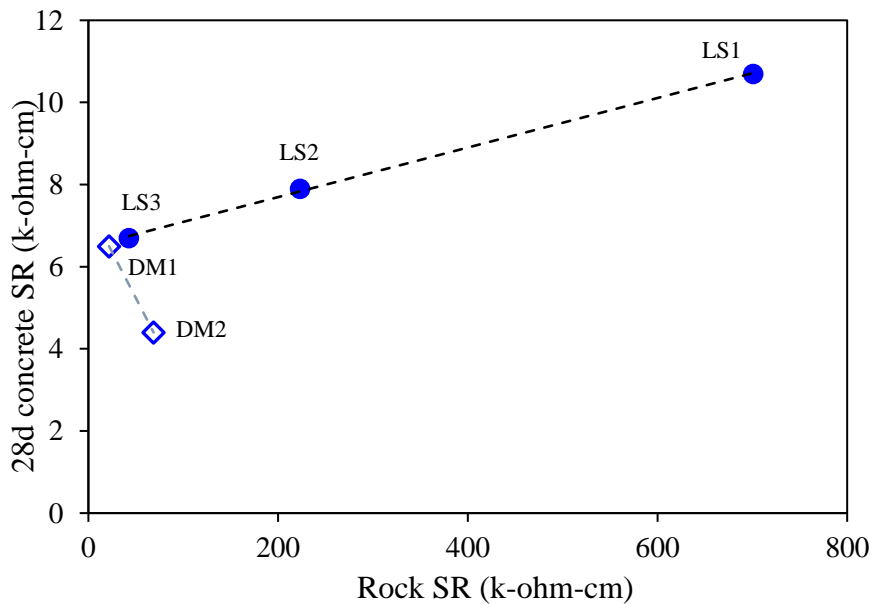


Figure 4.30. Rock SR versus 28-day concrete SR

In Figure 4.29, a power relationship was fitted between the rock pore parameters (threshold and critical pore throat diameters) and the 28-day concrete SR. The 28-day concrete SR was observed to correlate better with the critical pore throat diameter than with the threshold pore throat diameter. An increase in the critical pore throat diameter resulted in a decrease in the 28-day concrete SR.

In Figure 4.30, a linear relationship exists between the rock SR and the 28-day concrete SR when evaluating the rock samples by rock type (i.e., limestone versus dolostone). The correlation was found to be strong, aside from DM2's 28-day concrete SR value, which fell below the trend for the rest of the samples. In any case, it is more reasonable to consider the limestone and dolostone samples' SR results separately for reasons that will be explained below. Figure 4.31 shows the variation of the concrete SR values with the aggregate ASTM C127 absorption values.

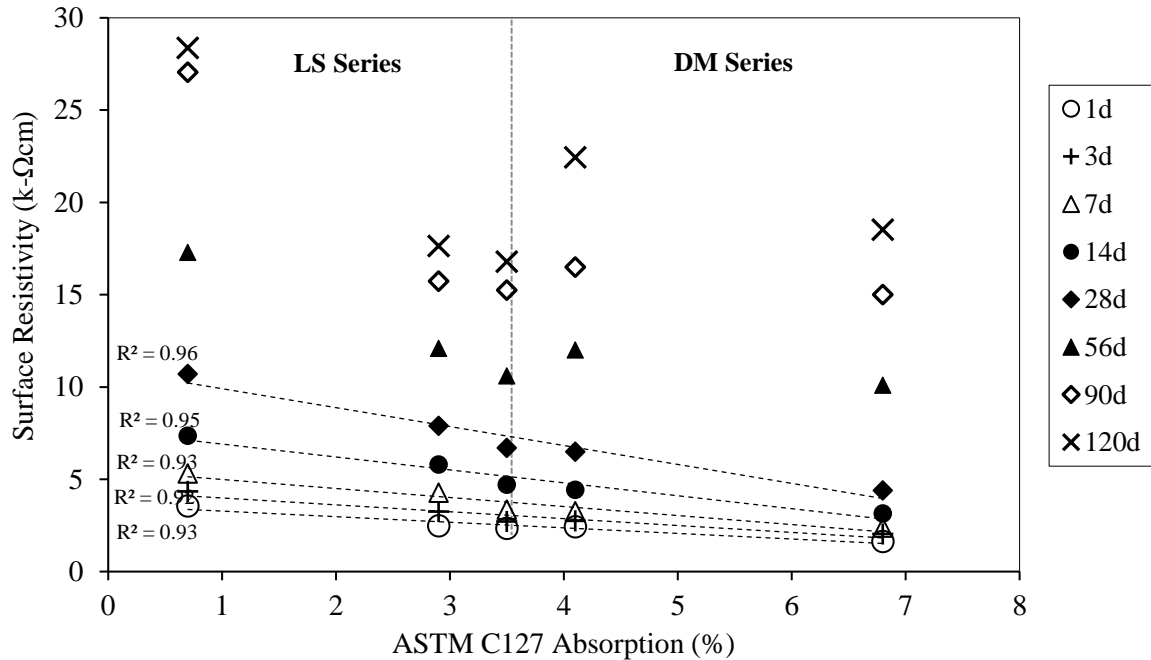


Figure 4.31. Variation of concrete SR values with aggregate absorption values

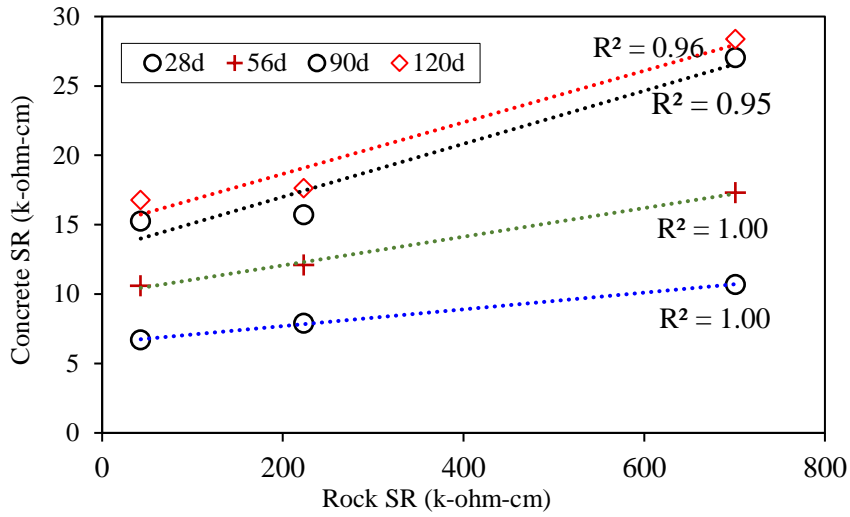
Figure 4.31 indicates that an increase in the coarse aggregate absorption possibly resulted in an increase in the number of connected pores and thereby an increase in permeability and a decrease in SR. However, this trend was seen among all mixes only up to a sample age of 28 day (Figure 4.31), as mentioned above. Up to 28 days, the decrease in the SR values was linear with very strong correlation coefficients (greater than 0.91). After a sample age of 28 days, there was a change in the trend. Despite dolostone coarse aggregates DM1 and DM2 having absorption values higher than limestone coarse aggregates LS2 and LS3, the concretes containing dolostone DM1 and DM2 developed higher SR values after an age of 90 days than the concretes with limestone LS2 and LS3. This indicates a possible interaction between the cementitious matrix and the surfaces of the dolostone aggregate particles, which might have densified the interfacial transition zone and isolated highly porous coarse aggregates.

It is also highly possible that, at later ages, the highly absorptive dolomitic aggregates improved the microstructure of the bulk concrete through internal curing because the aggregates were used in their SSD condition after being soaked in water for 24 hours prior to mixing. Pores in such highly absorptive aggregates can act as water reservoirs that store water and eventually release it into the interior of the system. However, the effectiveness of this process varies significantly depending on the aggregates' rate of absorption and desorption (Castro et al. 2011, Savva and

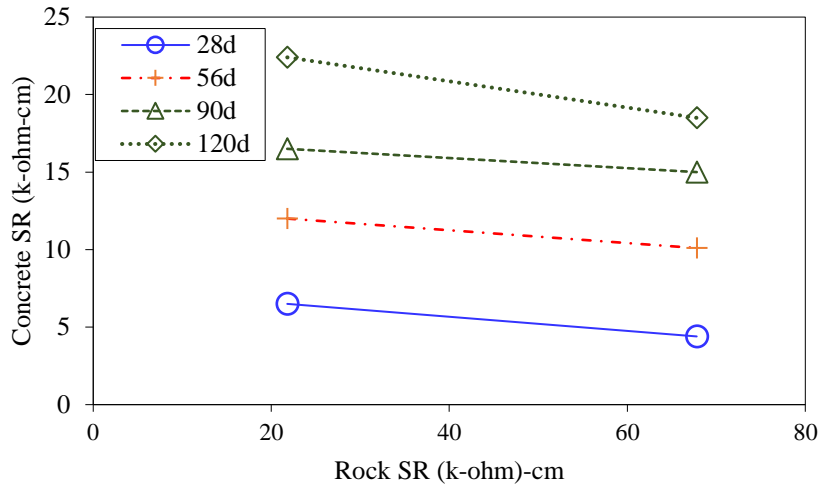
Petrou 2018, Zou et al. 2015). Such an observation was also made by Savva and Petrou (2018), who demonstrated the feasibility of achieving internal curing using highly absorptive normal weight coarse aggregates (with a water absorption of 5.2%), resulting in reduced autogenous shrinkage. In addition to improved restrained shrinkage behavior, rapid chloride permeability and compressive strength test results improved.

In the present study, the absorption values of the dolomitic coarse aggregates were in a similar absorption range (4.1% to 6.8%) to the aggregates studied by Savva and Petrou (2018), which supports the speculation that these aggregates might be used to achieve internal curing. Moreover, the 24-hour water absorption of the DM2 coarse aggregate, 6.8%, overlaps with the 24-hour water absorption range of lightweight aggregates (6% to 30%) (Castro et al. 2011). Another recent study (Zou et al. 2015) showed that incorporating artificial normal-weight highly porous fine aggregate (with a water absorption of 23.6%) into a mix enhanced the mortar properties, which also substantiates the claim made in the present study regarding effects of using highly absorptive dolomitic coarse aggregates.

However, in the present research, details regarding any actual cement reaction with the surfaces of dolostone aggregate particles or internal curing in the samples were beyond the scope of the study. Nonetheless, it could be concluded that, as a result of different possible mechanisms operating in the samples containing either limestone or dolomitic coarse aggregates, the SR comparison could only be made among the mixes containing coarse aggregates of same type. Hence, SR trends at different ages were more apparent in the LS and DM series when the two aggregate types were considered separately, as shown in Figure 4.32.



(a) Limestone series



(b) Dolostone series

Figure 4.32. Concrete SR versus rock SR considered separately for the limestone (a) and dolostone (b) series

4.4.4 Nord Test

Figure 4.33 shows the variation in the DNSSM values obtained in this study with the aggregates' ASTM C127 absorption values. Since, the variation in the DNSSM values with the aggregates' Phunque absorption values follow the same trend, the variation is shown here with respect to the ASTM C127 absorption values only.

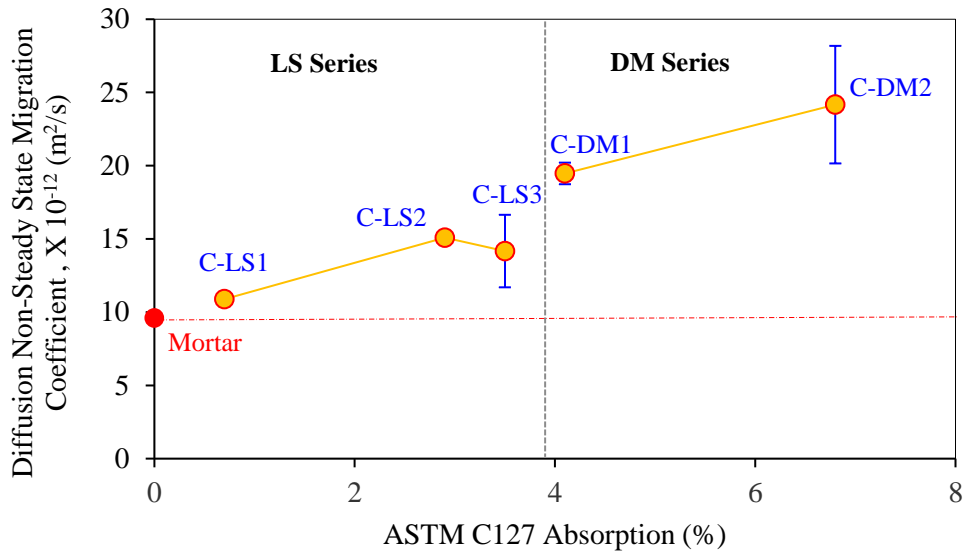


Figure 4.33. Concrete DNSSM values versus aggregate ASTM C127 absorption values

From Figure 4.33, it is clear that the DNSSM coefficients (measured at a sample age of 28 days) of the mixes increased with an increase in the absorption values of the coarse aggregates. Even though this was the overall trend, the variation needs to be compared and viewed independently for the mixes containing the LS and DM series aggregates. This is because of the change in the SR values of the DM samples that was observed after a sample age of 28 days.

Among the LS series mixes, C-LS1 exhibited the lowest DNSSM coefficient of $10.89 \times 10^{-12} m^2/s$. C-LS2 exhibited a slightly higher DNSSM coefficient value compared to C-LS3, even though the latter was expected to exhibit the highest DNSSM coefficient value among LS series. However, this finding might be because of the variation in the experimental values, as indicated by the error bars. Among the DM series mixes, C-DM2 showed a higher DNSSM coefficient value, $24.17 \times 10^{-12} m^2/s$, compared to that of C-DM1, which had a coefficient value of $19.47 \times 10^{-12} m^2/s$, indicating a higher chloride intrusion in the C-DM2 mix than in the C-DM1 mix.

All concrete mixes showed a higher DNSSM coefficient than that of the mortar mix (indicated by the dashed line in Figure 4.33, with the DNSSM value for the mortar mix indicated on the Y-axis). This indicates that the bulk chloride permeability of the concrete mixes increased due to the presence of porous aggregates and that the chloride permeability of the concrete mixes increased with an increase in coarse aggregate porosity. Even though C-LS1 showed a slightly higher DNSSM than the mortar mix, the values were very close to each other.

Figure 4.34 shows the variation in the concrete DNSSM coefficients with the rock pore throat diameter. Though not very strong, the correlation between the concrete DNSSM coefficients was relatively better with the critical rock pore throat diameter than with the threshold rock pore throat diameter.

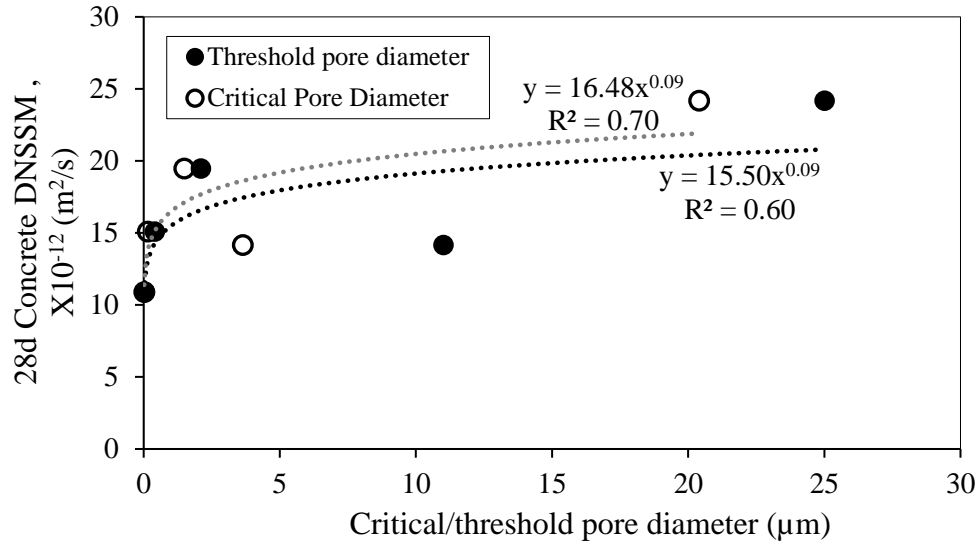


Figure 4.34. Concrete DNSSM values versus rock pore throat diameter values

Figure 4.35 shows the relationship between the accelerated tests (i.e., SR and DNSSM) at a sample age of 28 days. This is an important relationship because lately there has been an emphasis on using SR as an indicator for the transport properties in cementitious systems because it is an easy and a rapid non-destructive test with advantages over other electrical tests. It is known that a mix with a higher SR value exhibits a lower chloride intrusion susceptibility and hence a lower DNSSM coefficient. Accordingly, overall, C-LS1 indicated the highest 28-day SR value of 10.7 kΩ-cm with the lowest 28-day DNSSM coefficient of $10.89 \times 10^{-12} \text{ m}^2/\text{s}$, and C-DM2 showed the lowest 28-day SR value of 4.4 kΩ-cm with the highest 28-day DNSSM coefficient of $24.17 \times 10^{-12} \text{ m}^2/\text{s}$. Thus, the test results confirm the trends observed in this study.

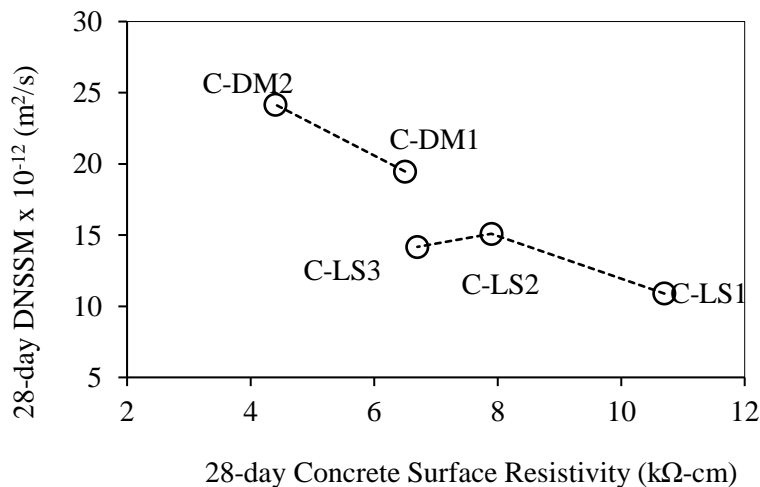


Figure 4.35. Relationship between SR values and DNSSM

4.4.5 Water Sorptivity

Figure 4.36 shows the variation in the 28-day water sorptivity of the mixes with the coarse aggregate ASTM C127 absorption values. Since the variation in the 28-day water sorptivity of the mixes versus coarse aggregate Phunque absorption values follows the same trend, the variation is shown with respect to the ASTM C127 absorption values only.

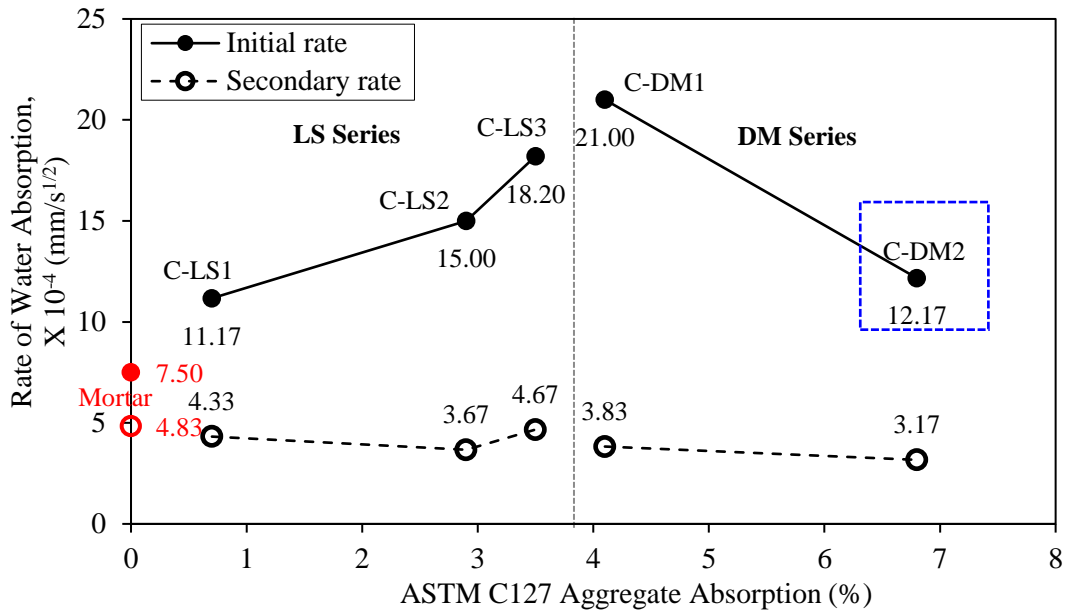


Figure 4.36. 28-day water sorptivity of concrete mixes versus ASTM C127 aggregate absorption values

The sorptivity values of the mortar mix are presented on the y-axis of Figure 4.36. The figure indicates that the initial rate of water absorption (or initial sorptivity) of mixes belonging to the LS series increased with an increase in the aggregate absorption values, whereas the DM series mixtures show the opposite trend. The secondary rate of absorption (or secondary sorptivity) of mixtures belonging to both the LS and DM series did not vary significantly and was similar to that of the mortar mix, which had a secondary sorptivity value of $4.83 \times 10^{-4} \text{ (mm/s)}^{1/2}$.

Among the LS series mixes, mix C-LS1 showed the lowest initial sorptivity of $11.17 \times 10^{-4} \text{ (mm/s)}^{1/2}$, and mix C-LS3 showed the highest of $18.20 \times 10^{-4} \text{ (mm/s)}^{1/2}$. Mixes belonging to the DM series did not exhibit this trend. It should be noted that the initial sorptivity of mix C-DM2 in Figure 4.36 is a reliable value because the R^2 value of the linear regression of the test data (I versus $s^{1/2}$) is not higher than 0.98, as required by ASTM C1585. This can be attributed to the lack of bilinear behavior (i.e., two fitting lines with clearly different slopes), and such instances are not uncommon; this was also observed by Zhutovsky and Hooton (2019).

In Figure 4.36, the initial sorptivity value for mix C-DM2 is indicated just for completeness. Mix C-DM1 showed an initial sorptivity value of $21.00 \times 10^{-4} \text{ (mm/s)}^{1/2}$, which was greater than that of

all mixes in the LS series. Overall, all of the concrete mixes showed an initial sorptivity value greater than that of the mortar mix, indicating increased chloride intrusion in the concrete mixtures. It should be re-emphasized that initial sorptivity can be related to permeability, and a higher initial sorptivity value indicates a higher permeability to deleterious ions is likely (Zhutovsky and Hooton 2019). Thus, concrete mixes containing more highly absorptive aggregates exhibit a higher permeability with respect to chloride intrusion than mixes containing aggregates of a relatively lower absorption.

The variation in the initial sorptivity of the concrete mixes with the initial sorptivity of the corresponding rock cores and their threshold and critical pore throat diameters are shown in Figures 4.37 and 4.38, respectively.

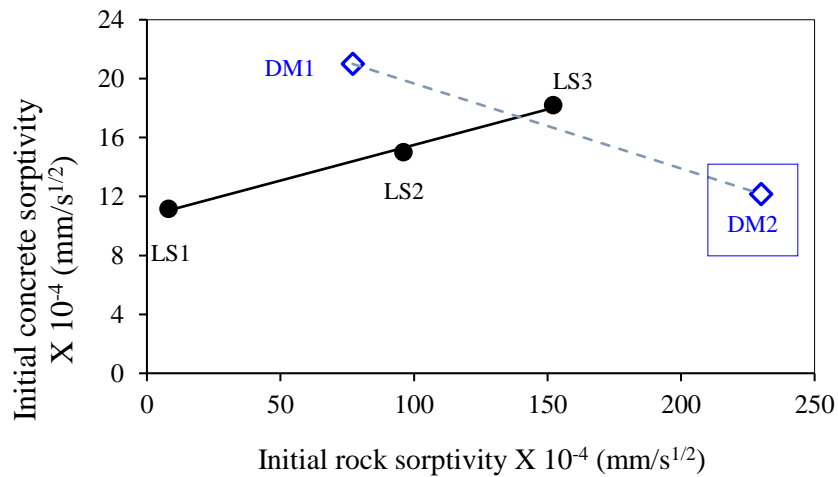


Figure 4.37. 28-day initial sorptivity in concrete versus initial sorptivity in LS rocks

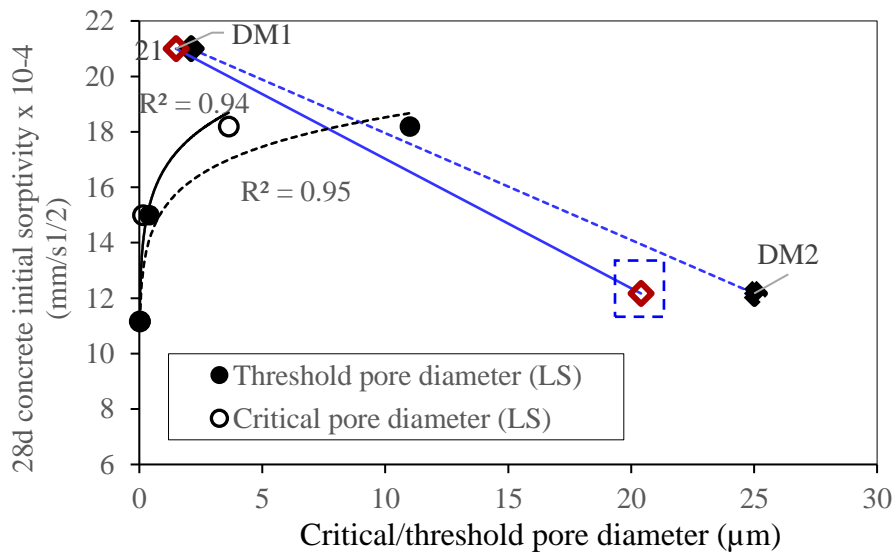


Figure 4.38. 28-day initial sorptivity of concrete versus pore throat diameter of rocks

From Figure 4.37, it can be observed that rocks having a higher sorptivity resulted in concrete mixes with a higher initial sorptivity. Thus, a very good linear relationship was seen among the rock and concrete specimens that belonged to the LS series. It can be observed from Figure 4.38 that the 28-day initial sorptivity of the concrete mixes was very well related to both the threshold and critical pore diameters in their rocks. LS1 rock, which had the smallest critical pore throat diameter of $0.02 \mu\text{m}$, exhibited the lowest initial sorptivity of $11.17 \times 10^{-4} \text{ mm/s}^{1/2}$ in mix C-LS1, and LS3 rock, which had the largest critical pore throat diameter of $3.63 \mu\text{m}$, exhibited the highest initial sorptivity of $18.2 \times 10^{-4} \text{ mm/s}^{1/2}$ in mix C-LS3.

4.4.6 Salt Ponding Test

The chloride content of the concrete mixes, shown in Figure 4.39, was calculated as the difference between the chloride content determined from the ponded slab samples and the chloride content present in the base cylinder samples of the respective mixes. The chloride content was determined using slab samples taken at two different depths, i.e., one sample collected from the top 1/16 to 1/2 inch of the slab and one sample collected from the bottom 1/2 to 1 inch of the ponded slab surface.

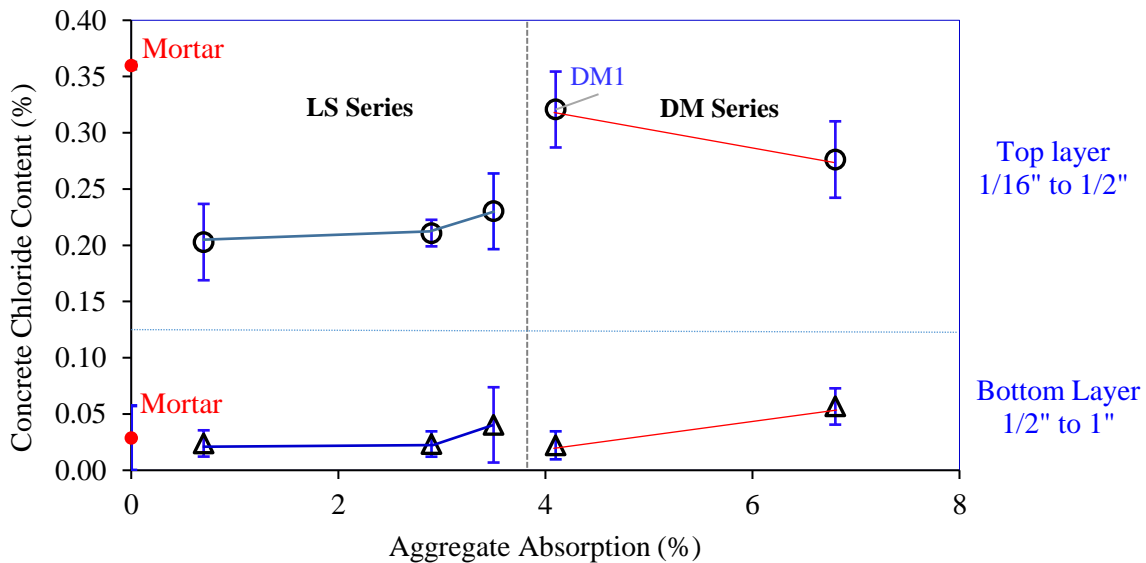


Figure 4.39. Chloride content in concrete versus ASTM C127 absorption values

Figure 4.39 shows the variation in the mixes' chloride content values with the aggregates' ASTM C127 absorption values. In Figure 4.39, the concrete chloride content represents the average of six samples from two slabs made with the same batch of concrete (three samples per slab). However, the mortar chloride content was the average of three samples obtained from one mortar slab specimen.

Figure 4.39 also shows that the chloride content was higher in the top layer (1/16 to 1/2 inch) than in the bottom layer (1/2 to 1 inch), as expected. The variation in the chloride content was

visually obvious in the top layer, whereas that in the bottom layer was not very apparent. On comparing the chloride content in the top layers of the different specimens, the DM concrete mixes, which contained highly porous dolostone aggregates (DM1 and DM2), were found to have a higher chloride content than the mixes containing low-absorption limestone aggregates (i.e., LS1, LS2, and LS3). It should be noted that it was not the concrete with the highest aggregate absorption value (C-DM2) but the one with the largest amount of fine, connected pores (C-DM1) that had the highest chloride content in the top layer of the concrete slab. Apart from mix C-DM2, the chloride content values in the top layer of the mixes increased with an increase in the aggregate ASTM C127 absorption values.

Among the LS series mixes, mix C-LS1 showed the lowest chloride content in both the top and bottom layers, with chloride content values of 0.20% and 0.02%, respectively, and mix C-LS3 showed the highest chloride content values of 0.23% and 0.04% in the top and bottom layers, respectively. In mixes belonging to the DM series, mix C-DM2 unexpectedly exhibited a lower chloride content value than mix C-DM1. However, mix C-DM2 exhibited a higher chloride content value of 0.06% in the bottom layer than mix C-DM1, which had a chloride content value of 0.02%. This indicates that mix C-DM2 had a higher chloride permeability than mix C-DM1. It should also be noted that the chloride content value in the bottom layer of mix C-DM2 was the highest among all the mixes.

Figure 4.40 shows the variation in the chloride content with the rock critical and threshold pore throat diameters for the LS series mixes. The variation is shown only for the LS series since a clear trend in the chloride content values versus the aggregate ASTM C127 absorption values was obtained only for the LS series mixes.

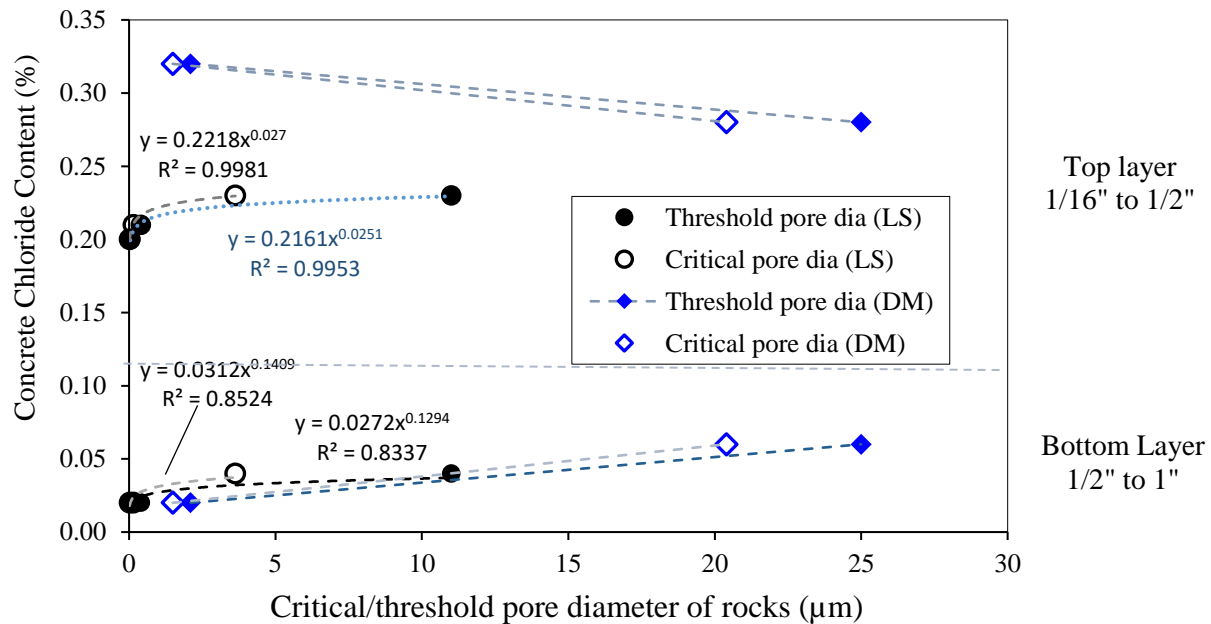


Figure 4.40. Concrete chloride content versus the critical and threshold pore throat diameters of the corresponding rocks in the concrete

A power function was fitted to the data points (Figure 4.40), and it was found that the chloride content values in both the top and bottom layers correlate well with both the threshold and critical rock pore throat diameters. LS1, which had the smallest critical and threshold pore throat sizes, showed the lowest chloride content, whereas LS3, which had the largest **critical and threshold** pore throat sizes, showed the highest chloride content in both the top and bottom layers.

Figure 4.41 shows the relationship between 28-day concrete sorptivity and 28-day concrete SR for the LS series mixes.

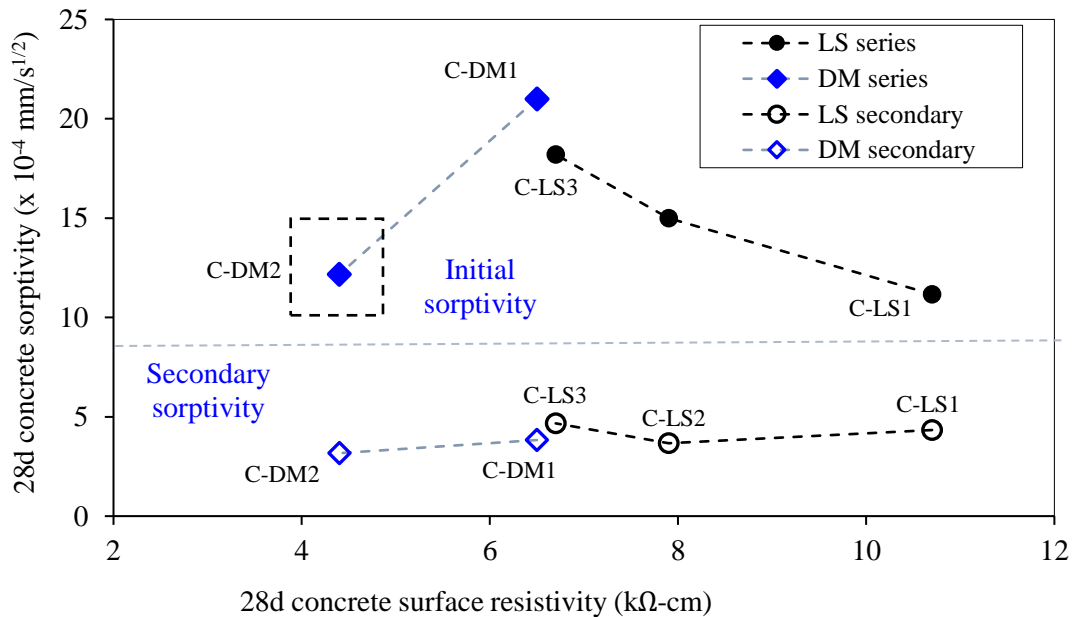


Figure 4.41. 28-day concrete sorptivity versus 28-day concrete SR

No variation in the secondary sorptivity values was observed as concrete SR varied. However, a clear variation was seen in the initial sorptivity as concrete SR varied. In the LS series, concrete mixes with higher SR showed lower initial sorptivity, while concrete mixes with lower SR showed higher initial sorptivity. Accordingly, mix C-LS1, which had the highest 28-day SR of 10.7 kΩ-cm, exhibited the lowest 28-day initial sorptivity, $11.17 \times 10^{-4} \text{ (mm/s)}^{1/2}$, and mix C-LS3, which had the lowest SR of 6.7 kΩ-cm, exhibited the highest 28-day initial sorptivity, $18.20 \times 10^{-4} \text{ (mm/s)}^{1/2}$.

Figure 4.42 shows the variation in chloride content with concrete SR for sample ages of 28 days and 56 days.

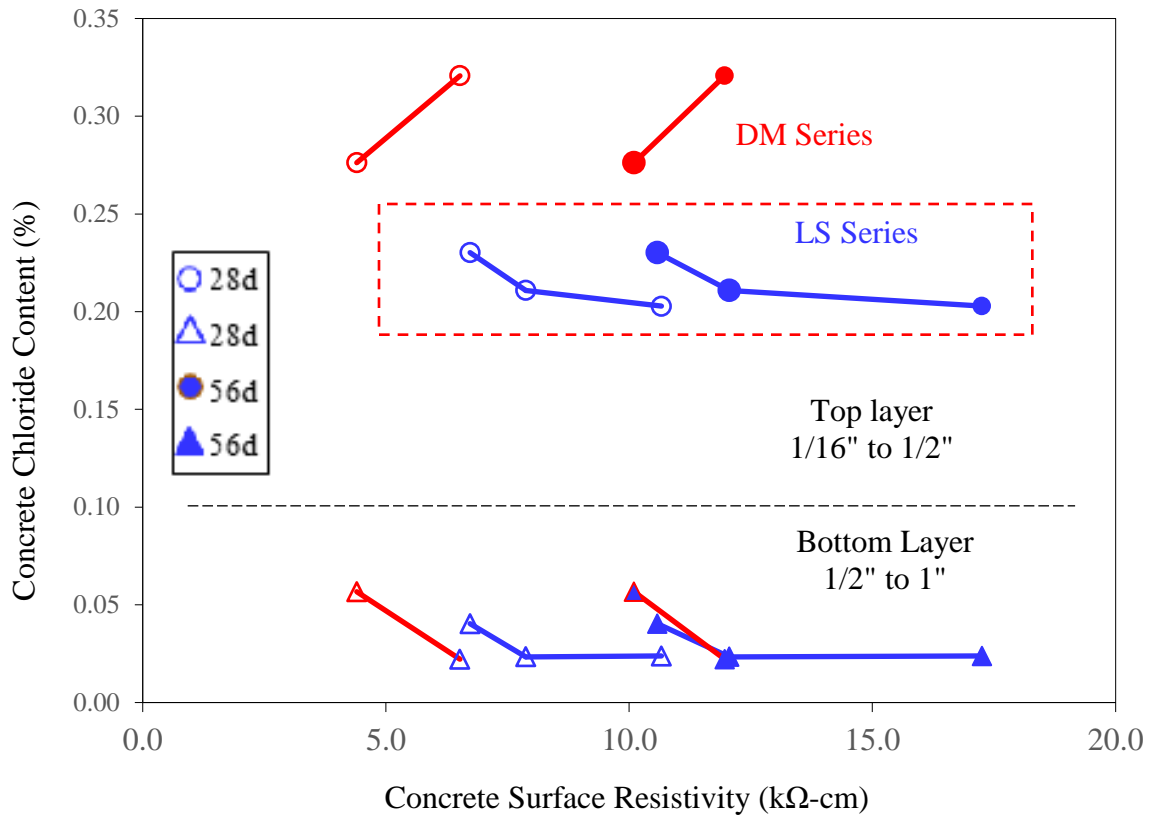


Figure 4.42. Concrete chloride content versus concrete SR at 28 days and 56 days

The trends observed in Figure 4.42 are similar in both the top and bottom layers of the tested slab samples at both ages. Overall, there was a fairly good relationship between chloride content and concrete SR, with SR and chloride content being positively correlated. In both layers, this relationship was clearer in the LS series mixes than in the DM series mixes. Accordingly, in both layers of the LS series mixes, mix C-LS1 exhibited the highest SR and the lowest chloride content, whereas mix C-LS3 exhibited the lowest SR and the highest chloride content.

Figure 4.43 shows the relationship between chloride content and concrete initial sorptivity.

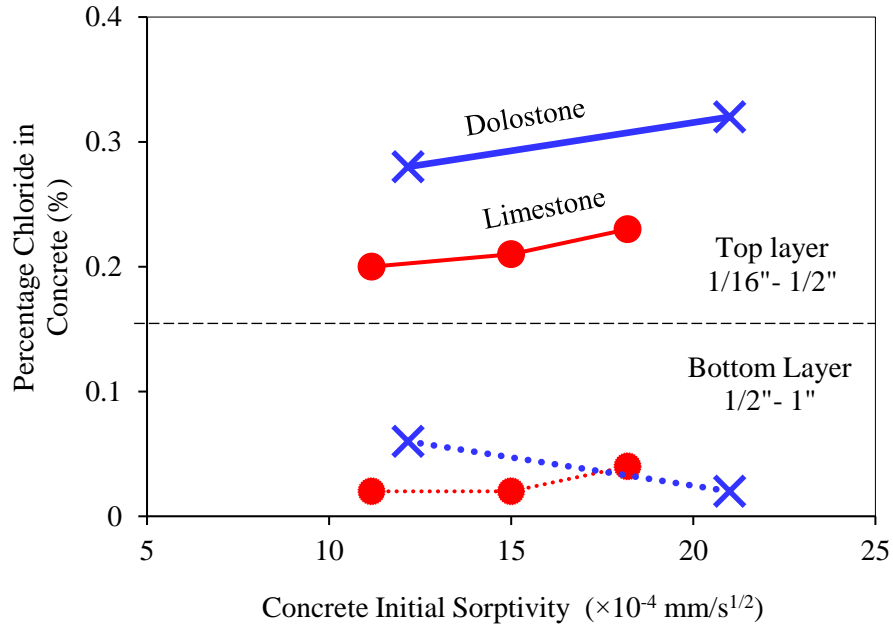


Figure 4.43. Concrete chloride content versus concrete initial sorptivity

Overall, it can be seen in Figure 4.43 that for concrete made with a given type of aggregate (either limestone or dolostone), the chloride content in the top layer of the concrete increased with an increasing rate of sorption for the concrete.

Figure 4.43 also shows that for both aggregate types studied (limestone and dolostone), the chloride content measured from the salt ponding tests increased with the initial sorptivity of the aggregate. Consequently, the short-term sorptivity test (which takes 6 hours based on ASTM C1585) can be used instead of the 90-day salt ponding test (as specified in AASHTO T 259) for a quick evaluation of chloride intrusion in concrete.

5 CONCLUSIONS AND RECOMMENDATIONS

This study evaluated the influence of coarse aggregate porosity and pore throat size distribution on chloride penetration in HPC mixes. The coarse aggregates utilized were limestone and dolostone aggregates that had different water absorption capacities. The aggregates and their corresponding rock samples were analyzed for pore characteristics, and the mortar and HPC specimens were evaluated for chloride intrusion using electrical and non-electrical tests. Relationships were determined between the various properties of the aggregates/rocks and the results obtained from the concrete tests.

The major findings of this study are as follows:

1. The coarse aggregate correction factor increased exponentially with aggregate absorption. This factor must be considered in concrete air void measurements.
2. Concrete compressive strength did not significantly vary for the carbonate coarse aggregate absorption values ranging from 0.7% to 6.8% used in the present study.
3. The main features of the pore structure of the aggregates studied are summarized in Table 5.1.

Table 5.1. Main features of the pore structure of the aggregates studied

Rock ID	Absorption (%)	Mean He porosity (%)	Mean MIP porosity (%)	Mean pore throat size (mm)	Critical pore throat size (mm)	Threshold pore throat size (mm)
LS1	0.7	1.0	3.2	0.02	0.02	0.04
LS2	2.9	6.7	8.4	0.29	0.15	0.4
LS3	3.5	12.5	15.9	1.94	3.63	11
DM1	4.1	15.0	18.4	1.25	1.49	2.1
DM2	6.8	21.0	25.8	5.34	20.4	25

4. The following observations were made regarding the test methods for quantifying the pore system of coarse aggregates:
 - Absorption test – Simple, quick, and easy to run, but not directly related to concrete chloride penetration
 - Sorptivity test – Related to concrete chloride penetration (ponding test results); rock plugs and knowing coring orientation are required
 - Helium test – Measures the total porosity of samples and has a good relationship with the total porosity measured from MIP tests

- MIP test – Provides more information on pore structure, but equipment and operational skills are required
 - Thin section test - Provides more information on mineralogy, grain size, and visualized pore structures (for relatively larger pores).
5. Variation was observed in the results of the electrical and non-electrical tests on concrete made with limestone and dolostone coarse aggregates:
 - In the electrical tests, concrete surface resistivity decreased with increasing aggregate absorption, while the Nord chloride migration coefficient (DNSSM) increased with increasing aggregate absorption.
 - In the non-electrical tests, the same trends were obtained from the sorptivity and ponding tests. Concrete initial sorptivity and chloride content in the top surface layer (top 1/16 to 1/2 inch) increased with limestone aggregate absorption, but they decreased with dolostone aggregate absorption.
 6. There are close relationships between aggregate absorption and specific gravity and between aggregate absorption and helium porosity. There is a strong linear relationship between aggregate helium and MIP porosity.
 7. The critical and threshold throat pore sizes determined from MIP testing of the rock samples had a strong exponential relationship with concrete SR and initial sorptivity. However, the effects of the critical and threshold pore throat sizes seemed not to be significant on the chloride penetration values resulting from the salt ponding tests.
 8. Concrete made with a higher absorption limestone aggregate had higher chloride content after the salt ponding tests. This is probably because more fluids/chloride can penetrate from the mortar into more porous coarse aggregate.
 9. Concrete made with dolostone aggregate had reduced chloride content with increasing aggregate absorption. This is probably due to a potential cement reaction with the surfaces of dolostone aggregate particles and the internal curing ability provided by the stored water in the more porous aggregates.
 10. The mortar samples sieved from the C-LS1 Ames mix had a higher chloride content than all of the five concrete mixes made. This result is related to the high porosity and the critical and threshold pore throat diameters of the mortar.
 11. Before the age of 28 days, the surface resistivity of the concrete mixes decreased linearly with the absorption values of the coarse aggregates. After 28 days, the surface resistivity of the concrete mixes made with dolostone coarse aggregate increased significantly, implying potential cement reactions with the surface of the dolostone aggregate particles and/or internal curing effects provided by water in the highly porous dolostone aggregate.

12. The surface resistivity of concrete made with limestone coarse aggregate increased linearly and the surface resistivity of concrete made with dolostone coarse aggregate decreased linearly with surface resistivity of the corresponding rocks.
13. The chloride content in the top layer of the concrete slabs measured during the salt ponding tests noticeably increased with the limestone aggregate absorption values but decreased with the dolostone absorption values measured through ASTM C127.
14. The surface resistivity, DNSSM, and initial rate of water absorption of the concretes were all higher than those of the mortar mix. However, the chloride content in the top layer of the five concrete mixes were all lower than that of the mortar mix. This suggests that all aggregates, even those with high porosity or high absorption, helped reduce chloride penetration in the HPC compared to the corresponding mortar mix.
15. In the present study, it was not the concrete with the highest aggregate absorption values (Bowser) but the one with the largest amount of fine, connected pores (Douds) that had the highest chloride content in the top layer of the concrete slab subjected to a salt ponding test. The chloride content in the top layer obtained from the salt ponding tests was 0.36% for the mortar mix, 0.32% for the concrete made with Douds aggregate (absorption of 4.1%), 0.28% for the concrete made with Bowser aggregate (absorption of 6.8%), and 0.2% for the concrete made with Ames aggregate (absorption of 0.7%).
16. For a given aggregate type, the concrete chloride content measured from salt ponding tests noticeably increased with the initial sorptivity (or initial rate of water sorption) of the aggregate. This reinforces that sorptivity provides a good indication of the pore structure and connectivity (capillary network) that governs the penetration of aggressive ions into concrete in severe environments.
17. Because thin section petrography, helium porosity, and mercury pore throat sizes were shown to be effective in predicting rock sorption and resistivity values, the numerous reports of these properties in the geological literature can be used to predict the performance of rocks in engineering tests and guide aggregate exploration programs.

The following recommendations are proposed for further study:

1. Recommendations for aggregate pore structure characterization:
 - Aggregate absorption is a key parameter related to many other aggregate and concrete properties. However, the effects of aggregate absorption on concrete sorptivity and chloride intrusion also depend upon aggregate type. Therefore, aggregate absorption should not be used as a sole criterion for concrete durability control.
 - The critical and threshold pore sizes of aggregate obtained from MIP testing can be used to provide quantitative information on the pore connectivity of aggregates, mortar, and concrete as needed.

- Thin-section tests can provide detailed information on aggregate quality, e.g., aggregate grain size, pore characteristics, and bond with mortar. Thin-section tests should be conducted more regularly on Iowa aggregates.

2. Recommendations for concrete permeability and chloride intrusion tests:

- Concrete surface resistivity was shown to be related to concrete initial sorptivity and chloride content. However, opposite trends for this relationship were found for the limestone aggregate concrete and the dolostone aggregate concrete. Therefore, when the surface resistivity test is used, one should know the coarse aggregate type in the concrete tested.
- For all aggregate types, the chloride content measured from the salt ponding tests always increased with the initial sorptivity of the concrete. The initial sorptivity test (which takes six hours) can be performed instead of a 90-day salt ponding test for a quicker evaluation of chloride intrusion in concrete.

3. Recommendations for future study:

- Only aggregates from three limestone sources and two dolostone sources were examined in this study. There are currently 720 crushed rock sources in the Iowa DOT's T203 list of approved sources. More Iowa aggregates should be studied to verify the trends observed in the present study.
- In the present study, mortar had the highest chloride content after 90 days of the ponding test, and fluids and chemicals can penetrate into aggregate through the mortar. In the future, concrete mixes with a lower w/b should also be studied. As the mortar becomes less permeable with a lower w/b, it can wrap and seal the permeable aggregate particles, thus preventing chloride penetration into the aggregate and improving the chloride resistance of the concrete.
- Most tests in the present study showed opposite trends between the limestone aggregate concrete and dolostone aggregate concrete. These results are probably due to a potential cement reaction with surfaces of dolostone aggregate particles and the internal curing ability provided by the stored water in the more porous dolostone aggregates. High-porosity dolostone aggregates should be further studied. In addition, high-resolution imaging (e.g., scanning electron microscopy) of the cement-aggregate interface could reveal more detail about the processes and products in this vital zone of interaction.
- A comparison study can be conducted involving the construction of two field HPC overlays, one made with a low-absorption and low-sorptivity aggregate and the other made with a high-absorption and especially high-sorptivity aggregate. The aggregates could be either limestone or dolostone. The overlays can be monitored for surface resistivity and chloride penetration over time. The results can be used to verify the findings from the present study.

REFERENCES

- Andrade, C. 1993. Calculation of Chloride Diffusion Coefficients in Concrete from Ionic Measurements. *Cement and Concrete Research*, Vol. 23, No. 3, pp. 724–742.
- Andrade, C. and C. Alonso. 1996. Corrosion Rate Monitoring in the Laboratory and On-Site. *Construction and Building Materials*, Vol. 10, No. 5, pp. 315–328.
- Andrade, C., R. Polder, and M. Basheer. 2007. Non-Destructive Methods to Measure Ion Migration. In *Non-Destructive Evaluation of the Penetrability and Thickness of the Concrete Cover*. State-of-the-Art Report of RILEM Technical Committee 189-NEC. International Union of Laboratories and Experts in Construction Materials, Systems and Structures, Bagnex, France, pp. 91–112.
- Andrade, C., M. Prieto, P. Tanner, F. Tavares, and R. d'Andrea. 2013. Testing and Modelling Chloride Penetration into Concrete. *Construction and Building Materials*, Vol. 39, pp. 9–18.
- Andrade, C., C. Alonso, J. Gulikers, R. Polder, R. Cigna, Ø. Vennesland, M. Salta, A. Raharinaivo, and B. Elsener. 2004. Test Methods for On-Site Corrosion Rate Measurement of Steel Reinforcement in Concrete by Means of the Polarization Resistance Method. RILEM TC 154-EMC: Electrochemical Techniques for Measuring Metallic Corrosion, *Materials and Structures*, Vol. 37, No. 9, pp. 623–643.
- Basheer, L., J. Kropp, and D. J. Cleland. 2001. Assessment of the Durability of Concrete from Its Permeation Properties : A Review. *Construction and Building Materials*, Vol. 15, Nos. 2–3, pp. 93–103.
- Bektas, F., K. Wang, and J. Ren. 2015. *Carbonate Aggregate in Concrete*. Minnesota Department of Transportation, St. Paul, MN.
<http://www.dot.state.mn.us/research/TS/2015/201514.pdf>.
- Bektas, F., W. Cai, K. Wang. 2016. Aggregate Freezing-Thawing Performance Using the Iowa Pore Index. Midwest Transportation Center, Iowa State University, Ames, IA.
https://intrans.iastate.edu/app/uploads/2018/03/aggregate_freezing-thawing_using_iowa_pore_index_w_cvr.pdf.
- Bentz, D. P., S. Z. Jones, P. E. Stutzman, J. Arnold, M. Boisclair, P. Rothfeld, J. Tanesi, H. Kim, J. Munoz, and M. Beyene. 2017. *Influence of Aggregate Characteristics on Concrete Performance*. NIST Technical Note 1963. U.S. Department of Commerce, National Institute of Standards and Technology, Gaithersburg, MD.
- Bjegović, D., M. Serdar, I. S. Oslaković, F. Jacobs, H. Beushausen, C. Andrade, A. V. Monteiro, P. Paulini, and S. Nanukuttan. 2015. Test Methods for Concrete Durability Indicators. In *Performance-Based Specification and Control of Concrete Durability*. State-of-the-Art Report of RILEM Technical Committee TC 230-PSC. International Union of Laboratories and Experts in Construction Materials, Systems and Structures, Bagnex, France, pp. 51–105.
- Castro, J., L. Keiser, M. Goliás, and J. Weiss. 2011. Absorption and Desorption Properties of Fine Lightweight Aggregate for Application to Internally Cured Concrete Mixtures. *Cement and Concrete Composites*, Vol. 33, No. 10, pp. 1001–1008.
- Choquette, P.W. and L.C. Pray. 1970. Geologic Nomenclature and Classification of Porosity in Sedimentary Carbonates. *AAPG Bulletin*, Vol. 54, No. 2, pp. 207–250.

- Derluyn, H., M. Griffa, D. Mannes, I. Jerjen, J. Dewanckele, P. Vontobel, A. Sheppard, D. Derome, V. Cnudde, E. Lehmann, and J. Carmeliet. 2013. Characterizing Saline Uptake and Salt Distributions in Porous Limestone with Neutron Radiography and X-Ray Micro-Tomography. *Journal of Building Physics*, Vol. 36, No. 4, pp. 353–374.
- Dhandapani, Y. and M. Santhanam. 2017. Assessment of Pore Structure Evolution in the Limestone Calcined Clay Cementitious System and Its Implications for Performance. *Cement and Concrete Composites*, Vol. 84, pp. 36–47.
- Dong, H., H. Zhang, Y. Zuo, P. Gao, and G. Ye. 2018. Relationship Between the Size of the Samples and the Interpretation of the Mercury Intrusion Results of an Artificial Sandstone. *Materials*, Vol. 11, No. 2, 201, pp. 1–17.
- Gane, P. A. C., C. J. Ridgway, E. Lehtinen, R. Valiullin, I. Furó, J. Schoelkopf, H. Paulapuro, and J. Daicic. 2004. Comparison of NMR Cryoporometry, Mercury Intrusion Porosimetry, and DSC Thermoporosimetry in Characterizing Pore Size Distributions of Compressed Finely Ground Calcium Carbonate Structures. *Industrial and Engineering Chemistry Research*, Vol. 43, No. 24, pp. 7920–7927.
- Giesche, H. 2006. Mercury porosimetry: a general (practical) overview. *Particle & Particle Systems Characterization*, Vol. 23, No. 1, pp. 9–19.
- Gustafson, K. J., R. Dawson, K. B. Jones, and N. Tieck. 2015. *Carbonate Rock Pore Size Distribution Determination through Iowa Pore Index Testing*. Iowa Department of Transportation, Highway Division, Office of Construction and Materials, Ames, IA.
- Hall, C. and T. K-M. Tse. 1986. Water Movement in Porous Building Materials—VII: The Sorptivity of Mortars. *Building and Environment*, Vol. 21, No. 2, pp. 113–118.
- KDOT. 2007. *Standard Specifications for State Road and Bridge Construction*. Kansas Department of Transportation, Bureau of Construction and Materials, Topeka, KS. <https://www.ksdot.org/burconsmain/specprov/2007SSDefault.asp>.
- Khanzadeh Moradillo, M., C. Qiao, M. Keys, H. Hall, M. T. Ley, S. Reese, and W. J. Weiss. 2019. Quantifying Fluid Absorption in Air-Entrained Concrete Using Neutron Radiography. *Materials Journal*, Vol. 116, No. 6, pp. 213–226.
- Lucia, F.J. 1995. Rock-Fabric/Petrophysical Classification of Carbonate Pore Space for Reservoir Characterization. *AAPG Bulletin*, Vol. 79, No. 9, pp. 1275–1300.
- Lawler, J. S., P. D. Krauss, and C. Abernathy. 2005. *Development of High-Performance Concrete Mixtures for Durable Bridge Decks in Montana Using Locally Available Materials*. ACI Special Publication 228-55, pp. 883–902.
- Li, X., Y. Kang, and M. Haghghi. 2018. Investigation of Pore Size Distributions of Coals with Different Structures by Nuclear Magnetic Resonance (NMR) and Mercury Intrusion Porosimetry (MIP). *Measurement*, Vol. 116, pp. 122–128.
- Luping, T. and L.-O. Nilsson. 1992. Chloride Diffusivity in High Strength Concrete at Different Ages. *Nordic Concrete Research*, Vol. 11, No. 1, pp. 162–171.
- McLeod, H. A. K. 2009. Development and Construction of Low-Cracking High-Performance Concrete (LC-HPC) Bridge Decks: Construction Methods, Specifications, and Resistance to Chloride Ion Penetration. PhD dissertation. University of Kansas, Lawrence, KS.
- MDOT. 2012. *Standard Specifications for Construction*. Michigan Department of Transportation, Lansing, MI. <https://mdotcf.state.mi.us/public/specbook/2012/main.cfm>.
- Mehta, P. K. and P. J. M. Monteiro. 2014. *Concrete: Microstructure, Properties, and Materials*. Fourth Edition. McGraw-Hill, New York, NY.

- MnDOT. 2018. *Minnesota Standard Specifications for Construction*. Minnesota Department of Transportation, St. Paul, MN. <http://www.dot.state.mn.us/pre-letting/spec/2018/2018-spec-book-final.pdf>.
- Myers, J. D. and W. Dubberke. 1980. *Iowa Pore Index Test*. Interim Report. Iowa Department of Transportation, Highway Division, Office of Materials, Ames, IA.
- Nilsson, L.-O., E. Poulsen, P. Sandberg, H. E. Sorensen, and O. Klinghoffer. 1996. *Chloride Penetration into Concrete, State-of-the-Art, Transport Processes, Corrosion Initiation, Test Methods and Prediction Models*. HETEK Report No. 53.
- NJDOT. 2007. *Standard Specifications for Road and Bridge Construction*. New Jersey Department of Transportation, Ewing Township, NJ. <https://www.state.nj.us/transportation/eng/documents/BDC/pdf/attachmentbdc07s03.pdf>.
- PennDOT. 2003. *Specifications*. Commonwealth of Pennsylvania Department of Transportation, Harrisburg, PA. http://www.dot.state.pa.us/public/PubsForms/Publications/Pub_408/408_2003/408_2003_IE/408_2003_IE.pdf.
- de Oliveira, G. L. P., M. A. R. Ceia, R. M. Missagia, N. L. Archilha, L. Figueiredo, V. H. Santos, and I. L. Neto. 2016. Pore Volume Compressibilities of Sandstones and Carbonates from Helium Porosimetry Measurements. *Journal of Petroleum Science and Engineering*, Vol. 137, pp. 185–201.
- Qiao, C., W. Ni, Q. Wang, and J. Weiss. 2018. Chloride Diffusion and Wicking in Concrete Exposed to NaCl and MgCl₂ Solutions. *Journal of Materials in Civil Engineering*, Vol. 30, No. 3, pp. 1–10.
- Richards, S. and A. Bouazza. 2007. Determination of Particle Density Using Water and Gas Pycnometry. *Geotechnique*, Vol. 57, No. 4, pp. 403–406.
- Ridzuan, M. F. A. 2016. Understanding the Geological Basis of the Iowa Pore Index. MS thesis. Iowa State University, Ames, IA.
- Rouquerol, J., D. Avnir, C. W. Fairbridge, D. H. Everett, J. M. Haynes, N. Pernicone, J. D. F. Ramsay, K. S. W. Sing, and K. K. Unger. 1994. Recommendations for the Characterization of Porous Solids. *Pure and Applied Chemistry*, Vol. 66, No. 8, pp. 1739–1758.
- Rouquerol, J., G. V. Baron, R. Denoyel, H. Giesche, J. Groen, P. Klobes, P. Levitz, A. V. Neimark, S. Rigby, R. Skudas, and K. Sing. 2011. Liquid Intrusion and Alternative Methods for the Characterization of Macroporous Materials. *Pure and Applied Chemistry*, Vol. 84, No. 1, pp. 107–136.
- Rouquerol, J., G. V. Baron, R. Denoyel, H. Giesche, J. Groen, P. Klobes, P. Levitz, A. V. Neimark, S. Rigby, R. Skudas, and K. Sing. 2012. The Characterization of Macroporous Solids: An Overview of the Methodology. *Microporous and Mesoporous Materials*, Vol., pp. 2–6.
- Rushing, J. A., K. E. Newsham, and T. A. Blasingame. 2008. Rock Typing: Keys to Understanding Productivity in Tight Gas Sands. Society of Petroleum Engineers (SPE) Unconventional Reservoirs Conference, February 10–12, Keystone, CO.
- Savva, P. and M. F. Petrou. 2018. Highly Absorptive Normal Weight Aggregates for Internal Curing of Concrete. *Construction and Building Materials*, Vol. 179, pp. 80–88.
- Scholle, P.A. and D. S. Ulmer-Scholle. 2003. *AAPG Memoir 77: A Color Guide to the Petrography of Carbonate Rocks: Grains, Textures, Porosity, Diagenesis*. American Association of Petroleum Geologists, Tulsa, OK.

- Soja, W., F. Zunino, and K. Scrivener. 2019. *Mercury Intrusion Porosimetry (MIP). Laboratory of Construction Materials*. École Polytechnique Fédérale de Lausanne, Lausanne, Switzerland. <https://www.epfl.ch/labs/lmc/wp-content/uploads/2019/08/03-Wioletta-Franco-MIP.pdf>.
- Stanish, K. D., R. D. Hooton, and M. D. A. Thomas. 1997. *Testing the Chloride Penetration Resistance of Concrete: A Literature Review*. Federal Highway Administration, Turner-Fairbank Highway Research Center, McLean, VA.
- Ulmer-Scholle, D.S., P.A. Scholle, J. Schieber, and R. J. Raine. 2015. *AAPG Memoir 109: A Color Guide to the Petrography of Sandstones*. American Association of Petroleum Geologists, Tulsa, OK.
- Vaysburd, A. 1992. Durability of Lightweight Concrete and Its Connections with the Composition of Concrete, Design and Construction Methods. In *SP-136: Structural Lightweight Aggregate Concrete Performance*. American Concrete Institute, Farmington Hills, MI.
- Wattanapornprom, R. and T. Ishida. 2017. Modeling of Chloride Penetration into Airborne Chloride Environmental Conditions Combined with Washout Effects. *Journal of Advanced Concrete Technology*, Vol. 15, pp. 126–142.
- Wei, J., B. Tao, and W. J. Weiss. 2017. Water Absorption in Cementitious Materials at Different Temperatures Water. *Advances in Civil Engineering Materials*, Vol. 6, No. 1, pp. 280–295.
- Yan, Z., C. Chen, P. Fan, M. Wang, and X. Fang. 2015. Pore Structure Characterization of Ten Typical Rocks in China. *Electronic Journal of Geotechnical Engineering*, Vol. 20, No. 2, pp. 479–494.
- Yang, L., D. Gao, Y. Zhang, J. Tang, and Y. Li. 2019. Relationship between Sorptivity and Capillary Coefficient for Water Absorption of Cement-Based Materials: Theory Analysis and Experiment. *Royal Society Open Science*, Vol. 6, No. 6, pp. 1–12.
- Yao, Y. and D. Liu. 2012. Comparison of Low-Field NMR and Mercury Intrusion Porosimetry in Characterizing Pore Size Distributions of Coals. *Fuel*, Vol. 95, pp. 152–158.
- Zeng, Q., Z. Lin, C. Zhou, and J. Wang. 2019. Capillary Imbibition of Ethanol in Cement Paste Traced by X-Ray Computed Tomography with CsCl-Enhancing Technique. *Chemical Physics Letters*, Vol. 726, pp. 117–123.
- Zhang, N., M. He, B. Zhang, F. Qiao, H. Sheng, and Q. Hu. 2016. Pore Structure Characteristics and Permeability of Deep Sedimentary Rocks Determined by Mercury Intrusion Porosimetry. *Journal of Earth Science*, Vol. 27, pp. 670–676.
- Zhutovsky, S. and R. D. Hooton. 2019. Role of Sample Conditioning in Water Absorption Tests. *Construction and Building Materials*, Vol. 215, pp. 918–924.
- Zou, D., H. Zhang, Y. Wang, J. Zhu, and X. Guan. 2015. Internal Curing of Mortar with Low Water to Cementitious Materials Ratio using a Normal Weight Porous Aggregate. *Construction and Building Materials*, Vol. 96, pp. 209–216.

**THE INSTITUTE FOR TRANSPORTATION IS THE FOCAL POINT FOR TRANSPORTATION
AT IOWA STATE UNIVERSITY.**

InTrans centers and programs perform transportation research and provide technology transfer services for government agencies and private companies;

InTrans contributes to Iowa State University and the College of Engineering's educational programs for transportation students and provides K–12 outreach; and

InTrans conducts local, regional, and national transportation services and continuing education programs.



**IOWA STATE
UNIVERSITY**

Visit InTrans.iastate.edu for color pdfs of this and other research reports.